Exploring the role of RNA modifications in phage-host dynamics

Dissertation

Zur Erlangung des Doktorgrades der Naturwissenschaften

(Dr. rer. nat.)

der Fakultät für Biologie

der Ludwig-Maximilians-Universität München

vorgelegt von

Bibakhya Saikia

aus Assam, Indien

München, 2025

Diese Dissertation wurde angefertigt
unter der Leitung von Prof. Dr. Kirsten Jung
im Bereich der Fakultät für Biologie
an der Ludwig-Maximilians-Universität München

This dissertation was prepared
under the guidance of Prof. Dr. Kirsten Jung
in the Faculty of Biology
at the Ludwig-Maximilians-Universität München

Gutachter (Reviewers):

1. Prof. Dr. Kirsten Jung

2. Prof. Dr. Simon Heilbronner

Datum der Abgabe (Date of submission): 29.01.2025

Tag der mündlichen Prüfung (Date of the oral examination): 27.02.2025

Eigenständigkeitserklärung

Hiermit versichere ich an Eides statt, dass die vorliegende Dissertation mit dem Titel „Exploring the role of RNA modifications in phage-host dynamics“ von mir selbstständig verfasst wurde und dass keine anderen als die angegebenen Quellen und Hilfsmittel benutzt wurden. Die Stellen der Arbeit, die anderen Werken dem Wortlaut oder dem Sinne nach entnommen sind, wurden in jedem Fall unter Angabe der Quellen (einschließlich des World Wide Web und anderer elektronischer Text- und Datensammlungen) kenntlich gemacht. Weiterhin wurden alle Teile der Arbeit, die mit Hilfe von Werkzeugen der künstlichen Intelligenz de novo generiert wurden, durch Fußnote/Anmerkung an den entsprechenden Stellen kenntlich gemacht und die verwendeten Werkzeuge der künstlichen Intelligenz gelistet. Die genutzten Prompts befinden sich im Anhang. Diese Erklärung gilt für alle in der Arbeit enthaltenen Texte, Graphiken, Zeichnungen, Kartenskizzen und bildliche Darstellungen.

Bibakhya Saikia München, 29.01.2025

Affidavit

Herewith I certify under oath that I wrote the accompanying dissertation myself.

Title: Exploring the role of RNA modifications in phage-host dynamics

In the thesis, no other sources and aids have been used than those indicated. The passages of the thesis that are taken in wording or meaning from other sources have been marked with an indication of the sources (including the World Wide Web and other electronic text and data collections). Furthermore, all parts of the thesis that were de novo generated with the help of artificial intelligence tools were identified by footnotes/annotations at the appropriate places and the artificial intelligence tools used were listed. The prompts used were listed in the appendix. This statement applies to all text, graphics, drawings, sketch maps, and pictorial representations contained in the Work.

Bibakhya Saikia Munich, 29.01.2025

Erklärung

Hiermit erkläre ich,

- dass die Dissertation nicht ganz oder in wesentlichen Teilen einer anderen Prüfungskommission vorgelegt worden ist.
- dass ich mich anderweitig einer Doktorprüfung ohne Erfolg nicht unterzogen habe.

Bibakhya Saikia München, 29.01.2025

Declaration

Hereby I declare,

- that this work, complete or in parts, has not yet been submitted to another examination institution.
- that I did not undergo another doctoral examination without success.

Bibakhya Saikia Munich, 29.01.2025

Contributions to Publications Presented in this Thesis

Citations in chapters: Some parts of 2.2-2.13, 2.15-2.18, 2.27, 3.1.1, 3.1.2., 3.2.1, 3.2.2, 3.2.4, 3.3

Bibakhya Saikia, Sebastian Riquelme-Barrios, Thomas Carell, Sophie Brameyer and Kirsten Jung. 2024. Depletion of m^6A-RNA in *Escherichia coli* reduces the infectious potential of T5 bacteriophage. Microbiology Spectrum, 12 (12), e0112424. Doi: 10.1128/spectrum.01124-24.

Author Contributions

Bibakhya Saikia – Conceptualisation, Investigation, Writing – original draft, Writing – review and editing, and Methodology. Sebastian Riquelme-Barrios – Conceptualisation, Methodology, Writing – original draft and Writing – review and editing. Thomas Carell – Methodology and Writing – review and editing. Sophie Brameyer – Conceptualisation, Funding acquisition, Methodology, Supervision, Writing – original draft and Writing – review and editing. Kirsten Jung – Conceptualisation, Funding acquisition, Methodology, Supervision, Writing – original draft and Writing – review and editing.

We hereby confirm the above statements.

Bibakhya Saikia Prof. Dr. Kirsten Jung

Table of Contents

Nomenclature

All bacterial strains as written in italics, e.g. *Escherichia coli* or *E. coli*

All genes are written in italics, e.g., *flu*

All proteins are written with a first capital letter, e.g., Flu

All plasmids are written with p, e.g., pET28a

Gene deletions are marked by Δ, e.g., Δ*flu*

P indicates as the promoter of a gene, e.g., P*flu*.

Promoter fusion with fluorescence reporters are written as, e.g., P*flu*-*mNeonGreen*.

Abbreviations

6His	hexa histidine
A	adenine
ADP	adenosine diphosphate
ALKBH5	alpha-ketoglutarate dependent dioxygenase homolog 5
Arm	aminoglycoside resistance methyltransferase
ART	adenosine diphosphate ribosyltransferases
ATP	adenosine triphosphate
BASEL collection	Bacteriophage Selection for your Laboratory collection
bp	basepairs
BSA	bovine serum albumin
C	cytosine
cDNA	complementary DNA
CFU	colony-forming units
Ct	threshold cycle
DAP	diaminopimelic acid
DENV	dengue virus
DIA	data independent acquisition
DNA	deoxyribonucleic acid
dsDNA	double-stranded deoxyribonucleic acid
dsRNA	double-stranded ribonucleic acid
DTT	dithiothreitol

ELISA	enzyme-linked immunosorbent assay
EOP	efficiency of plaquing
FST	first step transfer
FTO	fat mass- and obesity-associated protein
G	guanine
GO	Gene Ontology
HCV	Hepatitis C virus
HIV-1	Human immunodeficiency virus-1
IAV	Influenza A virus
ICTV	International Committee on Taxonomy of Viruses
IPTG	isopropyl-β-D-1-thiogalactopyranoside
kb	kilobase
KEGG	Kyoto Encyclopedia of Genes and Genomes
LB	lysogeny broth
LC-MS/MS	liquid chromatography-tandem mass spectrometry
LFQ	label-free quantification
LM	lysogeny broth with 2x NaCl
m^2A	2-methyladenosine
$m^{6,6}A$	$N^{6,6}$-dimethyladenosine
m^6A	N^6-methyladenosine
m^6A-meRIP-seq	m^6A-methylated RNA immunoprecipitation sequencing
m^7G	N^7-methylguanosine
MC	mitomycin C

METTL1	methyltransferase-like 1
METTL14	methyltransferase-like 14
METTL3	methyltransferase-like 3
MOI	multiplicity of infection
mRNA	messenger ribonucleic acid
NAD^+	nicotinamide adenine dinucleotide
NB	nutrient broth
Ni-NTA	nickel nitriloacetic acid
OD_{600}	optical density at 600 nm
ORF	open reading frame
PCl	phenol-chloroform-isoamyl alcohol
PCR	polymerase chain reaction
PFU	plaque-forming units
PMSF	phenylmethylsulfonyl fluoride
pNPP	para-nitrophenyl phosphate
qPCR	quantitative polymerase chain reaction
RBS	ribosome binding site
RF	relative fluorescence intensity
RNA	ribonucleic acid
Rol-LAMP	rolling circle extension-assisted loop-mediated isothermal amplification
ROS	reactive oxygen species
RP	ribosomal protein
rRNA	ribosomal ribonucleic acid

RT	reverse transcriptase
SAM	S-adenosylmethionine
SD	Shine-Dalgarno
Sgm	Sisomicin-gentamicin methyltransferase
ssDNA	single stranded deoxyribonucleic acid
ssRNA	single stranded ribonucleic acid
SST	Second step transfer
SV40	simian vacuolating virus 40
TBST	Tris-buffered saline with 0.1 % (v/v) Tween 20
TCA	tricarboxylic acid
tRNA	transfer ribonucleic acid
U	uracil
UTR	untranslated region
w/v, v/v	weight per volume, volume per volume
WDR4	WD repeat domain 4
WTAP	Wilms tumor 1-associated protein
YTHDC1	YT521-B homology domain containing 1
ZIKV	Zika virus

List of Figures and Tables

List of Figures

List of Tables

Summary

This thesis investigates the role of bacterial rRNA modifications in phage-host dynamics, focusing on two bacterial model systems: *V. campbellii* and *E. coli*. In *V. campbellii*, m^6A-RNA depletion did not influence lysogenic phage induction or susceptibility to the lytic phage Virtus. In *E. coli*, the study was extended to include several members of the T-phages and λ phage. T5 phage exhibited a significant reduction in plaquing efficiency in the m^6A-RNA depleted mutant compared to the wild-type strain. Cellular-level studies of T5 phage infections showed that while phage adsorption was similar in both strains, the m^6A-RNA depleted mutant exhibited a delayed host cell lysis, resulting in asynchronous bursts.

Molecular-scale investigations to assess how m^6A depletion influences T5 phage infection revealed an increase in ribosome-associated proteins in the wild-type strain upon infection, whereas the m^6A-RNA depleted mutant showed a reduction in these proteins. Furthermore, the m^6A-RNA depleted mutant showed reduced polysome (multiple ribosomes bound to an mRNA) abundance and increased monosome (free ribosome or single ribosome bound to an mRNA) levels, indicating impaired translation efficiency. This was accompanied by a significantly higher abundance of some T5 phage transcripts. Thus, the m^6A-RNA depleted mutant may compensate for diminished translational efficiency by increasing transcript levels or decreasing mRNA turnover to maintain protein levels.

Additional analyses explored RNA modifications in RNA phages, reporting for the first time the presence of modifications such as m^6A, m^2A, $m^{6,6}A$, and m^7G in genomic RNA from the phages MS2 and Qβ. Single knockout mutants for the host rRNA methyltransferases catalysing the observed modifications did not affect Qβ replication. However, a mutant lacking *rsmA* which codes for RsmA responsible for $m^{6,6}A$ methylation, was found to increase MS2 phage infectivity. This result suggests a physiological role of $m^{6,6}A$ modifications in protecting the host against MS2 infection.

In conclusion, this thesis provides the first insights into the roles of rRNA modifications, particularly m^6A in bacteria, highlighting their impact on phage–host interactions.

Zusammenfassung

Diese Arbeit untersucht den Effekt bakterieller rRNA-Modifikationen auf die Phagen-Wirt-Dynamik und konzentriert sich dabei auf zwei bakterielle Modellorganismen: *Vibrio campbellii* und *Escherichia coli*. In *V. campbellii* hatte die m^6A-RNA-Depletion keinen Einfluss auf die Induktion lysogener Phagen oder die Infektion mit dem lytischen Phagen. Bei *E. coli* wurde die Studie auf mehrere Mitglieder der T-Phagen und λ-Phagen ausgeweitet. T5-Phagen hatten in der m^6A-RNA-depletierten Mutante im Vergleich zum Wildtypstamm eine signifikante geringere Effizienz in der Plaquebildung. Zelluläre Studien zur Infektion mit T5-Phagen zeigten, dass die Phagenadsorption bei beiden Stämmen ähnlich war, die m^6A-RNA-depletierte Mutante jedoch eine verzögerte Lyse der Wirtszellen aufwies, was zu einer asynchronen Lyse führte.

Untersuchungen auf molekularer Ebene zur Beurteilung, wie sich m^6A-RNA-Depletion auf die Infektion mit T5-Phagen auswirkt, ergaben einen Anstieg der Ribosomen-assoziierten Proteine im Wildtyp nach der Infektion, während die m^6A-RNA-depletierte Mutante eine Abnahme dieser Proteine aufwies. Darüber hinaus zeigte die m^6A-RNA-depletierte Mutante eine verringerte Anzahl an Polysomen (mehrere Ribosomen auf einer mRNA) und eine erhöhte Anzahl an Monosomen (ein freies Ribosom oder ein einzelnes Ribosom auf einer mRNA), was auf eine verringerte Translationseffizienz hindeutete. Diese Veränderungen gingen mit einem Anstieg einiger T5-Phagentranskripte einher. Die m^6A-RNA-depletierten Mutanten kompensiert vermutlich diese verminderte Translationseffizienz, indem die generelle Menge an Transkript erhöht wird und somit die Menge an Proteinen konstant zu halten.

Weitere Untersuchungen ermöglichten den Nachweis von RNA-Modifikationen in RNA-Phagen. Damit konnte erstmals die Präsenz der Modifikationen m^6A, m^2A, $m^{6,6}A$ und m^7G in den genomischen RNA-Phagen MS2 und Qß nachgewiesen werden. Einzelne Knockout-Mutanten für die rRNA-Methyltransferasen des Wirts, die die beobachteten Modifikationen katalysieren, hatten keinen Einfluss auf die Qβ-Replikation. Es zeigte sich jedoch, dass das Fehlen von RsmA, das die $m^{6,6}A$ Methylierung katalysiert, zu einer Erhöhung der Infektiosität der MS2-Phagen führte. Dieses Ergebnis deutet auf eine Rolle von $m^{6,6}A$-Modifikationen beim Schutz des Wirts vor einer MS2-Infektion hin.

Diese Arbeit gibt erste Einblicke in die Rolle von rRNA-Modifikationen, insbesondere m^6A, in Bakterien und demonstriert deren Einfluss auf die Wechselwirkung zwischen Phagen und Wirt.

1 Introduction

Back in 1957, during a lecture at the Society for Experimental Biology, Dr. Francis Crick, who later received the Nobel prize in 1962 alongside his colleagues for discovering the molecular structure of deoxyribonucleic acid (DNA), introduced the concept of the central dogma of molecular biology. He described a unilateral transfer of information from DNA to ribonucleic acid (RNA) to proteins and later published it in his paper titled "On Protein Synthesis" (Crick, 1958). The discovery of RNA-dependent DNA polymerase (also called reverse transcriptase) in retroviruses (Baltimore, 1970; Temin and Mizutani, 1970) strongly challenged the central dogma. Crick then refined the central dogma and described a detailed residue-by-residue flow of sequential genetic information in a biological system (Crick, 1970). He further stated that genetic information cannot be transferred from protein to either protein or nucleic acid (Crick, 1970). However, over time, exceptions (Shapiro, 2009) — particularly, alternative splicing (Chow et al., 1977), junk DNA (Ohno, 1972), non-coding RNAs (Mattick, 2003), RNA viruses, epigenetics (Jablonka and Lamb, 2002) and prions (Prusiner, 1998) — expanded our understanding of molecular biology and introduced additional layers to gene flow regulation. One such extra layer is post-transcriptional modification of RNA.

1.1 RNA modifications

Epitranscriptomics, by definition, describes the functionally relevant changes to the RNA that do not alter or mutate its sequence. The word transcriptome refers to the coding and non-coding RNA transcripts of a cell. The loanword from the Greek prefix epi – means over, upon or above – implies the addition of "something" on top of the traditional RNA transcript sequence. Examples of mechanisms that produce such changes are chemical modifications of the most common building blocks of RNA – adenine (A), uracil (U), guanine (G), and cytosine (C) (Fig. 1.1). To date, over 170 RNA modifications have been identified across all domains of life (Fig. 1.1) which are stored in an online database for RNA modification pathways called MODOMICS (Cappannini et al., 2024; Czerwoniec et al., 2009). These chemical changes can regulate RNA metabolism, structure, stability, function and fate (Wilkinson et al., 2022). Among the earliest RNA modifications to be

discovered were the infamous 5´cap (m^7G modification), which protects messenger RNA (mRNA) and enhances translation efficiency (Shatkin, 1976) and the poly(A) tail, which stabilizes mRNA and facilitates its export from the nucleus (Edmonds et al., 1971). These modifications are essential for efficient splicing, demonstrating that RNA modifications are key regulators of gene expression and translation.

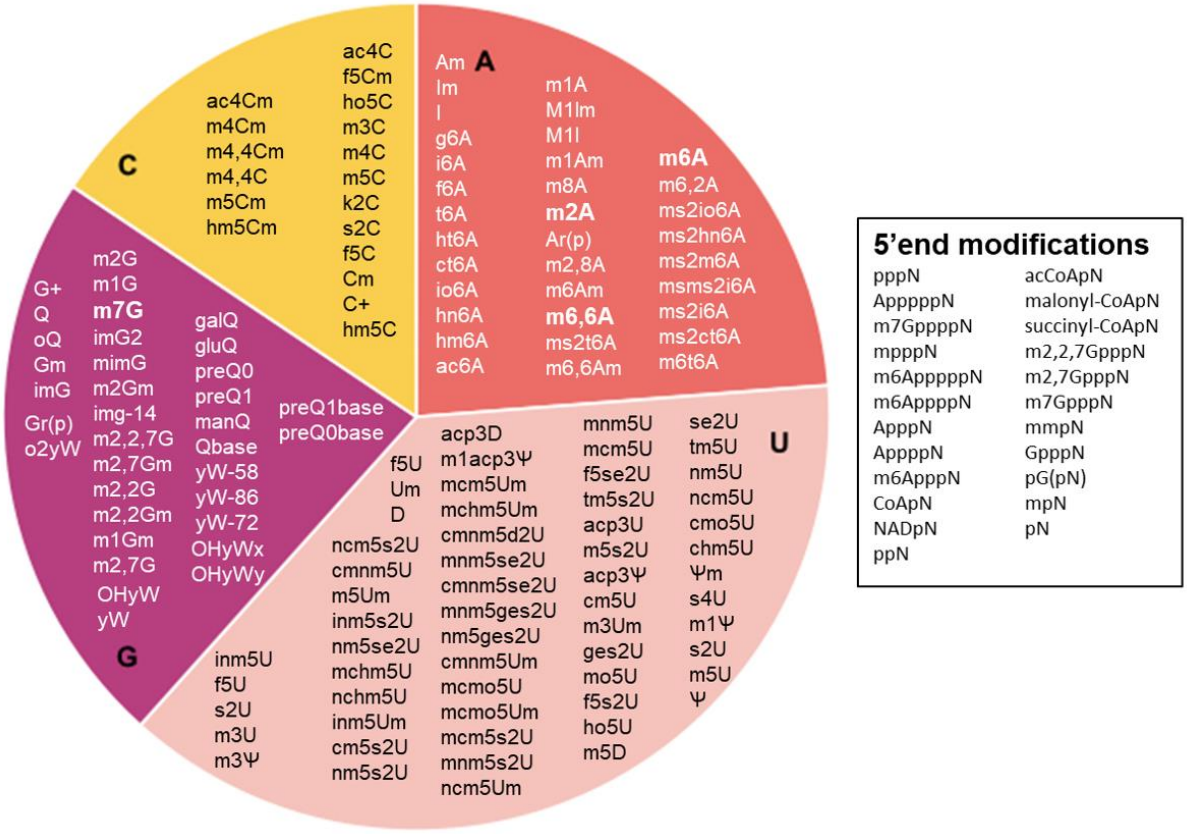

Figure 1.1 Known RNA modifications classified by their nucleotide (C, A, U, G) and 5'end modifications. Four modifications (m^6A, $m^{6,6}A$, m^2A and m^7G) that are studied in this thesis are marked in bold. Modified and adapted from Cappannini et al., 2024 and Lucas and Novoa, 2023.

Numerous modifications present in different forms of RNA (Fig. 1.1) could influence its fate. This thesis will provide a brief overview of some essential methyl modifications such as m^7G, m^2A and $m^{6,6}A$, with a primary focus on the m^6A modification, which has emerged as the most prevalent, abundant and conserved modification in eukaryotic RNA (Jiang et al., 2021).

S-adenosylmethionine (SAM) is involved in methyl group transfers and acts as a common methyl donor for several substrates, including RNA.

1.1.1 m^7G modification

N^7-methylguanosine (m^7G) is a modified guanosine nucleotide with a methyl group at position N7 (Fig. 1.2). Initially studied for its role at the 5′cap of eukaryotic and virus mRNA (Furuichi, 2015; Shatkin, 1976; Abraham et al., 1975; Furuichi and Miura, 1975), m^7G has also been found in internal positions within mammalian mRNA, microRNA (miRNA), transfer RNA (tRNA) and ribosomal RNA (rRNA) (Cheng et al., 2022; Zhang et al., 2019). William-Beuren syndrome chromosome region 22 (WBSCR22) adds m^7G at position G1639 of human 18S rRNA, which is known to impact pre-rRNA processing and biosynthesis of the 40S ribosomal subunit (Zhang et al., 2019). Additionally, methyltransferase-like 1 (METTL1) forms a complex with WD repeat domain (WDR4) to add m^7G in miRNA and mRNA (Liu et al., 2024; Zhang et al., 2019) and at the position of G46 of mammalian tRNAs (Cheng et al., 2022). m^7G modification in G46 of tRNA is a relatively conserved modification across humans, yeast and bacteria (Tomikawa, 2018). The absence of m^7G modification can impact pathogenic fungal infectivity, regulate the presence of other tRNA modifications and is associated with several diseases, including tumours as reviewed by Tomikawa, 2018.

Escherichia coli and *Bacillus subtilis* use methyltransferase TrmB to methylate G46 at the N7 position in the variable loop of the tRNA, generating a positive charge (Zhou et al., 2009; De Bie et al., 2003). However, deletion of the *trmB* gene is not essential for the growth of *E. coli* (De Bie et al., 2003). Conserved in bacteria, the methyltransferases RsmG and RlmKL are responsible for the addition of m^7G methylation to G527 in the 16S rRNA and G2069 in the 23S rRNA (Lesnyak et al., 2006; Okamoto et al., 2007). Moreover, RlmKL is a fused methyltransferase that is also known to methylate G2445 at the N2 position (Kimura et al., 2012). Deletions of either *rsmG* or *rlmKL* do not influence ribosomal assembly or growth rate in *E. coli* (Pletnev et al., 2020). However, the deletion of *rlmKL* leads to reduced efficiency of constitutive and induced exogenous protein synthesis (Pletnev et al., 2020). Additionally, a new methyltransferase RlmQ is responsible for the addition of m^7G methylation to G2601 in the 23S rRNA of *Staphylococcus aureus* (Bahena-Ceron et al., 2024). Deletion of *rlmQ* influences the growth rate and biofilm formation of *S. aureus*

along with its cytotoxicity on human cells (Bahena-Ceron et al., 2024). This modification was conserved among clinical isolates of *S. aureus* but was absent in *E. coli* (Bahena-Ceron et al., 2024).

Interestingly, m^7G modification in bacteria has a unique association with antibiotic resistance. Aminoglycoside-producing organisms, such as *Micromonospora zionensis* protect themselves against their own secondary metabolite by modifying its ribosomes by encoding aminoglycoside resistance methyltransferase (Arm) such as Sisomicin-gentamicin methyltransferase (Sgm) (Kojic et al., 1996). Sgm confers resistance to antibiotics such as sisomicin, gentamicin and kanamycin by adding m^7G methylation at G1405 in bacterial 16S rRNA (Husain et al., 2010). Remarkably, many human pathogenic bacteria have acquired Arm family proteins through horizontal gene transfer, a key mechanism for spreading antibiotic resistance (Husain et al., 2010). Additionally, the loss of the conserved G527 modification in the 16S rRNA of *Mycobacterium tuberculosis* confers streptomycin resistance (Okamoto et al., 2007). These findings highlight the role of m^7G modification in bacterial antibiotic resistance.

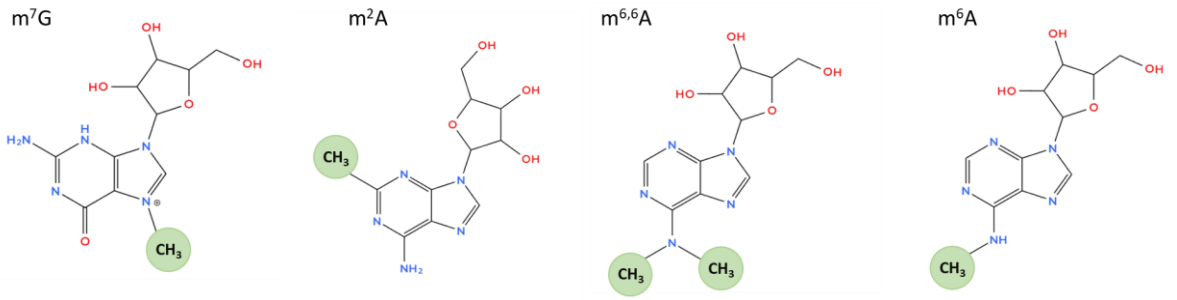

Figure 1.2 Chemical structures of N^7-methylguanosine (m^7G), 2-methyladenosine (m^2A), N^6, N^6-dimethyladenosine ($m^{6,6}A$), and N^6-methyladenosine (m^6A), respectively. Nitrogen atoms and amino groups are marked in blue. Oxygen atoms and hydroxy groups are marked in red. The methyl group is highlighted in green. The images were generated using MolView.

1.1.2 m^2A modification

2-methyladenosine (m^2A) is a modified adenosine nucleotide with a methyl group at position C2 (Fig. 1.2). This modification was first reported in 1972 at position A37 in *E. coli* tRNAs such as $tRNA_{ACG}$, $tRNA_{GUC}$, $tRNA_{UUC}$, and $tRNA_{GUG}$ (Saneyoshi et al., 1972). In 1975, m^2A was also detected at A37 of $tRNA_{UUG}$ and $tRNA_{CUG}$ (Yaniv and Folk, 1975), though the enzyme responsible for this conserved modification remained unknown. Nearly two decades later, m^2A modification was discovered in position A2503 in the 23S rRNA of *E. coli* (Kowalak et al., 1995). Subsequent work by Mankin and colleagues identified RlmN, a methyltransferase responsible for the m^2A modification in position A2503 in 23S rRNA of *E. coli* (Toh et al., 2008). Four decades after the initial investigations on the modification at A37 on specific tRNAs, RlmN was reported to be a dual methyltransferase responsible for the addition of the m^2A modification in both tRNA and rRNA (Benítez-Páez et al., 2012). RlmN is a conserved methyltransferase across other bacteria (Pletnev et al., 2020). In *Enterococcus faecalis*, RlmN is described as a model for sensing reactive oxygen species (ROS) and influencing the proteome by regulating the m^2A modification in the rRNA and tRNA (Lee et al., 2023). Deletion of *rlmN* causes inefficient production of exogenous proteins (Pletnev et al., 2020), probably because it has an error-prone characteristic that increases the misreading of the stop codon, UAG (Benítez-Páez et al., 2012).

Primarily thought to be a bacteria-specific RNA modification, m^2A is also reported in the Plant kingdom, especially in the chloroplast rRNA and at position A37 in chloroplast and cytosolic tRNA (Duan et al., 2024). Particularly, in *Arabidopsis thaliana*, RlmN-like proteins such as RLMNL1, RLMNL2 and RLMN3 were identified, which are responsible for the addition of m^2A in chloroplast rRNA, chloroplast tRNA and cytosolic tRNA, respectively (Duan et al., 2024).

1.1.3 $m^{6,6}A$ modification

N^6, N^6-dimethyladenosine is modified adenosine nucleotide with two methyl groups at the N6 position (Fig. 1.2). This modification drew considerable attention in the early 1970s when it became apparent that, unlike previous mutations affecting ribosomal structure and functions — primarily found in ribosomal proteins, which led to antibiotic resistance or defects in ribosomal assembly — kasugamycin (ksg) resistance was caused by a change in methylation of 16S rRNA

(Helser et al., 1971). Ksg sensitivity is due to the presence of $m^{6,6}A$ modification at positions A1518 and A1519 (referred to as KsgA locus) and methylated by KsgA (also known as RsmA) methyltransferase (Helser et al., 1972, 1971). Later, it was reported that lack of modification at position A1519 is essential to confer ksg resistance in *E. coli* and dimethylation of the adjacent adenosine nucleotides is independent of each other (Vila-Sanjurjo et al., 1999). RsmA is especially important for cell growth at low temperatures and pre-rRNA processing (Connolly et al., 2008) — to segregate immature 30S subunits from mature ones for forming a complete 70S free ribosome to participate in translation (Xu et al., 2008). Deletion of RsmA causes a decreased ability to synthesize exogenous proteins and an increase of 17S rRNA precursors at 20°C (Pletnev et al., 2020).

RsmA is a highly conserved methyltransferase, present in all three domains of life (Pletnev et al., 2020). In archaea and eukaryotes, the enzyme is termed as Dim1 and is required for pre-ribosomal processing and ribosome biogenesis (Zorbas et al., 2015; Lafontaine et al., 1995). In *A. thaliana*, Dim1 is essential for root epidermal patterning and growth (Wieckowski and Schiefelbein, 2012) as well as the development of chloroplast at low temperatures (Tokuhisa et al., 1998).

1.2 m^6A modification in Eukaryotes

N^6-methyladenosine (m^6A) is a modified adenosine nucleotide with a methyl group at position N6 (Fig. 1.2). It is the most abundant, predominant and conserved internal modification of eukaryotic RNA, especially the mRNA (Jiang et al., 2021). In the early 1970s, chromatography first revealed the presence of m^6A modification in human and mouse mRNA (Desrosiers et al., 1974; Perry and Kelley, 1974). However, it was the development of m^6A-methylated RNA immunoprecipitation sequencing (m^6A-meRIP-seq), combining antibodies specific to m^6A with next-generation high throughput sequencing, that enabled transcriptome-wide mapping of the m^6A positions (Dominissini et al., 2012; Meyer et al., 2012). This breakthrough led the way to further advancement in m^6A mapping technologies which assisted in unmasking the fundamental role of m^6A in the regulation of gene expression in eukaryotes. A conserved m^6A motif DRACH (D = G or A or U, R = G or A, A = m^6A-modified A, H = A or U or C) was established using the m^6A-meRIP-seq (Linder et al., 2015; Dominissini et al., 2012; Meyer et al., 2012) in agreement with previously reported biochemical studies (Harper et al., 1990; Narayan et al., 1994; Rottman et al.,

1994). In the last ten years, several studies have shown that m^{6}A modification can influence 1) physiological behaviours such as neurodevelopment, learning and memory; 2) immunoregulation such as T-cell homeostasis and inflammatory response; 3) diseases such as cancer, neuronal disorders, autoimmune diseases, osteoporosis, metabolic diseases and viral infection (Chen et al., 2024; Jiang et al., 2021; Luo et al., 2021; Shan et al., 2024; Xu et al., 2021; Yang et al., 2020; Zhang et al., 2020; Zhou et al., 2020).

1.2.1 Mammalian m^{6}A modification machinery

The first component of an evolutionary conserved methyltransferase complex, methyltransferase-like 3 (METTL3), was discovered and characterised in 1997 (Bokar et al., 1997). In 2014, METTL3 was reported to form a complex with methyltransferase-like 14 (METTL14) and Wilms tumor 1 (WT1) – associated protein (WTAP) to add m^{6}A modification on mRNA (Ping et al., 2014) (Fig. 1.3). There are four more evolutionary conserved methyltransferases, also called as "writers" that can methylate adenines at the N6 position of different types of eukaryotic RNA (Sendinc and Shi, 2023) — methyltransferase-like 16 (METTL16) (Pendleton et al., 2017; Warda et al., 2017), methyltransferase-like 5 (METTL5) (Tran et al., 2019), phosphorylated CTD interacting factor 1 (PCIF1) (Sendinc et al., 2019) and CCHC zinc-finger containing protein (ZCCHC4) (Ma et al., 2019).

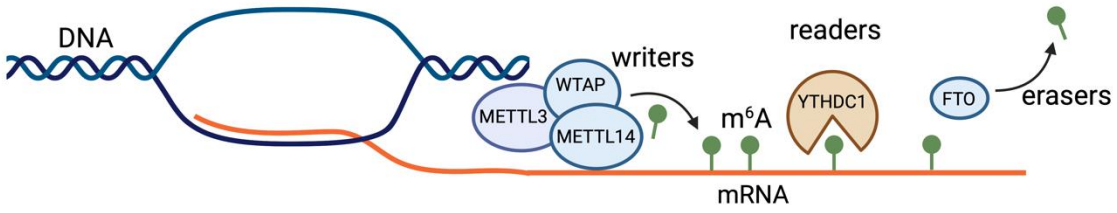

Figure 1.3 Machinery for the addition, removal and recognition of m^{6}A modification in the mammalian mRNA. Methyltransferase-like 3 (METTL3), methyltransferase-like 14 (METTL14), Wilms tumor 1-associated protein (WTAP), YT521-B homology domain containing 1 (YTHDC1) and fat mass- and obesity-associated protein (FTO). Figure was generated using Biorender.com.

The discovery of fat mass- and obesity-associated protein (FTO) and alpha-ketoglutarate dependent dioxygenase (AlkB) homolog 5 (ALKBH5) as demethylases (or "erasers") for m^6A mRNA methylation (Fig. 1.3) brought to light that m^6A modification is a highly dynamic and reversible process (Jia et al., 2011; Zheng et al., 2013). The ability of writers and erasers to add and remove methyl groups, respectively, highlights the complexity and specificity with which these enzymes modulate mRNA metabolism and function. The discovery and characterisation of m^6A-reader proteins (or "readers") that recognise and bind to m^6A-modified mRNAs (Fig. 1.3) provided significant insights into the m^6A-mediated post-transcriptional regulation of genes. YT521-B homology (YTH) domain-containing reader proteins such as YTH domain family 1-3 (YTHDF1-3) and YTH domain containing 1-2 (YTHDC1-2) are an important class of m^6A-reader proteins (Shi et al., 2019). The conserved carboxy-terminal YTH domain is well-characterized for its ability to recognize and bind m^6A methylation (Dominissini et al., 2012; Schwartz et al., 2013). Other classes of readers include eukaryotic initiation factor 3 (eIF3), fragile X mental retardation 1 (FMR1) insulin-like growth factor 2 mRNA-binding proteins 1-3 (IGF2BP1-3), leucine-rich pentatricopeptide repeat-containing (LRPPRC) and heterogeneous nuclear ribonucleoproteins (HNRNPs) (Shi et al., 2020, 2019). HNRNPC/G and HNRNPA2B1 recognize RNA binding motifs (RBM) due to the m^6A switch, the process in which the presence of m^6A modification in the mRNA can alter the local mRNA structure exposing RBMs (Liu et al., 2015). The systematic understanding of the molecular machinery that modulates m^6A modification has significantly enhanced our current knowledge of gene expression regulation by this post-transcriptional modification.

1.2.2 m^6A modification and viral epitranscriptome

The first evidence of m^6A modification in viral transcripts was identified in the simian vacuolating 40 (SV40) virus (Canaani et al., 1979; Lavi and Shatkin, 1975), inspiring a cascade of similar findings in other viruses. This domino effect led to the discovery of m^6A modification in viral transcripts of adenovirus (Hashimoto and Green, 1976; Moss and Koczot, 1976), influenza A virus (IAV) (Krug et al., 1976; Narayan et al., 1987), avian sarcoma virus (Stoltzfus and Dimock, 1976), Rous sarcoma virus (Beemon and Keith, 1977; Kane and Beemon, 1985) and herpes simplex virus type 1 (Moss et al., 1977). These discoveries came to a natural halt due to technological limitations

of that time, which hindered further exploration into the role of m^6A modification in viral infections. However, recent advancements in m^6A mapping technologies (Chen et al., 2015; Dominissini et al., 2012; Meyer et al., 2012) and liquid chromatography-mass spectrometry with tandem mass spectrometry (LC-MS/MS) techniques for detecting and quantifying overall m^6A levels (Fu et al., 2015; Jia et al., 2011), have reignited interest to study the molecular mechanism of m^6A modification and its role in cellular and viral transcripts. For example, three independent groups showed that m^6A modification positively regulates human immunodeficiency virus-1 (HIV-1) infection (Kennedy et al., 2016; Lichinchi et al., 2016a; Tirumuru et al., 2016). Lichinchi et al., 2016a reported that depletion of METTL3/METTL14 (or "m^6A writers") decreased HIV-1 replication while depletion of ALKBH5 (or "m^6A erasers") increased HIV-1 replication. Additionally, the HIV-1 genome was also reported to have m^6A modifications (Kennedy et al., 2016; Tirumuru et al., 2016), especially in the 3′untranslated region (UTR) that promoted viral gene expression by recruiting YTHDF (or "m^6A readers") (Kennedy et al., 2016). Around the same time, m^6A modification was also identified as a conserved regulatory marker across the RNA genomes of the *Flaviviridae* family such as Zika virus (ZIKV), dengue virus (DENV), West Nile virus, yellow fever virus and hepatitis C virus (HCV) (Gokhale et al., 2016). Interestingly, m^6A modification has an anti-viral role during HCV and ZIKV infection as it negatively modulates HCV particle production (Gokhale et al., 2016) and ZIKV viral RNA abundance (Lichinchi et al., 2016b). In contrast, m^6A modification plays a pro-viral role during IAV and SV40 infection as overexpression of m^6A reader protein YTHDF2 enhances IAV replication (Courtney et al., 2017) and inactivation of m^6A residues on late viral transcripts resulted in delayed replication of SV40 (Tsai et al., 2018). In summary, m^6A modification can have pro- or anti-viral functions (Horner and Reaves, 2024; Zhang et al., 2023; Baquero-Perez et al., 2021; Manners et al., 2019), which can be elucidated by modulating the main components of the m^6A modification machinery through overexpression or depletion of writers, erasers and readers. Moreover, targeted alterations of DRACH motifs in the host or viral mRNA to eliminate certain m^6A residues provide an additional strategy to understand the role of this modification, thereby offering potential targets for antiviral interventions.

1.3 m^6A modification in Prokaryotes

M^6A modification was first found in bacterial rRNA, the most abundant of all RNA (Hayashi et al., 1966; Starr and Fefferman, 1964; Littlefield and Dunn, 1958), followed by in valine-specific tRNA (Saneyoshi et al., 1969). Quite recently, m^6A modification was also reported in bacterial mRNA (Deng et al., 2015). They experimentally demonstrated that the mRNA of Gram-negative bacteria has higher m^6A/A ratios than Gram-positive bacteria (Deng et al., 2015). Moreover, they report that most of the m^6A-modified transcripts are associated with respiration, amino acid metabolism, stress response and small RNAs (Deng et al., 2015).

1.3.1 Prokaryotic m^6A modification machinery

Although m^6A modification is reported to occur in most types of bacterial RNA– the enzymes responsible for catalysing this modification have been identified only in rRNA and tRNA. In *E. coli*, a single m^6A modification occurs at position A37 in the valine-specific tRNA, catalysed by methyltransferase TrmM (Golovina et al., 2009). Additionally, *E. coli* has two m^6A modification sites at position A1618 and A2030 of the 23S rRNA which are catalysed by methyltransferases, RlmF and RlmJ, respectively (Golovina et al., 2012; Sergiev et al., 2007). TrmM, RlmF and RlmJ belong to the family of Rossman fold methyltransferases (Sergiev et al., 2016, 2007), with RlmJ displaying an additional helical subdomain (Punekar et al., 2013). While the structure of RlmF remains unresolved, it has been reported as a structural homolog of METTL16, m^6A-methyltransferase for eukaryotic mRNA (Breger et al., 2023). RlmJ is widely conserved throughout the phylum Proteobacteria while RlmF is primarily confined to the class *Gammaproteobacteria* (Pletnev et al., 2020). Single deletions of either *rlmF* or *rlmJ* do not disrupt ribosomal assembly or affect the growth rate of *E. coli*; however, they do result in reduced production of exogenous proteins (Pletnev et al., 2020). In addition, deletion of *rlmJ* is associated with an increased growth rate of *E. coli* in an anaerobic environment (Golovina et al., 2012).

Although most studies on RlmF and RlmJ have been conducted in *E. coli*, these proteins are also well conserved in the marine bacterium *Vibrio campbellii* BAA-1116, which serves as a model organism for quorum sensing. Recent studies from our group utilised LC-MS/MS to quantify m^6A content in tRNA-depleted mRNA and rRNA samples of wild type *V. campbellii* and *E. coli*. We

found that the m^6A/A ratio in *V. campbellii* was approximately 0.2 % (Saikia et al., 2024), while in *E. coli*, the ratio is approximately 0.15 % (Riquelme-Barrios et al., 2024) (Fig. 1.4). The double knockout of genes *rlmF* and *rlmJ* in *E. coli* and *V. campbellii* resulted in a decrease of at least 95 % in m^6A levels of the tRNA-depleted mRNA and rRNA samples (Riquelme-Barrios et al., 2024; Saikia et al., 2024) (Fig. 1.4). These m^6A-depleted mutants are used in this thesis to examine the role of m^6A modification in bacteriophage infection, given the well-established role of m^6A in regulating viral infection in eukaryotic cells (Refer to section 1.2.2).

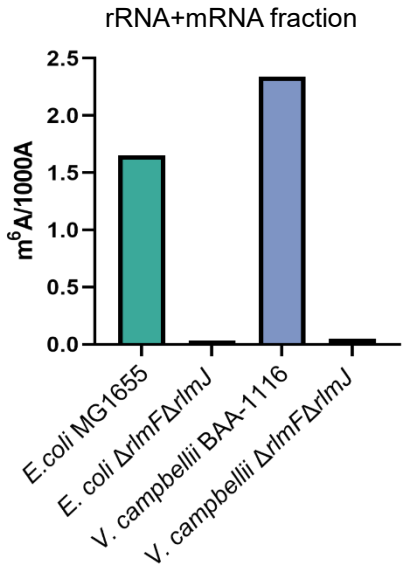

Figure 1.4 Presence of m^6A modification in *E. coli* and *V. campbellii*. Quantitative analysis of m^6A to 1000A of isolated rRNA and mRNA fraction from wild type *E. coli* and *V. campbellii* and their double knockout *rlmF* and *rlmJ* mutants. Figure is adapted from Riquelme-Barrios et al., 2024; Saikia et al., 2024.

1.4 Bacteriophages

In 1915, Frederick William Twort noticed contaminating bacterial cultures with mysterious clear spots while trying to propagate the Vaccinia virus (Twort, 1915). Out of the three possible hypotheses discussed by him for this unusual phenomenon, one stood out – the novel "ultra-microscopic virus". Around the same time, Félix Hubert d'Herelle also independently published

similar findings wherein he noticed an invisible antagonist against bacteria grown in agar that could pass through a Chamberland filter and enthusiastically labelled them as “bacteriophages” (d’Hérelle, 1917). The term bacteriophage originates from the English word bacterium and the Greek term phagein, meaning to devour or to eat, perfectly describing the role of bacteriophages as an obligate intracellular parasite of bacteria. Bacteriophages (or phages) are acellular entities that use archaea and bacteria as hosts to replicate and propagate. Through their parasitic life cycle, phages play a crucial role in shaping microbial ecosystems and influencing the dynamics of bacterial evolution, virulence and community structure(Salmond and Fineran, 2015; Batinovic et al., 2019). They are ubiquitous and among the most abundant biological entities, prevalent in all ecosystems rich in bacteria, including soils, aquatic environments and the human microbiome (Batinovic et al., 2019).

1.4.1 Bacteriophage diversity and lifestyle

Felix d’Herelle, one of the original co-discoverers of phages, devoted the remainder of his career to their study, marking the beginning of a golden period of phage research and the subsequent birth of molecular biology. This period not only witnessed the discovery of phages with diverse nucleic acid types in their genomes but also benefited from the emergence of the electron microscope (EM), which enabled detailed study of their shape, size and structure (Ackermann, 2009). Phages with double-stranded DNA (dsDNA), single-stranded DNA (ssDNA), double-stranded RNA (dsRNA) or single-stranded RNA (ssRNA) were the initial form of classification along with capsid shapes such as filamentous, icosahedral or pleomorphic (Ackermann, 2009). In addition to icosahedral capsids, these phages exhibited tail diversities such as long contractile tails, long non-contractile tails, short tails or no tails at all. Moreover, the recent availability of phage genomic sequences reveals that their genomes vary in size from 3.4 kilobases (kb) to almost 500 kb and the lack of an omnipresent gene found in all phages contributes to their remarkable complexity (Keen, 2015; Ackermann, 2009). Each phage genome is a distinct blend of shared elements that have evolved over billions of years, representing a melting pot of unknown genes and proteins in the biosphere (Keen, 2015). This continually expanding genomic and morphological diversity of phages necessitates ongoing revision to their taxonomy and classification, prompting Hans-W. Ackermann to describe this process as “as much an art as a science.” (Ackermann, 2009). In the

present times, the International Committee on Taxonomy of Viruses (ICTV) is given the task of developing a uniform and universal taxonomy for all eukaryotic and prokaryotic viruses.

Given their ubiquity and diversity, it is unsurprising that phages exhibit a range of life cycles from the well-known lytic and lysogenic cycles to the less common but eminent pseudo-lysogeny and chronic cycles (Fig. 1.5 A-D). All life cycles begin with the attachment or adsorption of the phages to their specific receptors in the bacterial cell wall, followed by the injection of their genomic material (DNA or RNA) or fusion and uncoating of the capsid to release the genomic material into the host cell. In the lytic cycle, the phage hijacks the host's machinery to produce new phage particles and ruptures the host to release its progeny virions, thereby allowing further cycles of infection (Fig. 1.5 A) (Orlova, 2012). In contrast, the lysogenic cycle involves the integration of the phage DNA into the host genome, where it remains dormant across many bacterial generations (now called prophage) until triggered by stress, at which point it may enter the lytic phase (Fig. 1.5 B) (Lwoff, 1953). In addition, free phages have been found in lysogenic bacteria in the absence of stress (or any inducing agent) which supports the idea of spontaneous prophage induction (Carrolo et al., 2010; Lwoff, 1953). The pseudo-lysogeny cycle is usually maintained when nutrients and bacterial hosts are limited (Fig. 1.5 C). Hence, the phage genomic material acts inactive and silently resides in the host (Mäntynen et al., 2021; Naureen et al., 2020). The chronic cycle (also called the carrier phase) is a stable, long-term infection of the phages to the bacterial hosts wherein the phage progenies are continuously budding off the cells or are asymmetrically passed to daughter cells without any immediate lysis (Fig. 1.5 D) (Mäntynen et al., 2021; Naureen et al., 2020). Pseudo-lysogeny and chronic cycles are unique and exciting life cycles, however, this thesis will primarily focus on the two common life cycles – lytic and lysogenic.

1.4.1.1 Obligate lytic phages

Phages that cannot undergo lysogeny and are released from a lysed-infected cell are obligately lytic. Since the early 1940s, a special series of seven such obligately lytic DNA phage types have been used as model systems upon which fundamentals of molecular biology are built. These phages, known collectively as the T-series or T-phages, include types T1, T2, T3, T4, T5, T6 and T7, where "T" denotes types (Demerec and Fano, 1945). Research on these T-phages has contributed significantly to the birth of molecular biology and genetics, including DNA as the

genetic material and its replication mechanisms, gene expression and transcription, and phage-host interactions, in addition to the genetic code underlying protein synthesis (Ofir and Sorek, 2018).

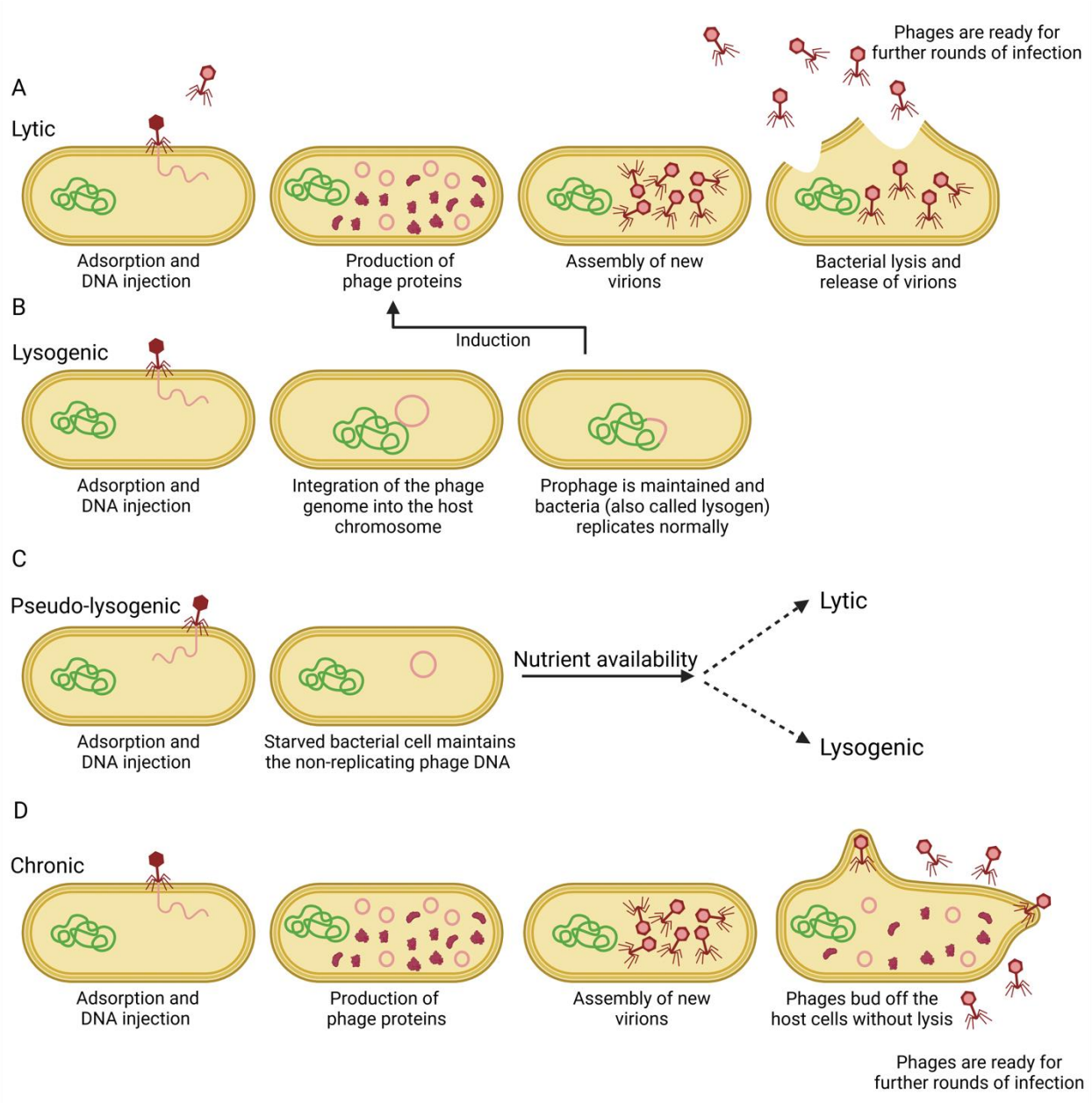

Figure 1.5 Different phage lifecycles reported in bacterial hosts. The production of new virions is shown via lytic cycle (A), lysogenic cycle (B), pseudo-lysogenic cycle (C) and chronic cycle (D). Figure was generated in Biorender.com.

T2, T4 and T6 are often referred to as T-even series (Abedon, 2000) as they are quite similar in morphology and genetics — contain 5-hydroxymethyl cytosine (instead of cytosine) in their approximately 165 kbp dsDNA (Subedi and Barr, 2021; Kutter and Wiberu, 1968) and have a characteristic contractile tail. T1, T3, T5 and T7 (T-odd series) have simple noncontractile tails and contain the usual four nucleotides in their dsDNA (Subedi and Barr, 2021). However, T1, T3 and T7 are clustered together due to a relatively similar genome size of approximately 43 kb. T5 phage is different from the other T-phages.

1.4.1.1.1 T5 and T5-like phages

According to Demerec and Fano, phage T5 was isolated from a mixture of phages supplied by Dr. Tony Rakieten from the Long Island College of Medicine in 1945. Morphologically, it has a long, flexible, noncontractile tail and an icosahedral head with a genome of about 121,300 base pairs (bp) with terminal repeats of about 8.4 % of the total genome length (Rhoades, 1982). The left terminal repeats are essential as part of the first step transfer (FST) of T5 DNA injection, wherein about 8 % of the whole genome is injected into the host, followed by the second step transfer (SST) which corresponds to the remaining 92 % of the genome (Lanni, 1968). The FST controls two phage-induced functions – degradation of host DNA and transfer of the rest of the T5 genome (Lanni, 1968). The host DNA is degraded within the first few minutes of FST which leads to the production of free nucleotides that are eliminated from the host (Warner et al., 1975). It is interesting that the phage T5 does not recycle the free host nucleotides but instead synthesises its own nucleotides from scratch, a process that is both energy-intensive and time-consuming (Warner et al., 1975). Additionally, the T5 genome contains nicks in 3`to 5`strand and is insensitive to several restriction enzymes (Davison, 2015; Davison and Brunel, 1979a, 1979b).

FhuA, an outer membrane protein that transports ferrichrome, a type of siderophore that binds to iron to make it accessible to *E. coli* is also the receptor for phage T5 (Heller and Schwarz, 1985). However, most of the T5-like phages use BtuB as a receptor, an outer membrane protein responsible for the transport of cobalamin (vitamin B_{12}) (Heller and Schwarz, 1985; Maffei et al., 2021). According to ICTV, T5 and T5-like phages are classified within the *Demereciviridae* family. A recent study introduced sixty-eight new obligate lytic phages, including nine new T5-like phages that could infect *E. coli*, (Maffei et al., 2021) which have now been deposited in the Deutsche

Sammlung von Mikroorganismen und Zellkulturen GmbH (DSMZ – German Collection of Microorganisms and Cell Cultures). These nine T5-like phages are from the Bacteriophage Selection for your Laboratory (BASEL) collection and use BtuB as the receptor (Maffei et al., 2021).

1.4.1.1.2 MS2 and Qβ phages

The first report on phages containing RNA as a genetic material was in 1961 when Loeb and Zinder discovered phage f2, which can only infect *E. coli* strains containing the fertility factor (F-plasmid, F+) (Loeb and Zinder, 1961). Soon after, several RNA phages were identified, including MS2 (Strauss and Sinsheimer, 1963; Davis et al., 1961a) and Qβ (Nonoyama et al., 1963). According to ICTV, both phages belong to family *Leviviridae*, with MS2 in genera *Levivirus* and Qβ in genera *Allolevivirus* (Callanan et al., 2020; Olsthoorn and van Duin, 2011). MS2, the first biological entity to have its complete genome sequenced, has a small ssRNA genome of size 3569 nucleotides which contains four genes encoding proteins for maturation, coat, lysis and replicase enzyme (Fiers et al., 1976). Qβ has a relatively larger ssRNA genome as compared to MS2, with 4220 nucleotides which have three open reading frames that encode four proteins for maturation-lysis (A2), major coat, minor coat (A1), and replicase enzyme (Mekler, 1981; Meyer et al., 1981). They both contain icosahedral shells with one copy of their positive sense ssRNA genome and infect their hosts via F-pili (Olsthoorn and van Duin, 2011; Overby et al., 1966a, 1966b). The ssRNA genomes of RNA phages have a unique secondary structure that plays role in its overall replication cycle (Olsthoorn and van Duin, 2011). Maturation protein is bound to the ssRNA of the phage and recognises the host by interacting with the F-pili, thereby initiating entry into the host through a combination of collision and pili retraction (Gorzelnik and Zhang, 2021; Meng et al., 2019; Callanan et al., 2018; Clarke et al., 2008). However, the maturation protein of Qβ has a dual functionality – which includes ssRNA genome entry into the host as well as the ability to lyse the host once Qβ replication is successful and fully-formed virions are produced (Mekler, 1981; Meyer et al., 1981; Olsthoorn and van Duin, 2011). The replicase enzyme coded by the ssRNA phages, is one of the four subunits that make up the replicase holoenzyme. The other three subunits are ribosomal protein (RP) S1 and translational elongation factors EF-Tu and EF-Ts that are recruited by the phage to assist in RNA synthesis and translation (Takeshita and Tomita, 2010; Wahba et al., 1974;

Blumenthal et al., 1972). MS2 and Qβ are heavily dependent on their host translational machinery to complete their virulent replication.

1.4.1.2 Temperate phages

Phages that can undergo lysogeny, wherein their genetic material gets integrated into the host chromosome are called temperate phages (Lwoff, 1953). The bacteria then become a lysogen as the phage genome becomes a prophage (Fig. 1.5 B). At some point, the prophage gets excised from the chromosome under stress conditions (or spontaneity) which initiates the lytic life cycle of the temperate phage. Thus, temperate phages have the ability to choose between the lytic and lysogenic life cycles and this decision-making process was first studied in λ phage (Jacob and Wollman, 1953; Lederberg and Lederberg, 1953; Weigle, 1953). Phage λ was discovered by Esther Lederberg in 1951 at the University of Wisconsin (Lederberg, 1951), a finding that led to extensive studies on λ phage and contributed to the foundation of genetics and molecular biology.

Prophages can have a big impact on the lifestyle and virulence of the bacterial hosts, the lysogens, by encoding factors that can enhance pathogenicity and adaptation (Wendling et al., 2021; Fortier and Sekulovic, 2013; Brüssow et al., 2004; Casjens, 2003). Some of the greatest examples include pathogenic bacteria such as *Corynebacterium diphtheriae*, *Clostridium botulinum* and *E. coli* O157:H7 that derive their pathogenicity from their respective prophages that encode the toxin (Brüssow et al., 2004). Prophage acquisition also increases bacterial fitness and their evolution through horizontal gene transfer (HGT) of beneficial genes such as antibiotic resistance (Wendling et al., 2021). Our research group has identified ten putative prophage regions in the chromosomes of *V. campbellii* using the bioinformatic tool PHAST (Fig. 1.6) (Lorenz et al., 2016). Among these, four regions were classified as putative intact prophage regions – ΦHAP-1-like, VfO4K68-like, VfO3K6-like and *Vibrio* kappa-like (Lorenz et al., 2016). Notably, ΦHAP-1-like and *Vibrio* kappa-like prophages are induced into their lytic cycle in response to oxidative or heat stress as evidenced by transmission EM (TEM) analysis (Lorenz et al., 2016), highlighting their potential role in environmental adaption.

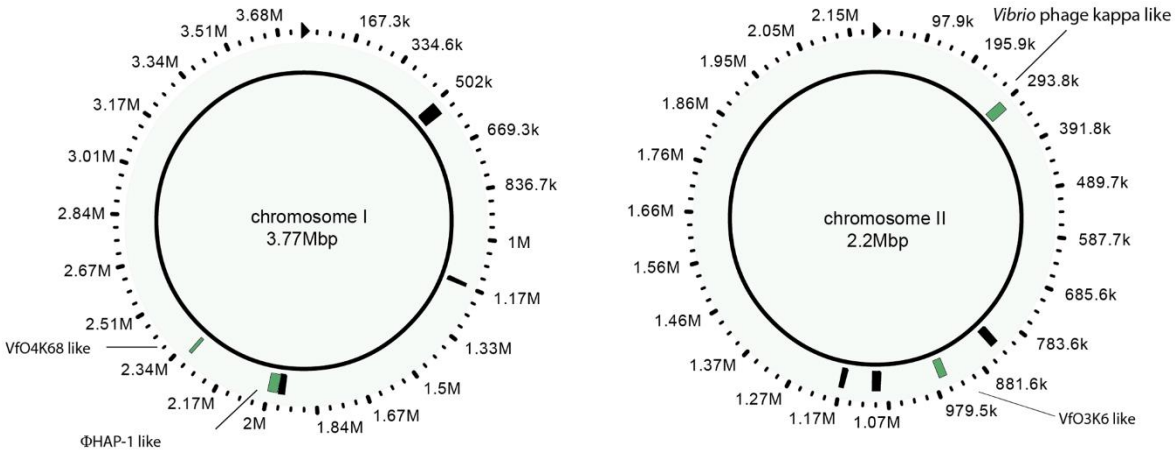

Figure 1.6 Chromosome I and II of *V. campbellii* contain putative prophage regions. Five potential prophages are identified across both chromosomes. Intact prophage regions are highlighted in green, while incomplete prophages are marked in black. Figure adapted from Lorenz et al., 2016.

Most of the putative prophages identified in *V. campbellii* are incomplete or cryptic, marked in black in Fig. 1.6. Evolution and genome rearrangements may cause a prophage to be imprisoned into the host chromosome, rendering it unable to enter a lytic cycle. These dormant prophage remnants are referred to as incomplete or cryptic prophages and they support their host to survive hostile conditions such as antibiotics, acid fluctuations, osmotic and oxidative stress, in addition to influencing biofilm formation (Wang et al., 2010). For instance, the *E. coli* K-12 genome contains nine cryptic prophage elements from CP4-6, DLP12, e14, Rac, Qin, CP4-44, CSP-53, CPZ-55 and CP4-57 that account for 3.6 % of its genome (Wang et al., 2010).

1.4.2 RNA modifications in phages

Recent studies have begun to shed light on the potential regulatory roles of RNA modifications in phage-bacteria dynamics. For example, Phage T4 encodes three adenosine diphosphate (ADP)-ribosyltransferase enzymes – Alt, ModA and ModB that could modify over thirty host proteins, including *E. coli* RNA polymerase (RNAP) for a successful takeover of *E. coli* transcriptional and translational machinery (Depping et al., 2005; Tiemann et al., 2004; Koch et al., 1995; Goff, 1974). ADP-ribosyltransferase is an enzyme that catalyses the transfer of ADP-ribose from nicotinamide

adenine dinucleotide (NAD^+) onto target proteins or nucleic acids in a process called ADP-ribosylation (Groslambert et al., 2021; Kim et al., 2020). Until recently, ModB was only reported to utilise NAD^+ as a substrate, however, a new study now identified NAD-capped RNA as an additional substrate for ModB (Wolfram-Schauerte et al., 2023). This study describes the installation of RNA chains by ModB onto the specific host translational proteins through a process called RNAylation (Wolfram-Schauerte et al., 2023). Ribosomal proteins rS1 and rL2 are RNAylated at their RNA-binding regions, suggesting a coordinated shutdown of host gene expression by inactivating specific host ribosomes (Wolfram-Schauerte et al., 2023). Additionally, the inactivation of ModB causes delayed host cell lysis and reduced burst size of phage T4, highlighting its importance in efficient T4 infection (Wolfram-Schauerte et al., 2023).

Complementary to this, another study has identified a unique RNA modification mechanism as part of a bacterial defence system against phage infection. They report the first internal mRNA modification of phage transcripts by a chaperone-mediated defence toxin-antitoxin chaperone (CmdTAC) system (Mets et al., 2024; Vassallo et al., 2024). The addition of ADP-ribose at the N6 position of adenine in GA dinucleotides in phage mRNAs blocks the translation of phage proteins (Vassallo et al., 2024). This system operates in a competitive binding manner, whereby the major capsid protein of the phage outcompetes the antitoxin CmdA for interaction with CmdC, thus allowing the free toxin CmdT to initiate this targeted modification (Vassallo et al., 2024).

Such studies not only broaden our understanding of the molecular mechanisms of phage-host interactions but also generate keen interest in investigating the phage epitranscriptome during bacterial infection. Thus, this thesis aims to contribute to the growing field of exploring RNA modification during phage replication in bacteria.

1.5 Scope of the thesis

The aim of this thesis is to investigate the role of rRNA modifications in bacteria and their influences on phage replication, with a particular focus on phage–host dynamics. To conduct this investigation, two model bacteria, *V. campbellii* and *E. coli*, are employed.

In *V. campbellii*, the study primarily examines the induction of lysogenic phages and the infection dynamics of the lytic phage Virtus using both wild-type and m^6A-RNA depleted mutant bacterial

strains. In *E. coli*, the impact of m^6A depletion is screened on a more diverse range of lytic phages, with particular emphasis on the T5 phage. The phenotype is validated and further characterised at a range of scales, from whole-population to single-cell resolution, using classical methodologies. T5 Phage–host interactions are also assessed, focusing on different stages of infection, including phage adsorption to the host, intracellular replication and the subsequent production of progeny phage particles.

To delve deeper into the molecular mechanisms of T5 phage–host interactions, a dual proteomic analysis is conducted. This approach is designed to reveal global changes in phage and host protein levels, enabling the identification of differentially regulated biological pathways during infection in both wild-type and m^6A-RNA depleted bacteria. This is complemented by studies of ribosome composition and transcript abundance to determine the impacts of m^6A modification on phage gene expression.

Additionally, this thesis examines the presence of RNA modifications in RNA phages such as MS2 and Qβ using LC-MS/MS analysis, followed by genetic knockout studies to understand their influences on phage–host interactions.

2 Materials and methods

Some parts are cited from the publication: Bibakhya Saikia, Sebastian Riquelme-Barrios, Thomas Carell, Sophie Brameyer and Kirsten Jung. 2024. Depletion of m^6A-RNA in *Escherichia coli* reduces the infectious potential of T5 bacteriophage. Microbiology Spectrum, 12 (12), e0112424. Doi: 10.1128/spectrum.01124-24.

2.1 Preparation of culture media

Table 1: Different culture media and their components used in the study

Culture media	Components
Lysogeny broth (LB)	10g/L tryptone, 5g/L yeast extract, 10g/L sodium chloride
Double strength (ds) LB	20g/L tryptone, 10g/L yeast extract, 20g/L sodium chloride
LM	10g/L tryptone, 5g/L yeast extract, 20g/L sodium chloride
M9 salt solution (10x)	75.2 g/L disodium hydrogen phosphate, 30 g/L potassium dihydrogen phosphate, 5 g/L sodium chloride, 5 g/L ammonium chloride
Trace elements solution (100x)	5 g/L ethylenediaminetetraacetic acid (EDTA), 0.8 g/L ferric chloride hexahydrate, 84 mg/L zinc chloride, 13 mg/L cupric chloride dihydrate, 10 mg/L cobalt chloride dihydrate, 10 mg/L boric acid and 1.6 mg/L manganese dichloride tetrahydrate
M9 media	1x M9 salt solution, 0.4 (w/v) % glucose, 1 mM magnesium sulphate, 0.3 mM calcium chloride, 1µg biotin, 1 µg thiamine and 1x trace elements solutions
Nutrient broth (NB)	5 g/L peptone, 3 g/L meat extract (N7519, Sigma-Aldrich, St. Louis, MO, USA)
NZYCM broth	1g/L casamino acids, 0.98g/L magnesium sulphate, 5g/L sodium chloride, 10g/L tryptone, 5g/L yeast extract (N3643, Sigma-Aldrich, St. Louis, MO, USA)

All the culture media mentioned in Table 1 were prepared with vollentsalztes (VE; distilled) water and sterilized by autoclaving. Agar plates (or base agar plates) were prepared by supplementing

the medium with 1.5 % (w/v) agar before autoclaving. Top agar (also called soft agar) was prepared by supplementing the medium with 0.7 % (w/v) agar before autoclaving. Freshly prepared top agar was used for all plaque assays. Trace elements solution (100x) was sterilised by 0.22 µM filter.

2.2 Strains, plasmids and oligonucleotides

The bacterial strains, bacteriophage strains and plasmids used in this study are listed in Table 2. Oligonucleotide sequences used for cloning and polymerase chain reaction (PCR) are listed in Table 3. Primers used for quantitative PCR (qPCR) are listed in Table 4.

Table 2: Bacterial strains, bacteriophages and plasmids used in this study

Strain	**Genotype**	**Reference/Source**
V. campbellii ATCC BAA-1116	*V. campbellii* wild type	(Lin et al., 2010)
V. campbellii Δ*rlmF*Δ*rlmJ*	Deletion of *rlmJ* and *rlmF* in *V. campbellii*	(Saikia et al., 2024)
V. campbellii Δ*rlmF*Δ*rlmJ* +	Insertion of *rlmJ* in *V. campbellii* Δ*rlmF*Δ*rlmJ*	This work
V. campbellii ΔΔ-compl.	Insertion of *rlmF* in the *glmS* region of *V. campbellii* Δ*rlmF*Δ*rlmJ*+	This work
V. harveyi VH2	GenBank: LGYS00000000	(Castillo et al., 2015)
E. coli WM3064	*thrB*1004 *pro thi rpsL hsdS lacZ*ΔM15 RP4-1360 Δ(*araBAD*)567 Δ*dapA*1341::[*erm pir*]	W. Metcalf, Univ. of Illinois, Urbana
E. coli BL21 (DE3)	F⁻ *ompT gal dcm lon* $hsdS_B$ (r_B^- m_B^-) λ(DE3)	(Studier and Moffatt, 1986)
E. coli DH5αλpir	*endA1 hsdR17 glnV44* (= *supE44*) *thi-1 recA1 gyrA96*	(Macinga et al., 1995)

	relA1 φ80d*lac*Δ(*lacZ*)M15 Δ(*lacZYA-argF*)U169 *zdg*-232::Tn10 *uidA*::*pir+*	
E. coli MG1655	K-12 F^- λ^- *ilvG*$^-$ *rfb-50 rph-1*	(Blattner et al., 1997)
E. coli MG1655 Δ*rlmF*Δ*rlmJ*	Deletion of *rlmJ* and *rlmF* in *E. coli* MG1655	(Riquelme-Barrios et al., 2024)
E. coli MG1655 ΔΔ-compl.	Insertion of *rlmF* and *rlmJ* in *E. coli* Δ*rlmF*Δ*rlmJ*	(Riquelme-Barrios et al., 2024)
E. coli MG1655 P_{flu}-*mNeonGreen*	Integration of P_{flu}-*mNeonGreen* at the native locus in *E. coli* MG1655	(Brameyer, 2024, unpublished)
E. coli MG1655 Δ*rlmF*Δ*rlmJ* P_{flu}-*mNeonGreen*	Integration of P_{flu}-*mNeonGreen* at the native locus in *E. coli* MG1655 Δ*rlmF*Δ*rlmJ*	(Brameyer, 2024, unpublished)
E. coli BW25113	K-12 F^- λ^- *rrnB3* Δ*lacZ4787 hsdR514* Δ(*araBAD*)*567* Δ(*rhaBAD*)*568 rph-1*	(Baba et al., 2006)
E. coli BW25113 Δ*rlmL*	Deletion of *rlmL* in *E. coli* BW25113	(Baba et al., 2006)
E. coli BW25113 Δ*rlmN*	Deletion of *rlmN* in *E. coli* BW25113	(Baba et al., 2006)
E. coli BW25113 Δ*rsmA*	Deletion of *rsmA* in *E. coli* BW25113	(Baba et al., 2006)
E. coli BW25113 Δ*rsmG*	Deletion of *rsmG* in *E. coli* BW25113	(Baba et al., 2006)
E. coli BW25113 Δ*trmB*	Deletion of *trmB* in *E. coli* BW25113	(Baba et al., 2006)

E. coli B	K-12 F^{-} *lon dcm malB*; NCBI Taxonomy ID: 37762; DSM 613	(Daegelen et al., 2009)
E. coli LE392	*Hsd*R514(rk- mk+) *gln*V(supE44) *tryT (*supF58), *lacY1* or Δ(*lacIZY)6, galK2, galT22, metB1, trpR55*; DSM 4230	(Murray et al., 1977)
E. coli Hfr 3000	Hfr (PO1) *relA1 spoT1 thi-1*; DSM 5210	(Loomis Jr. and Magasanik, 1967)
E. coli W1485	F+ *glnV42* (AS) met^{-} *λ*$^{-}$ *rpoS396* (Am) *rph-1*; DSM 5695	(Lederberg and Lederberg, 1953)
Bacteriophage strain	**Identifier**	**Source**
Virtus phage	GenBank: OK381870	(Droubogiannis and Katharios, 2022)
T3 phage	DSM 4621; GenBank: NC_047864.1	(Demerec and Fano, 1945)
T4 phage	DSM 4505; GenBank: AF158101.6	(Demerec and Fano, 1945)
T5 phage	DSM 16353; GenBank: AY543070.1	(Demerec and Fano, 1945)
T6 phage	DSM 4622; GenBank: MH550421.1	(Demerec and Fano, 1945)
T7 phage	DSM 4623; GenBank: NC_001604.1	(Demerec and Fano, 1945)
λ phage	DSM 4499; GenBank: J02459.1	(Lederberg and Lederberg, 1953)
vB_EcoS_GreteKellenberger	Bas26	(Maffei et al., 2021)
vB_EcoS_TrudiGerster	Bas27	(Maffei et al., 2021)

vB_EcoS_IrmaTschudi	Bas28	(Maffei et al., 2021)
vB_EcoS_SuperGirl	Bas29	(Maffei et al., 2021)
vB_EcoS_TrudiRoth	Bas30	(Maffei et al., 2021)
vB_EcoS_DaisyDussoix	Bas31	(Maffei et al., 2021)
vB_EcoS_IrisVonRoten	Bas32	(Maffei et al., 2021)
vB_EcoS_HildyBeyerler	Bas33	(Maffei et al., 2021)
vB_EcoS_SelmaRatti	Bas34	(Maffei et al., 2021)
MS2 phage	ATCC 15597; GenBank: V00642.1	(Davis et al., 1961)
Qβ phage	DSM 13768, GenBank: NC_001890.1	(Watanabe et al., 1967)
Plasmid	**Genotype**	**Reference**
pNTPS138-R6KT	*mobRP4*$^{+}$ *ori*-R6K *sacB*; suicide plasmid for in-frame deletions, Km^R	(Lassak et al., 2010)
pNPTS138-R6KT-KI-*rlmJ*	pNPTS-138-R6KT-derived suicide plasmid for insertion of *rlmJ* in *V. campbellii* Δ*rlmF*Δ*rlmJ*, Km^R	This work
pNPTS138-R6KT-*glmS*flank-*rlmF*-KI	pNPTS-138-R6KT-derived suicide plasmid for insertion of *rlmF* in the *glmS* region in *V. campbellii* Δ*rlmF*Δ*rlmJ* +, Km^R	This work
pET28a	Expression vector, Km^R	Novagen
pET28a-*V05027*	N-terminal 6His-tagged *VIBHAR_05027*, under the control of the T7 promoter, Km^R	This work

pET28a-*V01983*	N-terminal 6His-tagged *VIBHAR_01983*, under the control of the T7 promoter, Km^R	This work
F-plasmid	Conjugative plasmid, *oriT* *oriV* and *tra* operon	(Lederberg et al., 1952)

Table 3: Oligonucleotide sequences used for cloning and PCR in this study. Most primers are designed using *V. campbellii* ATCC BAA-1116 as a reference genome (NC_022269.1 and NC_022270.1).

Name	**Sequence**
*rlmJ*_FL_up_fwd	5‘-ctggcgccaagcttctctgcaggatctggtccagcttgggtttgcgttg-3‘
*rlmJ*_FL_down_rev	5‘-agctagcgaattcgtggatccagatgaagaacttggtttcaccagacag-3‘
pNPTS_*glmS*_Fwd	5´- ctggcgccaagcttctctgcaggatgccgcagcaaatcaacgcagcgctg-3´
*glmS_rlmF*_Rev	5´- gactttcatcttaggtttctcaaaaaagcgaagtcatgtgacttcg-3´
*rlmF_glmS*_Fwd	5´- gtaattatttagagaaagctatacccgtatatctactgacattgttatcttgttatac-3´
*glmS*_pNPTS_Rev	5´- gctagcgaattcgtggatccagatcatcaacgaaaccgagatcattgag-3´
*glmS_rlmF*_Fwd	5´-cgaagtcacatgacttcgctttttgagaaacctaagatgaaagtc-3´
*rlmF_glmS*_Rev	5´- gtataacaagataacaatgtcagtagatatacgggtatagctttctctaaataattac-3´
M13_rev	5‘-caggaaacagctatgacc-3‘
M13_uni	5‘-tgtaaaacgacggccagt-3‘
*rlmJ*_check_F	5‘-gaccaaatgcggctcaagc-3‘
*rlmJ*_check_R	5‘-gctttgacgatggcagcacg-3‘
*rlmF*_check_F	5‘-gtgggcatttgtctttgac-3‘
*rlmF*_check_R	5‘-caattgaccaatcttggcg-3‘
VC_*glmS*_check_F	5´- gccttcacgactcagctctc-3´
VC_*glmS*_check_R	5´- cgagacactttacaaccaac-3´
V05027-EcoRI-fwd	5´-tagccgaattcatgcttaatgccgtatcgactc-3´
V05027-Xhol-rev	5´-tagccctcgagttacccctcgcagattcaacaacg-3´

V01983-EcoRI-fwd	5´-tagccgaattcatgcctgataattacaccactcg-3`
V01983-Xhol-rev	5´-tagccctcgagttaaccgactttgacgacaacaa-3´
pET28a_check_F	5´-aagtggcgagcccgatcttcc-3´
pET28a_check_R	5´-gatatagttcctcctttcagc-3´
traI-F	5´-accacgacaccagtcgc-3´
traI-R	5´-ggtcagcagcgataatctg -3´

Table 4: Primers used for qPCR in this study. They were designed by using either *E. coli* MG1655 (U00096.3) or T5 phage (AY543070.1) as the reference genome.

Primer pair	**Sequences**	**Size (bp)**	**Primer efficiency**	**Description**
rpoA.F1 *rpoA*.R1	5´-tgactgcagccgatatcacc-3´ 5´-ccgcgctgaactttgatacg-3´	118	2.02	Amplify *E. coli* MG1655 rpoA, RNA polymerase subunit α
flu.F3 *flu*.R3	5´-tcacgataacaatggcggta-3´ 5´-gacataccggcaacctctgt-3´	111	1.91	Amplify *E. coli* MG1655 flu, self recognizing antigen 43 (Ag43) autotransporter
yeeR.F4 *yeeR*.R4	5´-ttcaccgtcactgatgtggt-3´ 5´-gttgagcaccggttgttctt-3´	145	1.98	Amplify *E. coli* MG1655 yeeR, inner membrane protein
lys.F2 *lys*.R2	5´-attagccaccgttaagcccg-3´ 5´-tgctactgtacgaataccttgca-3´	100	1.93	Amplify phage T5 endolysin or lysozyme
C1.F1 *C1*.R1	5´-cttttctcaaacgggtgcgg-3´ 5´-gctttatcggccaagtcagc-3´	129	1.94	Amplify phage T5 holin
N4.F1 *N4*.R1	5´-gccggtgatgcagctactat-3´ 5´-acaccagagccgtctttagc-3´	104	2.04	Amplify phage T5 major tail protein
T5.150.F2 *T5.150*.R2	5´-atcatcgtcgtccaatcggt-3´ 5´-aagatagccgggtcagaact-3´	100	1.94	Amplify phage T5 putative prohead protease
orf3.R1.1 *orf3*.F2	5´-tgcagaatacgaatgctatcaca-3´ 5´-accgtgtacgttcgcctaaa-3´	107	1.93	Amplify phage T5 tail assembly protein
T5.025.F1 *T5.025*.R1	5´-gcagatgaaggagtgggaga-3´ 5´-ctgaggtttctccagccaaa-3´	122	1.99	Amplify phage T5 capsid and scaffold protein

2.3 Plasmid and bacterial strain construction

Molecular methods were carried out according to the manufacturers' instructions. Chromosomal DNA isolation, plasmid isolation and PCR product clean-up kits were purchased from Süd-Laborbedarf Gauting (SLG) (Gauting, Germany). Enzymes and HiFi DNA Assembly Master Mix were purchased from New England BioLabs (Ipswich, MA, USA).

Complementation of the *rlmF* and *rlmJ* deletion in *V. campbellii* Δ*rlmF*Δ*rlmJ* was achieved using suicide vectors introduced into the strain using conjugative mating and selecting for clones after successful double homologous recombination (Brameyer et al., 2020).

To complement *rlmJ,* suicide plasmid pNPTS138-R6KT-*rlmJ*-KI was constructed. Briefly, *rlmJ* and 600-bp upstream and downstream flanking regions were amplified by PCR using genomic DNA from *V. campbellii* as a template and the primers *rlmJ*_FL_up_fwd and *rlmJ*_FL_down_rev. After purification, the 2030-bp long PCR fragment was cloned by Gibson assembly (Gibson et al., 2009) into the suicide plasmid pNPTS138-R6KT, which was first linearised by digestion with EcoRV. The correct plasmids were verified by colony PCR and sequencing using primers M13_rev and M13_uni.

Construction of the suicide plasmid pNPTS138-R6KT-*glmS*flank-*rlmF*-KI was slightly different due to the presence of transposable elements in the vicinity of the gene. Briefly, the regions surrounding *glmS* and *rlmF* (600 bp upstream and 24 bp downstream) were amplified to generate the suicide plasmid pNPTS138-R6KT-*glmS*flank-*rlmF* using *V. campbellii* genomic DNA as a template. Primer pairs used for amplification of *glmS* overhang fragments were pNPTS_*glmS*_Fwd and *glmS_rlmF*_Rev (upstream of *rlmF*) and *rlmF*_glmS_Fwd and *glmS*_pNPTS_Rev (downstream from *rlmF*). The primers *glmS_rlmF*_Fwd and *rlmF*_glmS_Rev were used to amplify *rlmF*. These DNA fragments were assembled via Gibson assembly (Gibson et al., 2009) into the pNPTS138-R6KT plasmid linearised with EcoRV. The plasmid was verified by colony PCR and sequencing using primers M13_rev and M13_uni.

The suicide plasmid pNPTS138-R6KT-*rlmJ*-KI was next introduced into *V. campbellii* Δ*rlmF*Δ*rlmJ* by conjugative mating using *E. coli* WM3064 as a donor in LB medium containing diaminopimelic acid (DAP) as previously described (Schwarz et al., 2023). Briefly, single-crossover integration mutants were selected on LM plates that contained kanamycin but lacked

DAP. Single colonies were grown for two days without antibiotics and plated on LB containing 10 % (w/v) sucrose to select for plasmid excision. Kanamycin-sensitive colonies were checked for gene insertion by colony PCR using primers bracketing the insertion sites. Insertion of *rlmJ* was verified by colony PCR and sequencing using the primers *rlmJ*_check_F and *rlmJ*_check_R.

Next, *rlmF* was added via the introduction of suicide plasmid pNPTS138-R6KT-*glmS*flank-*rlmF*-KI to *V. campbellii* Δ*rlmF*Δ*rlmJ*+ by conjugative mating with *E. coli* WM3064 as described above. Insertion of *rlmF* in the *glmS* region of *V. campbellii* was verified by colony PCR and sequencing using the primers VC_*glmS*_check_F and VC_*glmS*_check_R.

To generate plasmids encoding N-terminal 6His-tagged versions of major capsid proteins from *Vibrio* kappa-like prophage and ΦHAP-1-like prophage (*VIBHAR_05027* and *VIBHAR_01983,* respectively), *V. campbellii* genomic DNA was used as a template with primers *V05027*-EcoRI-fwd and *V05027*-Xhol-rev (*VIBHAR_05027*) or *V01983*-EcoRI-fwd and *V01983*-Xhol-rev (*VIBHAR_01983*). These two genes were cloned into the pET-28a vector using EcoRI and XhoI as restriction sites; the presence of the correct insert was confirmed by colony PCR and sequencing using primers pET28a_check_F and pET28a_check_R.

To generate an F+ strain of *E. coli*, F-plasmid from *E. coli* W1485 was introduced into an F– strain of interest through conjugation. Equal volume of exponentially grown strains was mixed and spotted on an LB plate with overnight incubation at 37 ºC. The spot was transferred into 1 mL of LB, washed and streaked out on an LB plate to obtain single clones. The clones were then patched on M9 medium with and without 50 µM L-methionine, followed by overnight incubation. *E. coli* W1485 is methionine auxotroph, which refers to its inability to synthesize methionine required for its growth. PCR was performed for the *traI* gene in the F-plasmid using primers *traI*-F and *traI*-R for clones grown in M9 without 50 µM L-methionine. PCR confirmed clones were infected with phage MS2 and Qβ to further confirm the introduction of F-plasmid.

2.4 Overproduction and purification of recombinant phage capsid proteins

The expression vectors, pET28a-*V05027* and pET28a-*V01983* were transformed into *E. coli* BL21 (DE 3) for overexpression of the major capsid proteins of *Vibrio* kappa-like prophage and ΦHAP-1-like prophage respectively. The cells were cultivated in LB supplemented with kanamycin (50

mg/mL) at 37 °C to an optical density at 600 nm (OD_{600}) of 0.5. Isopropyl-β-D-1-thiogalactopyranoside (IPTG) (0.5 mM) was added to the culture to induce *VIBHAR_05027* or *VIBHAR_01983* expression at 37 °C for 2.5 h. Cells were harvested (5000 × *g*, 20 min, 4 °C), resuspended, and disrupted with a high-pressure cell disrupter (Constant Systems Limited, Daventry, UK) in ice-cold disruption buffer (50 mM Tris-HCl [pH 7.5], 10 % [v/v] glycerol, 10 mM magnesium chloride, 1 mM dithiothreitol, 0.5 mM phenylmethylsulfonyl fluoride [PMSF], 3 mg DNase and 100 mM sodium chloride). Cell debris and intact cells were eliminated by centrifugation (5000 × *g*, 20 min, 4 °C) and the pellet was solubilized in 6 M urea and 10 mM Tris-HCl (pH 7.5) overnight with shaking at 4 °C. Any precipitates or insolubilized aggregates were removed by ultracentrifugation (20, 000 × *g*, 15 min, 4 °C) and the supernatant was loaded onto a nickel-nitrilotriacetic acid (Ni-NTA) column (Qiagen, Hilden, Germany). After a wash step (6 M urea, 10 mM Tris-HCl [pH 7.5] and 40 mM imidazole), the recombinant protein was eluted with elution buffer (6 M Urea, 10 mM Tris-HCl [pH 7.5] and 200 mM imidazole).

2.5 Protein determination using Bradford's method

Bradford's method for protein estimation was used as described (Bradford, 1976). Briefly, series of known concentrations of bovine serum albumin (BSA) standards (from 0.2 mg/mL to 1 mg/mL) or diluted proteins of interest were added to 1 mL of Bradford reagent (0.01 % [w/v] Coomassie Brilliant Blue G-250, 4.7 % [w/v] ethanol and 8.5 % [w/v] phosphoric acid). The mixture was incubated for 5 min, followed by absorbance measurement at 595 nm. Standard curve was prepared using the known concentrations of BSA to find out the unknown concentration of proteins of interest.

2.6 Generation of polyclonal antibodies against recombinant phage capsid proteins

Customized polyclonal rabbit antibodies against 6His-VIBHAR_05027 and 6His-VIBHAR_01983 were obtained from Kaneka Eurogentec (Seraing, Belgium). Heterologously produced and purified 6His-VIBHAR_05027 or 6His-VIBHAR_01983 were used as antigens in a Speedy 28-day Immunization Program with two rabbits per antigen as hosts. The specificity of the

polyclonal antibodies against 6His-VIBHAR_05027 and 6His-VIBHAR_01983 was verified by western blot analysis as described below.

2.7 Sodium dodecyl sulphate-polyacrylamide gel electrophoresis (SDS-PAGE) and western blot analysis of 6His-VIBHAR_05027 and 6His-VIBHAR_01983

SDS-PAGE. Stacking gels consisted of 4 % (w/v) acrylamide (in 50 mM Tris [pH 6.8]) and resolving gels of 12.5 % (w/v) acrylamide (in 300 mM Tris [pH 8.8]) and were run in a Tris-glycine buffer (25 mM Tris, 192 mM glycine, 0.1 % [w/v] SDS [pH 8.3]). Gels were stained overnight in Coomassie staining solution (0.25 % [w/v] Coomassie Brilliant Blue R-250, 9.2 % [v/v] concentrated acetic acid and 45.4 % [v/v] ethanol) and de-stained in de-staining solution (10 % [v/v] acetic acid and 40 % [v/v] ethanol).

Western blot analysis. Proteins were transferred to a nitrocellulose membrane using the Trans-Blot Turbo Transfer System (Bio-Rad, Hercules, CA, USA), then blocked with 5 % (w/v) milk powder prepared in Tris-buffered saline (TBS) (pH 7.6) containing 0.1 % (v/v) Tween-20 (TBST) for 1 h at room temperature. 6His-VIBHAR_05027 and 6His-VIBHAR_01983 were detected by incubating the membrane in TBST with primary polyclonal antibodies (Kaneka Eurogentec, Seraing, Belgium) or primary monoclonal antibodies against the 6His-tag (Thermo Fisher Scientific, Waltham, MA, USA). Membranes were then incubated with the alkaline phosphatase-conjugated goat anti-rabbit IgG (Thermo Fisher Scientific, Waltham, MA, USA) and developed using substrate solution (50 mM sodium carbonate buffer [pH 9.5], 0.1 % (w/v) Nitro-blue tetrazolium and 5 mg/mL 5-Bromo-4-chloro-3-indolylphosphate). PageRuler Prestained Protein ladder (10-180 kDa) (Thermo Fisher Scientific, Waltham, MA, USA) was used as a size standard ladder.

2.8 Phage induction assays

Wild type, Δ*rlmF*Δ*rlmJ* mutant and complemented mutant (ΔΔ-compl.) *V. campbellii* were exposed to stress conditions to assess the impact of m^6A-RNA modification on prophage induction. Bacterial strains grown in LM medium to an OD_{600} of 0.4 were exposed to either oxidative stress (by the addition of 1 µg/ml mitomycin C), heat stress (45 °C), or neither (control). After 30 min of

oxidative stress, mitomycin C was removed from the sample by centrifugation (5000 × *g*, 10 min, 4 °C) and the pellet was resuspended in a fresh, pre-warmed LM medium. After 30 min of heat stress, samples were shifted to 30 °C. Following 2 h of incubation at their physiological conditions, the supernatant containing the phage particles was harvested (5000 × *g*, 15 min, 4 °C), passed through a 0.22 µm filter Millipore Steriflip Vaccum filter (MilliporeSigma, Burlington, MA, USA) and stored at 4 °C.

2.9 Indirect enzyme-linked immunosorbent assay (ELISA)

Indirect ELISA was performed following previously described protocols (Andreolla et al., 2018; Lu et al., 2014) with slight modifications for the detection of major capsid proteins from the *Vibrio* kappa-like and ΦHAP-1-like prophages from *V. campbellii*. Briefly, 96 well F-bottom, polystyrene, chimney well, black, medium binding microplates (Greiner Bio-One GmbH, Kremsmünster, Austria) were coated with 100 µl of supernatant (derived from phage induction assays as described above) and 0.05 M carbonate buffer (pH 9.6) then incubated overnight at 4 °C. After washing three times with TBST, the plate was blocked with 200 µl of 5 % (w/v) milk powder prepared in TBST for 1 h at 30 °C. Following three washes with TBST, 100 µl of VIBHAR_05027- or VIBHAR_01983-positive serum in 5 % (w/v) milk powder with TBST was added to each well and the plate was incubated for 1 h at 30 °C. After three washes with TBST, 100 µl of alkaline phosphatase-conjugated goat anti-rabbit IgG (Thermo Fisher Scientific, Waltham, MA, USA) diluted in 5 % (w/v) milk powder in TBST was added to each well, followed by 1 h incubation at 30 °C and five washing steps with TBST. Subsequently, 100 µl of para-nitrophenyl phosphate (pNPP) substrate (Thermo Fisher Scientific, Waltham, MA, USA) was added to every well and incubated for 30 min in the dark. Last, 50 µl of 2N sodium hydroxide was added to each well to stop the reaction. Absorbance was measured immediately at 405 nm in a NanoQuant Infinite M200PRO plate reader (Tecan, Männedorf, Switzerland). All samples were analysed in technical duplicates.

Primary and secondary antibodies were optimised before indirect ELISA assays were performed with samples from the phage induction assays. Additionally, standard curves prepared using purified major capsid proteins with 6His-tag were included in every ELISA run to estimate the concentration of major capsid proteins in the sample.

2.10 Plaque assay and phage propagation

Plaque assay was performed using the double agar overlay method as described previously (Kropinski et al., 2009). Briefly, 100 µl of exponential-phase bacterial culture was mixed with 100 µl of diluted phages in top agar and poured onto a solid base agar medium. The total number of plaques formed was counted after an overnight incubation and the plaque-forming units (PFU) were determined.

To achieve high titer phage stocks, phages were propagated using the plate overlay method as described (Fortier and Moineau, 2009) with certain modifications. Briefly, top agar plates were prepared to cultivate nearly confluent plaques of each phage, followed by an overlay of 5-7 mL SM buffer (5.8 g/L sodium chloride, 2 g/L magnesium sulphate, 50 mL 1M Tris-Cl [pH 7.5] and 2 % [w/v] gelatin) and gentle shaking (40 rpm, 4 h). The suspension was then carefully pipetted off along with the top agar and centrifuged (5000 × *g*, 20 min, 4 °C). The supernatant was passed through a 0.22 µm filter Millipore Steriflip Vaccum filter (MilliporeSigma, Burlington, MA, USA) and stored at 4 °C.

The propagation host used for Virtus phage was *V. harveyi* VH2; λ phage was *E. coli* LE392 (DSM 4230); all T-phages and T5-like phages were *E. coli* B strain (DSM 613); MS2 phage was *E. coli* W1485 (DSM 5695) and Qβ phage was *E. coli* Hfr3000 (DSM 1520).

2.11 Selective enrichment of phages against *V. campbellii*

Selective enrichment of phages from seawater samples (Naples Sea and Red Sea) on *V. campbellii* as the host was carried out using a modified protocol described by Twest and Kropinski, 2009. Briefly, aqueous samples were centrifuged (5000 × *g*, 20 min, 4 °C), filtered using a 0.22 µm filter Millipore Steriflip Vaccum filter (MilliporeSigma, Burlington, MA, USA) and stored at 4° C with chloroform. Each sample was mixed with an equal volume of dsLB with 2 mM calcium chloride and 0.1 mL of an overnight culture of *V. campbellii*, followed by incubation at 30° C with gentle mixing (50 rpm). After 24 hours of incubation, the mixture was centrifuged (5000 × *g*, 20 min, 4 °C), filtered and stored at 4°C with chloroform. The phage lysate was then tested using spot assay. Briefly, 10 µl of the phage lysate was spotted on a lawn of *V. campbellii* in LB with 2 mM calcium

chloride plate and incubated at 30 °C for 24 hours. Plaque assay as described above was then employed to eliminate abortive infection. Further phage purification was performed by picking individual plaques with a sterile toothpick and propagated it at least 3 times.

Selective enrichment of phages from Codfish was processed as previously described (Echeverría-Vega et al., 2019). Briefly, 50 mL of sterile artificial seawater (23.2 g/L sodium chloride, 1.5 g/L potassium chloride, 3.84 g/L calcium chloride, 24.6 g/L magnesium sulphate heptahydrate) was mixed with 100 g of ground Codfish and centrifuged (5000 × *g*, 60 min, 4 °C), followed by sequential filtration using 5.0 µm, 0.45 µm and 0.22 µm filters (MilliporeSigma, Burlington, MA, USA) and stored at 4°C with chloroform. The supernatant was then processed for selective enrichment of phages and testing using spot assay with *V. campbellii* as a host as described above.

2.12 Efficiency of plaquing (EOP)

EOP was used to assess the relative infectivity or lytic efficacy of phage on different bacterial hosts. This was achieved by performing the plaque assay, wherein the phage lysate was tested against both the mutant bacterial strain and its corresponding wild-type strain. It was calculated as the ratio of the average PFU produced by the phage on a test strain (e.g., deletion strain) to the average PFU produced on a control strain (e.g., wild-type strain), expressed as a percentage (Kutter, 2009). The EOP of the wild-type strain was normalized to 100 %.

For Virtus phage, EOP was calculated as the percentage of the average PFU in Δ*rlmF*Δ*rlmJ* mutant compared to the wild-type *V. campbellii*.

For λ, T-phages and T5-like phages, EOP was calculated as the percentage of the average PFU in Δ*rlmF*Δ*rlmJ* mutant compared to the wild-type *E. coli* MG1655.

EOP was determined for phage T5, MS2 and Qβ using bacterial cultures in both the exponential phase (OD_{600} of 0.5) and the stationary phase (overnight cultures). It was calculated as the percentage of the average PFU in Δ*rlmF*Δ*rlmJ* mutant (or complemented, ΔΔ-compl. mutant) compared to the wild-type *E. coli* MG1655. Additionally, for phage MS2 and Qβ, EOP was calculated as the percentage of the average PFU in the single deletion mutant (e.g., Δ*rsmA* or Δ*rlmN* or *rlmL* or *rsmG* or *trmB*) compared to the wild-type *E. coli* BW25113.

2.13 Liquid infection assays

Exponential phase wild-type and Δ*rlmF*Δ*rlmJ* mutant *E. coli* MG1655 (~10^8 colony forming units [CFU]/mL) grown in NB (N7519, Sigma-Aldrich, St. Louis, MO, USA) were infected with T5 phage at a multiplicity of infection (MOI) of 10, 1, 0.1 or 0.01 to monitor phage–host dynamics in liquid culture based on growth. The mixture was added to 96-well plates (150 µl per well) and the OD_{600} was measured every 10 min using a NanoQuant Infinite M200PRO plate reader (Tecan, Männedorf, Switzerland) at 37 °C with continuous shaking.

Exponential phase *E. coli* BW25113 wild-type and its single deletion mutants from the Keio collection were grown in NZYCM (N3643, Sigma-Aldrich, St. Louis, MO, USA) and were infected with MS2 at an MOI of 2 or 0.2. These mixtures were then added to 96-well plates (150 µl per well) and the OD_{600} was measured every 10 min using a NanoQuant Infinite M200PRO plate reader (Tecan, Männedorf, Switzerland) at 37 °C with continuous shaking.

T5 phage was propagated on exponential phase wild-type and Δ*rlmF*Δ*rlmJ* mutant *E. coli* MG1655 at an MOI of 0.1 to assess the production of defective phage by the mutant. The infected cultures were sampled via centrifugation (5000 × *g*, 5 min, 4 °C) after 24 hours of shaking incubation at 37 °C. The supernatant containing the free phages was tittered by plaque assay on *E. coli* wild-type MG1655.

2.14 Synchronized infection assay

Synchronized infection experiments were performed as previously described (Brandão et al., 2021; Melo et al., 2022). Briefly, exponential phase wild type and Δ*rlmF*Δ*rlmJ* mutant *E. coli* MG1655 (~10^8 CFU/mL) were grown in NB (N7519, Sigma-Aldrich, St. Louis, MO, USA) and infected with T5 phage at a MOI of 10. Samples were collected at 0 min and 5 min after infection and immediately plated for CFU enumeration. Three biologically independent infection experiments showing a CFU reduction of at least 95 % within 5 min of infection were considered to show synchronized infection.

2.15 Time-lapse microscopy

A modified protocol from that of (Mandal et al., 2021) was used to demonstrate T5 phage-mediated bacterial lysis using time-lapse phase-contrast microscopy. Briefly, exponential phase wild-type and Δ*rlmF*Δ*rlmJ* mutant *E. coli* MG1655 (~10^8 CFU/mL) were grown in NB (N7519, Sigma-Aldrich, St. Louis, MO, USA) and infected with T5 phage at a MOI of 10 (or an equal volume of phage diluent as a control). After initial adsorption at 37 °C with shaking for 10 min, 2 µl of cells were spotted on pads of nutrient media (N7519, Sigma-Aldrich, St. Louis, MO, USA) solidified with 1 % (w/v) agarose, placed onto microscopic slides and covered with a coverslip. Subsequently, images were taken on a Leica DMi8 inverted microscope equipped with a Leica DFC365 FX camera (Wetzlar, Germany). Microscopic phase-contrast images were captured every two min in several positions for 3 h with a constant temperature of 37 °C using an incubator (PeCon, Erbach, Germany) around the DMi8 microscope. To set the focus plane, automatic autofocus was performed at every position and every time point using the adaptive focus control (AFC) and closed-loop focus system of the DMi8 microscope. To quantify non-lysed cells, phase-contrast images were analysed using the plugin MicrobeJ (Ducret et al., 2016) in ImageJ (Schneider et al., 2012). The default MicrobeJ settings were used for cell segmentation (Fit shape, rod-shaped bacteria) apart from the following settings: area: 1-max µm; length: 2.5–20 µm; width: 0.4–2 µm; curvature 0.0–0.15, angularity 0.0–0.25 and intensity 0.0–2000. Microscopy image analysis was performed from a total of 2,080 wild-type and 1,923 Δ*rlmF*Δ*rlmJ* mutant *E. coli* cells.

2.16 Fluorescence Microscopy

To assess the activity of *flu* promotor in *E. coli* wild-type and Δ*rlmF*Δ*rlmJ* mutant, transcriptional fusions with mNeonGreen were constructed. *E. coli* MG1655 P_{flu}-*mNeonGreen* and *E. coli* Δ*rlmF*Δ*rlmJ* P_{flu}-*mNeonGreen* were grown to an OD_{600} of 1.0 and were spotted onto phosphate buffer pads prepared with 1 % (w/v) agarose. Inoculated pads were placed onto microscopic slides, covered by coverslip and phase contrast and fluorescence images were captured on a Leica DMi8 inverted microscope equipped with a Leica DFC365 FX camera (Wetzlar, Germany). An excitation wavelength of 485 nm and a 510 nm emission filter with a 75 nm bandwidth were used for mNeonGreen fluorescence with an exposure of 500 ms, gain of 5 and 100 % intensity. In order to

calculate the relative fluorescence intensity (RF) associated with P_{flu}-*mNeonGreen* in individual cells, phase contrast and fluorescence images were analysed using the plugin MicrobeJ (Ducret et al., 2016) in ImageJ (Schneider et al., 2012). The default MicrobeJ settings were used for cell segmentation (Fit shape, rod-shaped bacteria) apart from the following settings: area: 1-max µm; length: 1.2–6 µm; width: 0.1–2 µm; curvature 0.0–0.15, angularity 0.0–0.25 and intensity 0.0–1800. Microscopy image analysis was performed for a minimum of 1,000 *E. coli* cells.

2.17 Adsorption assays

Adsorption assays were performed as previously described (Howard-Varona et al., 2018). Briefly, wild-type and Δ*rlmF*Δ*rlmJ* mutant *E. coli* MG1655 were grown in NB (N7519, Sigma-Aldrich, St. Louis, MO, USA) and infected with T5 phage at an MOI of 0.1. Free phages were sampled immediately post-infection (0 min), then every 5 min for 30 min using 0.22-µm sterile filtration. Plaque assays (Kropinski et al., 2009) were performed as described above to enumerate the free phage concentration.

2.18 One-step growth curve

One-step growth curves were performed as described previously (Brandão et al., 2021; Duarte et al., 2021). Briefly, exponential phase wild type and Δ*rlmF*Δ*rlmJ* mutant *E. coli* MG1655 (~10^8 CFU/mL) grown in NB (N7519, Sigma-Aldrich, St. Louis, MO, USA) were infected with T5 phage at an MOI of 0.001 and incubated at 37 °C with shaking for 10 min for initial adsorption. The remaining free phages were removed after the initial adsorption via centrifugation (5000 × *g*, 5 min, 4 °C) and the pellet was resuspended in fresh pre-warmed NB. Samples were incubated at 37 °C with shaking and collected (including t = 0) at 10-min intervals over 30 min, followed by 5-min intervals up to 105 min. Plaque assays (Kropinski et al., 2009) were performed as described above immediately after sample collection.

2.19 Production of phage MS2 and Qβ phage

Logarithmic phase *E. coli* W1485 (DSM 5695) and *E. coli* Hfr3000 (DSM 1520) grown in NZYCM (N3643, Sigma-Aldrich, St. Louis, MO, USA) and NB (N7519, Sigma-Aldrich, St.

Louis, MO, USA) supplemented with 0.8 % (w/v) sodium chloride were infected with MS2 and Qβ respectively at an MOI of 3.0. The MS2 phage propagation was during an overnight incubation while the Qβ phage propagation proceeded for 5 hours at 37 °C. After cell lysis, phage-containing supernatant was harvested via centrifugation (5000 × *g*, 30 min, 4 °C) to remove cell debris, followed by filtration using a 0.22 μm filter Millipore Steriflip Vaccum filter (MilliporeSigma, Burlington, MA, USA). Subsequently, polyethylene glycol 8000 (PEG8000; P2139, Sigma-Aldrich, St. Louis, MO, USA) was added to precipitate the phages, incubating the mixture for 2 hours for MS2 and overnight for Qβ at 4 °C. The precipitated phage particles were then subjected to ultracentrifugation (25,000 × *g*, 60 min, 4 °C) and resuspended in SM buffer (100 mM sodium chloride, 10 mM magnesium sulphate, 50 mM Tris-HCl [pH 7.5], 0.01 % [w/v] gelatin) for their genomic total RNA extractions.

2.20 Total RNA isolation

Total RNA was isolated using the phenol-chloroform-isoamyl alcohol (PCI) method as described (Riquelme-Barrios et al., 2024; Petrov et al., 2022; Sambrook and Russell, 2006). Briefly, a mixture of 1 % (v/v) phenol and 20 % (v/v) ethanol was added to bacterial cultures (or infected bacterial cultures) and immediately frozen in liquid nitrogen and stored at -80 °C freezer overnight. The next day, the samples were thawed, centrifuged (15,000 × *g*, 10 min, 4 °C) and resuspended in 500 μL of ice-cold 20 mM sodium acetate buffer (pH 5.2) with 1 mM EDTA. 500 μL of pre-warmed PCI and 25 μL of 10 % (w/v) SDS were added to the mixture, followed by incubation at 60 °C for 5 minutes at 1000 rpm. The samples were then cooled on ice for 30 minutes, followed by centrifugation (15,000 × *g*, 60 min, 4 °C) and transferring the top layer to phase-lock tubes (Phase Lock Gel, Quantabio, Beverly, MA, USA). An equal volume of PCI and 0.1 volume of 3 M sodium acetate (pH 5.2) were added to the phase-lock tubes and mixed well. The tubes were centrifuged (15,000 × *g*, 15 min, 4 °C) and the top layer was transferred into a fresh 2 mL RNA-free tube, followed by the addition of 3.0 volume of 100 % ethanol, mixed and incubated overnight at -80 °C freezer. The next day, the samples were centrifuged (15,000 × *g*, 20 min, 4 °C), washed with 70 % (v/v) ethanol, dried and resuspended in 100 μL of RNAse-free water. The samples were then treated with RNAse-free DNAse I (New England Biolabs, Ipswich, MA, USA) according to the manufacturer's instructions to remove DNA contaminants. The quality and integrity of RNA

were evaluated using chip gel electrophoresis on a 2100 Bioanalyzer with an RNA Nano chip kit from Agilent Technologies (Santa Clara, CA, USA). In addition, the RNA concentration was measured by using NanoDrop ND1000 (Peqlab, Erlangen, Germany) and its integrity was confirmed by determining the 260/280 and 260/230 ratios.

Genomic RNA extraction of MS2 and Qβ was also performed using the method described above with some modifications. Specifically, 1 volume pre-warmed PCI and 0.1 volume 10 % (w/v) SDS were directly added to the prepared phage lysate, followed by the steps described above. The quality and integrity of MS2 and Qβ RNA genomes were verified, followed by host ribosome depletion.

2.21 tRNA/rRNA removal

tRNA and rRNA depletion was carried out as described by (Riquelme-Barrios et al., 2024). Briefly, DNAse-free RNA samples were treated using the manufacturer's instructions for the RNA Clean and Concentrator Kit (Zymo Research, Irvine, CA, USA) to remove tRNAs. RNA integrity and elimination of tRNAs were validated using chip gel electrophoresis on a 2100 Bioanalyzer (Agilent Technologies, Santa Clara, CA, USA).

Subsequently, rRNA depletion was carried out for MS2 and Qβ RNA genome samples using the pan-riboPOOL rRNA Depletion Kit from siTOOLS (Planegg, Germany) following the manufacturer's protocols. The efficiency of rRNA depletion was evaluated using the 2100 Bioanalyzer (Agilent Technologies, Santa Clara, CA, USA) and reverse transcription qPCR (RT-qPCR) targeting the 23S and 16S rRNA as well as major coat protein markers for phage MS2 and Qβ. Ribosome depletion was quantified by comparing the ratio of 23S or 16S rRNA to major coat protein transcripts from phage MS2 or Qβ before and after the depletion process.

2.22 LC-MS/MS for RNA modification analysis

This work was done in collaboration with Prof. Dr. Stefanie Kaiser Group at Goethe University, Frankfurt. Members of Prof. Kaiser group performed LC-MS/MS analysis with the samples to detect and quantify modifications.

For accurate quantification of modified nucleosides in the RNA genome of phage MS2 and Qβ, absolute quantification analyses were performed using stable isotope labelled internal standards (SILIS) on an Agilent 1290 Infinity II ultrahigh-performance LC (ultra HPLC) series fitted with a diode-array detector combined with an Agilent 6470 triple quadrupole LC-MS system, electrospray ionization and Agilent jet stream as described (Barrios et al., 2024; Petrov et al., 2022; Borland et al., 2019). Briefly, an enzymatic mixture of benzonase, snake venom phosphodiesterase, and calf intestine phosphatase was used to digest RNA. The enzymatic mixture also contained tetrahydrouridin, butylated hydroxytoluene and pentostatin to safeguard the modifications. The improved gen $^{13}C/^{15}N$ SILIS from *Saccharomyces cerevisiae* tRNA was added to the digested RNA, followed by ribonucleoside separation using a Synergi Fusion-RP column, 2.5 µm particle size with 100 Å pore size at 35 °C column temperature and 0.35 mL/min flow rate (Phenomenex, Torrance, CA, USA).

The chromatography gradient began with 100 % buffer A (5 mM ammonium acetate, pH 5.3 adjusted with glacial acetic acid) for 1 min, followed by a gradual increase to 10 % buffer B (pure acetonitrile) over 4 mins and 40 % buffer B for 7 mins. Afterwards, the system was adjusted back to 100 % buffer A for the 2.5 mins. The MS was operated in dynamic multiple reaction monitoring mode with parameters such as positive ion, skimmer voltage 15 V, cell accelerator voltage 5 V, nitrogen gas -temperature 230 °C and flow 6 L/min, sheath gas - temperature 400 °C and flow 12 L/min, capillary voltage 2500 V, nozzle voltage, 0 V and nebulizer 40 psi.

Defined concentrations of ribonucleosides were used for calibration from ranges 0.05 pmol to 100 pmol for canonical nucleosides (A, U, G, C) and from 0.0025 pmol to 5 pmol for modified nucleosides. Data analysis was performed using Agilent's Quantitative Mass Hunter software.

2.23 Transcript quantification during T5 infection using RT-qPCR

To investigate the changes in transcript expression during T5 infection, exponential phase *E. coli* MG1655 and its Δ*rlmF*Δ*rlmJ* mutant were infected at an MOI of 10. 4 mL samples of the infected cells were collected at 0 (uninfected control), 5, 15, 25, 35 and 45 mins post-infection and immediately added to 16 mL of phenol-ethanol solution to stop the infection. The samples were then flash-frozen to preserve RNA integrity and were stored at -80 °C for total RNA extraction.

After RNA extraction, the samples were reverse transcribed using iScript™ Advanced cDNA Synthesis Kit (Bio-Rad, Hercules, CA, USA) following the manufacturer's protocols. Additionally, control reactions were maintained which lacked the reverse transcriptase enzyme (no RT) or lacked the template (no RNA). qPCR was used to evaluate the expression of certain host and phage transcripts as mentioned in Table 3. Primers were designed using Primer3 (Kõressaar et al., 2018; Untergasser et al., 2012; Koressaar and Remm, 2007) and their amplification efficiency was calculated using dilutions of T5 or *E. coli* MG1655 DNA genome (Table 3). Analysis of the relative expression of the transcripts was performed in technical duplicates using qPCR with CFX96™ Real-Time System with C1000 Touch™ Thermal Cycler (Bio-Rad, Hercules, CA, USA). Each well contained 4 µl of 1:100 dilution complementary DNA (cDNA) or no-RT control, 1 µl of 10 pmol of each primer and 5 µl of SsoAdvanced™ Universal SYBR® Green Supermix (Bio-Rad, Hercules, CA, USA). The substitution of nuclease-free water for cDNA templates served as a negative control. The amplification cycling parameters are an initial denaturation step at 95 °C for 30 s, followed by 40 cycles of oscillating between 95 °C for 10 s and 60 °C for 15 s. Additionally, melting curve analysis was also performed for each amplification reaction with a temperature gradient of 0.5 °C from 55 °C to 95 °C. The iCycler software identified a single fluorescence threshold corresponding to the exponential amplification in each target transcript in the samples. The threshold cycle (Ct) values were then used for further data analysis.

16S rRNA was used as an endogenous reference gene as it showed very small changes in expression levels across three biological replicates. The Pfaffl method was used to calculate the relative gene expression as it normalises the primer efficiencies of the target genes (Pfaffl, 2001).

2.24 Detection of m^6A modification in the 23S rRNA using rolling circle extension-assisted loop-mediated isothermal amplification (Rol-LAMP)

This work was done in collaboration with Leonardo Vásquez Camus from the AG Kirsten Jung at LMU. Mr. Camus performed the Rol-LAMP method with the samples.

Rol-LAMP method was employed to monitor changes in m^6A modifications of 23S rRNA during T5 phage infection as described (Li et al., 2023). RNA was extracted from samples infected with T5 and hybridised with padlock probes using a cooling gradient from 95 °C to 30 °C, followed by

the addition of Bst 2.0 DNA polymerase, SplintR, adenosine triphosphate (ATP) and deoxynucleotide triphosphates (dNTP). The mixture was incubated at 37 °C for 30 min, followed by 65°C for 10 min, and then stored at 4°C before proceeding with Rol-LAMP amplification. The ligated products were mixed with primers (forward inner primer [FIP], backward inner primer [BIP] and single loop primer [SLP], dNTPs, magnesium sulphate and isothermal amplification buffer (Tris-HCl, ammonium sulphate, potassium chloride, magnesium sulphate, Tween® 20 [pH 8.8], Bst 2.0 DNA polymerase and SYBR Green). Rol-LAMP amplification reactions were performed at 65 °C and fluorescence signals were measured every 30 seconds for 2 h.

2.25 Whole-cell proteomics

This work was done in collaboration with Dr. Ignasi Forné from the Protein analysis unit and Dr. Siobhan Cusack from AG Kirsten Jung at the LMU. Dr. Forné performed the LC-MS/MS analysis. Dr. Cusack performed the weighted gene co-expression network analysis (WGCNA) and generated the corresponding figures to illustrate the results from the analysis.

To investigate the changes in proteome abundance during T5 infection, exponential phase *E. coli* MG1655 and its Δ*rlmF*Δ*rlmJ* mutant were infected at an MOI of 10. 1 mL samples of the infected cells were collected at 0 (uninfected control), 15- and 35-mins post-infection, followed by centrifugation (15,000 × *g*, 2 min, 4 °C). The cell pellets were processed with an iST kit (Preomics, Planegg, Germany) as recommended by the manufacturer. The samples were resuspended to a final concentration of 1 μg/μL.

For LC-MS/MS analysis, desalted peptides were diluted to 0.1 μg/μL and 1 μL was injected into an UltiMate 3000 RSLCnano system (Thermo Fisher Scientific, Waltham, MA, USA). Peptide separation was carried out on a 25 cm analytical column (75 μm ID, 1.6 μm C18, Aurora-IonOpticks) using a 50-minute gradient from 2 % (v/v) to 35 % (v/v) acetonitrile in 0.1 % (v/v) formic acid. The effluent from the HPLC was directly electrosprayed into an Orbitrap Exploris 480 (Thermo Fisher Scientific, Waltham, MA, USA) operated in a data-independent mode to automatically switch between full-scan MS and MS/MS acquisition across 30 windows of 20 m/z each, covering the range of 380-390 m/z with 1 m/z overlap. Survey full scan MS spectra (m/z 380 to 980) were acquired at a resolution of R = 120,000 at m/z 400 (AGC target of 3×10^6) and max IT of 100ms. Data independent acquisition (DIA) scans were acquired with R = 30000 (AGC target

of 3×10^8), max IT set to "Auto" and normalized collision energy set at 30 %. Typical mass spectrometric conditions included a spray voltage of 1.5 kV and a heated capillary temperature of 275 °C.

DIA-NN (version 1.8.1.0) was used to identify and quantify the proteins from *E. coli* MG1655 and T5 phage, using a combined library created from the databases Uniprot_UP000000625_Ecoli_K12_MG1655_20231219 and Uniprot_UP000002107_Escherichia_phage_ T5_20231201 with the following parameters: MS tolerance of 10 ppm, MS/MS tolerance of 10 ppm, precursor FDR of 0.1, peptide length range of 7-30, precursor charge range of 1-4, precursor m/z range of 300-1800, fragment ion range of 200-1800 and modifications including N-term M excision, Ac (N-term) Oxidation (M), Carbamidomethyl (C). The quantification strategy employed was Robust LC with cross-run normalisation being RT-dependent.

Most statistical and bioinformatics analyses were performed using Perseus software (version 2.0.11.0). Proteins identified in the decoy reverse database, identified only by site modification or marked as potential contaminants were excluded from the analysis. Missing values were imputed based on a normal distribution. Weighted gene co-expression network analysis (WGCNA) was performed with the Python package pyWGCNA (Rezaie et al., 2023) using raw LFQ values as specified in the instructions for the package (https://github.com/mortazavilab/PyWGCNA/blob/main/tutorials/Data_format.md). Data visualisation was performed in R using the packages 'ggplot2' (Wickham, 2016) and 'ggpubr' (Kassambara, 2023).

2.26 Polysome profiling by sucrose density ultracentrifugation

Polysome profiling was performed to study bacterial 30S, 50S, 70S monosomes, and polysomes as described (Ero et al., 2024; Saito et al., 2022; Qin and Fredrick, 2013). Briefly, exponential phase wild-type and Δ*rlmF*Δ*rlmJ* mutant *E. coli* MG1655 grown in NB were noninfected or infected with T5 phage at MOI of 10 for 30 minutes before centrifugation at 10,397 × *g* for 5 min at 4 °C to prepare the bacterial crude lysate. The pellet was resuspended in a chilled lysis buffer (10 mM Tris-HCl [pH 8.0], 10 mM magnesium chloride and 1 mg/mL lysozyme) and immediately

flash-frozen in a liquid nitrogen bath. After thawing the samples in an ice-cool water bath, they were again flash-frozen in liquid nitrogen and stored at -80 °C until they were ready to be processed. The samples were thawed in a cool water bath, followed by the addition of 10 % (w/v) sodium deoxycholate and centrifugation at 9,391 × *g* for 10 min at 4 °C. The clarified lysate was loaded on top of a 10-50 % (w/v) sucrose density gradient, prepared using the gradient master in the Gradient Station™ (BioComp Instruments Ltd., New Brunswick, Canada) with gradient buffer (20 mM Tris-HCl [pH 8.0], 10 mM magnesium chloride, 100 mM ammonium chloride, 2 mM dithiothreitol) and ultra-centrifuged in a SW41 rotor (Beckman Coulter, Brea, CA, USA) at 35000 rpm for 3 h at 4 °C. Polysome profile of the noninfected and T5-infected samples were determined by uninterrupted monitoring of absorbance at 260 nm using piston gradient fractionator from Gradient Station™ (BioComp Instruments Ltd., New Brunswick, Canada) and the Triax™ Flow Cell (Science Services GmbH, Munich, Germany).

2.27 Statistical analysis and data presentation

If not indicated otherwise, all numerical data were analysed and graphs were prepared with GraphPad Prism version 10.0.2 (GraphPad Software, La Jolla, CA, USA). Functional analysis for WGCNA was performed using FUNAGE-Pro v2 (de Jong et al., 2022) and for differential protein expression analysis via volcano plot was performed using ShinyGo v0.741 (Ge et al., 2020). Peak bacterial density time and extinction time were calculated from growth curve data in R using package ‘gcplyr’ (Blazanin, 2024). Statistical analyses were performed in GraphPad Prism and R. Additional figure preparation was conducted with Affinity Designer version 2.2.1 (Serif, West Bridgford, UK).

All experiments were repeated at least three times to ensure reproducibility.

3 Results

3.1 Effect of m^{6}A-RNA depletion on phage replication in *V. campbellii*

Cited from publication: Bibakhya Saikia, Sebastian Riquelme-Barrios, Thomas Carell, Sophie Brameyer and Kirsten Jung. 2024. Depletion of m^{6}A-RNA in *Escherichia coli* reduces the infectious potential of T5 bacteriophage. Microbiology Spectrum, 12 (12), e0112424. Doi: 10.1128/spectrum.01124-24.

3.1.1 m^{6}A-RNA depletion does not influence prophage induction in *V. campbellii*

V. campbellii has four intact prophages in its genomes (Lorenz et al., 2016). Prophages are viral DNA segments that have integrated into the host genome and provide a competitive advantage to the host (Wendling et al., 2021). Prophage induction triggers a transition from the lysogenic to the lytic cycle, resulting in the activation of dormant viral DNA and subsequent viral replication and host cell lysis. In *V. campbellii*, ΦHAP-1-like prophage and *Vibrio* kappa-like prophage are triggered into their lytic cycle under oxidative or heat stress (Lorenz et al., 2016). To investigate whether the m^{6}A-RNA depleted mutant (Δ*rlmF*Δ*rlmJ*) affects prophage induction in *V. campbellii*, an indirect ELISA was developed to measure major capsid proteins in the supernatant to quantify total phage particles released by the host. While this assay does not directly evaluate phage infectivity, it provides a reliable measure of the phage load within the samples, supporting a comparative analysis of prophage release between wild-type and Δ*rlmF*Δ*rlmJ* mutant *V. campbellii*.

The genes *VIBHAR_05027* and *VIBHAR_01983*, which encode the major capsid proteins for *Vibrio* kappa-like prophage and ΦHAP-1-like prophage, respectively, were cloned into the pET28a vector and successfully overexpressed in *E. coli* BL21 cells through IPTG induction (Fig. 3.1 A). Confirmation of the overexpressed recombinant proteins was achieved via western blot analysis using anti-6His tag monoclonal antibodies (Fig 3.1 B). The resulting overexpressed 6His-tagged

proteins, 6His-VIBHAR_05027 and 6His-VIBHAR_01983 were localised in the inclusion bodies and subsequently solubilised using urea. The purification of the 6His-tagged recombinant proteins was carried out using Ni-NTA affinity chromatography, followed by quantification of the purified proteins using the Bradford reagent.

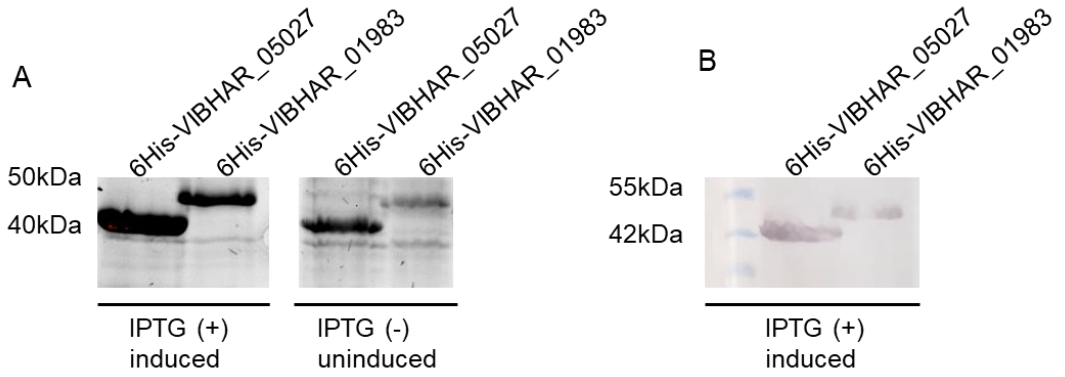

Figure 3.1 Expression of recombinant 6His-VIBHAR_05027 and 6His-VIBHAR_01983 proteins. A) SDS-PAGE analysis of the recombinant proteins under uninduced and IPTG-induced conditions. B) Confirmation of the recombinant proteins under IPTG induction using anti-6His tag antibodies via western blot.

The concentrations of purified 6His-VIBHAR_05027 and 6His-VIBHAR_01983 proteins were determined to be 2.9 mg/mL and 3.3 mg/mL, respectively. A total of sixteen vials, with eight vials for each of the two purified recombinant proteins (each at a concentration of 100 μg/mL) were sent to Kaneka Eurogentec (Seraing, Belgium) for antibody production via a Speedy 28-day immunisation programme, with two rabbits immunised per antigen. Following the successful generation of antibodies against major capsid proteins of both prophages, an indirect ELISA assay was established to enable quantitative measurement of the phage load in the samples (Fig 3.2 A). Standard curves were prepared from the purified recombinant proteins to reliably determine the concentration of capsid proteins in the indirect ELISA assay (Fig 3.2 B and C).

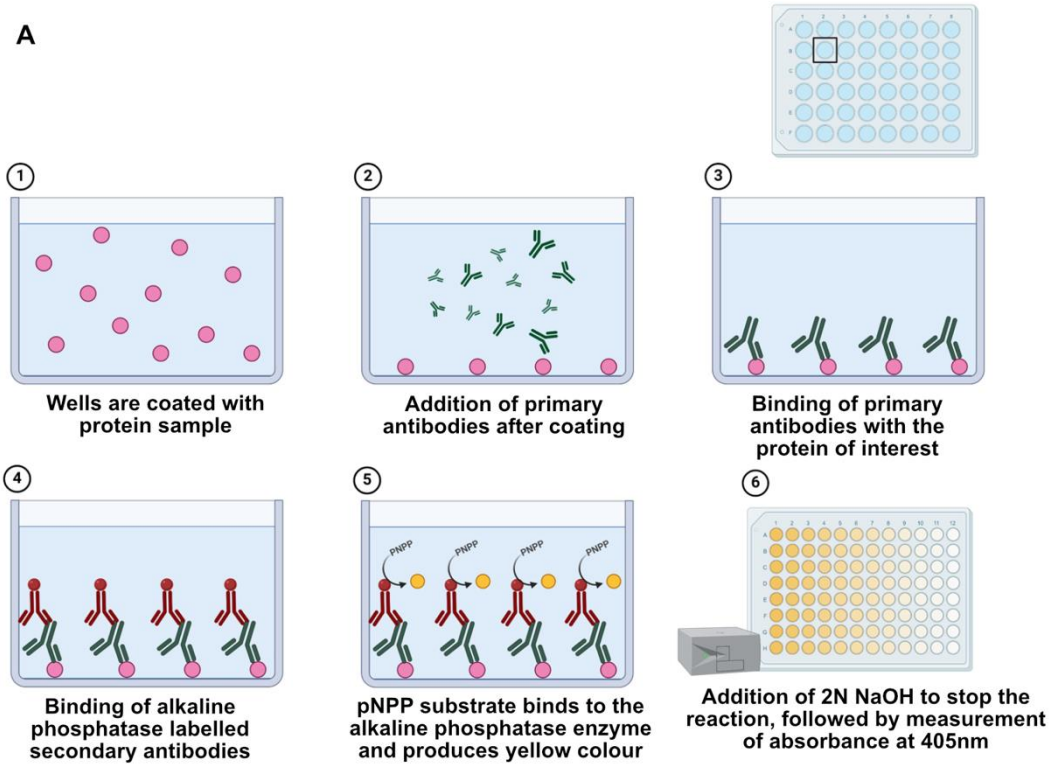
A
1
Wells are coated with protein sample
2
Addition of primary antibodies after coating
3
Binding of primary antibodies with the protein of interest
4
Binding of alkaline phosphatase labelled secondary antibodies
5
PNPP
pNPP substrate binds to the alkaline phosphatase enzyme and produces yellow colour
6
Addition of 2N NaOH to stop the reaction, followed by measurement of absorbance at 405nm

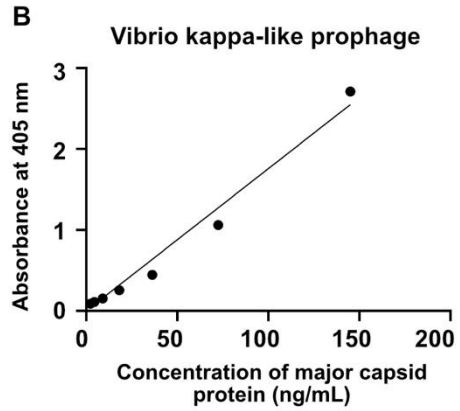
B
Vibrio kappa-like prophage
Absorbance at 405 nm
0
1
2
3
0
50
100
150
200
Concentration of major capsid protein (ng/mL)

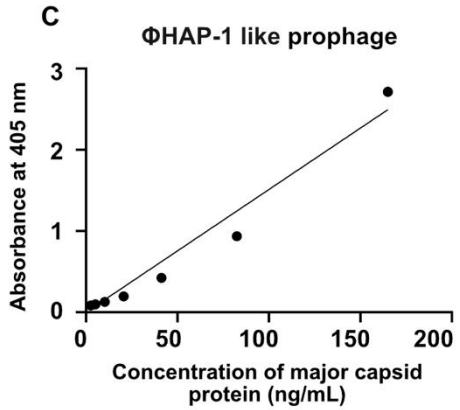
C
ΦHAP-1 like prophage
Absorbance at 405 nm
0
1
2
3
0
50
100
150
200
Concentration of major capsid protein (ng/mL)

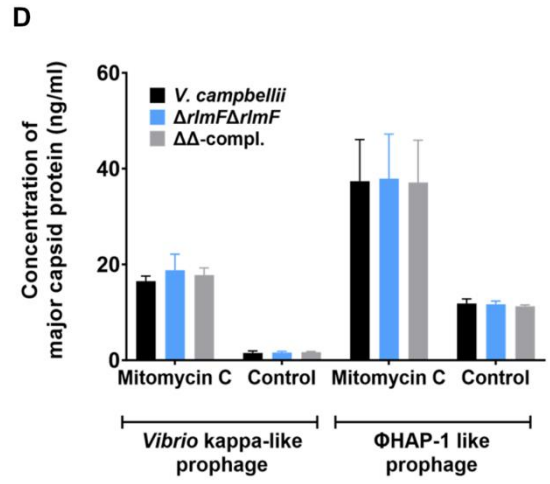
D
Concentration of major capsid protein (ng/ml)
0
20
40
60
V. campbellii
ΔrlmFΔrlmF
ΔΔ-compl.
Mitomycin C
Control
Mitomycin C
Control
Vibrio kappa-like prophage
ΦHAP-1 like prophage

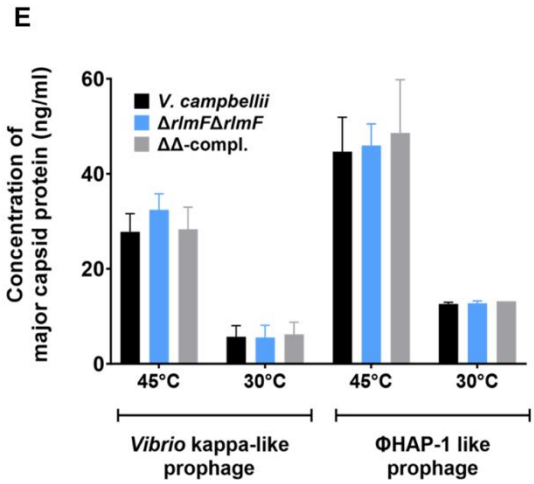
E
Concentration of major capsid protein (ng/ml)
0
20
40
60
V. campbellii
ΔrlmFΔrlmF
ΔΔ-compl.
45°C
30°C
45°C
30°C
Vibrio kappa-like prophage
ΦHAP-1 like prophage

Figure 3.2 Detection of major capsid proteins from *Vibrio* kappa-like prophage and ΦHAP-1 like prophage using indirect ELISA. A) Schematic representation depicts key steps of the indirect ELISA workflow developed for use in 96-well plates. The ELISA standard curves were prepared using purified recombinant VIBHAR_05027 from *Vibrio* kappa-like prophage (B) and VIBHAR_01983 from ΦHAP-1 like prophage (C). Lysogenic phages were induced in the indicated strains with 1 µg/mL mitomycin C (D) or heat at 45 °C (E) for 30 min. Untreated controls were also maintained. Two hours post-induction, culture supernatants were subjected to ELISA to estimate the release of phage particles. Figure 3.2 D and E are cited from publication: Bibakhya Saikia, Sebastian Riquelme-Barrios, Thomas Carell, Sophie Brameyer and Kirsten Jung. 2024. Depletion of m^6A-RNA in *Escherichia coli* reduces the infectious potential of T5 bacteriophage. Microbiology Spectrum, 12 (12), e0112424. Doi: 10.1128/spectrum.01124-24.

When the wild-type, Δ*rlmF*Δ*rlmJ* mutant, and the complemented mutant *V. campbellii* were subjected to oxidative or heat stress, higher levels of capsid proteins were detected for the ΦHAP-1-like prophage than for the *Vibrio* kappa-like prophage, suggesting that the former was more strongly induced under these stress conditions (Fig 3.2 D and E). However, no significant differences were observed between the wild type, the Δ*rlmF*Δ*rlmJ* mutant, or the complemented mutant (Fig 3.2 D and E). Additionally, low levels of capsid proteins were observed in the untreated cells, likely due to the spontaneous induction of prophages (Fig 3.2 D and E). Overall, the results indicate that m^6A-RNA modification does not modulate prophage induction in *V. campbellii* under oxidative or heat stress.

3.1.2 m^6A-RNA depletion does not influence Virtus replication in *V. campbellii*

The availability of the vibriophage Virtus, which can infect a wide range of *Vibrio* spp., including *V. campbellii* (Droubogiannis and Katharios, 2022), provided the unique opportunity to investigate the impact of m^6A-RNA modification on lytic phage replication in *V. campbellii* wild type and its Δ*rlmF*Δ*rlmJ* mutant. To evaluate this, the efficiency of plaquing by phage Virtus was tested on exponentially growing *V. campbellii* wild type, its Δ*rlmF*Δ*rlmJ* mutant and the complemented mutant (ΔΔ-compl.). Results indicated that infectivity by Virtus was comparable among all three strains (Fig. 3.3). Additionally, when stationary-phase cells were infected, no significant differences in susceptibility to Virtus were observed (Fig. 3.3). These findings suggest that m^6A-

RNA modification does not impact phage Virtus replication in *V. campbellii* under the tested conditions.

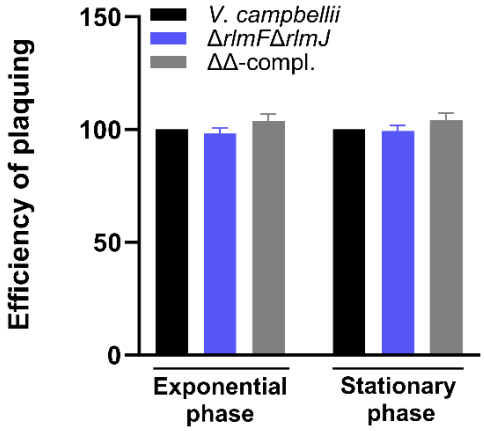

Figure 3.3 Efficiency of plaquing of phage Virtus to exponential and stationary phase *V. campbellii* wild-type strain, its Δ*rlmF*Δ*rlmJ* mutant and the complemented mutant (ΔΔ-compl.). The graph shows the efficiency of plaquing (EOP), which is calculated by dividing the number of plaques obtained from the mutant by the number of plaques obtained from the wild type. The EOP of the wild type was set to 100. Data are presented as the mean ± standard deviation of at least three independent experiments. Part of the figure (exponential phase) cited from publication: Bibakhya Saikia, Sebastian Riquelme-Barrios, Thomas Carell, Sophie Brameyer and Kirsten Jung. 2024. Depletion of m^6A-RNA in *Escherichia coli* reduces the infectious potential of T5 bacteriophage. Microbiology Spectrum, 12 (12), e0112424. Doi: 10.1128/spectrum.01124-24.

3.1.3 Unsuccessful enrichment of phages against *V. campbellii*

V. campbellii is notorious for causing luminous vibriosis in marine shrimp aquaculture facilities, marking it as an opportunistic pathogen (Srisangthong et al., 2023; Li et al., 2021). As a result, numerous studies have identified and characterised phages that infect this bacterium for potential biocontrol strategies (Srisangthong et al., 2023; Li et al., 2021; Nuidate et al., 2021; Sangseedum et al., 2017). However, none of these phages have been deposited to major culture collections like

DSMZ or ATCC, limiting their accessibility for further study. Thus, we sought to enrich and isolate *V. campbellii*-specific phages from the Naples Sea, Red Sea, and codfish to investigate further the influence of m^6A modification on phage replication in *V. campbellii*.

The samples were processed and tested to visualise the presence of phages. The codfish sample did not show any clearing, indicating the absence of lytic phages, and was excluded from further experiments. The Naples Sea sample exhibited faint clearing after enrichment, but subsequent isolation attempts were unsuccessful, and a second spot assay showed no clearing.

In contrast, the Red Sea sample produced clear spots after enrichment, indicating the presence of potential phages. However, attempts to isolate these phages from the spots — whether by touching a pipette tip or by sampling the soft agar — were unsuccessful. The plaque assay failed to yield distinct plaques. This lack of isolated plaques could be attributed to phenomena such as abortive infection or lysis from without.

Abortive infection occurs when phages overwhelm the bacterial cell, which often leads to the disruption of the cell wall, causing cell death without producing phage progenies. Cell wall disruption could be due to multiple phage adsorption or the action of the phage lysins. This process is sometimes referred to as bacterial suicide. Consequently, although initial signs of phage activity were observed in the Red Sea sample, these factors hindered the isolation and examination of individual phages, thus concluding the exploration into the role of m^6A-RNA modification in *V. campbellii*.

3.2 Effect of m^6A-RNA depletion on phage replication in *E. coli* MG1655

Cited from publication: Bibakhya Saikia, Sebastian Riquelme-Barrios, Thomas Carell, Sophie Brameyer and Kirsten Jung. 2024. Depletion of m^6A-RNA in *Escherichia coli* reduces the infectious potential of T5 bacteriophage. Microbiology Spectrum, 12 (12), e0112424. Doi: 10.1128/spectrum.01124-24.

In contrast to *V. campbellii*, the genome of *E. coli* contains cryptic prophages (Blattner et al., 1997) but offers a diverse array of well-characterized lytic phages (Demerec and Fano, 1945).

3.2.1 m^{6}A-RNA depletion in *E. coli* influences T5 phage infection

The most prominent lytic phages for *E. coli*, including the five of the "T-phages" (Abedon, 2000; Demerec and Fano, 1945) and phage λ, were screened to assess their ability to infect exponentially grown *E. coli* Δ*rlmF*Δ*rlmJ* mutant compared to the *E. coli* MG1655 (Fig. 3.4). All phages tested are dsDNA phages belonging to the class *Caudoviricetes* and characterised by their tail and icosahedral head (Ackermann, 1999).

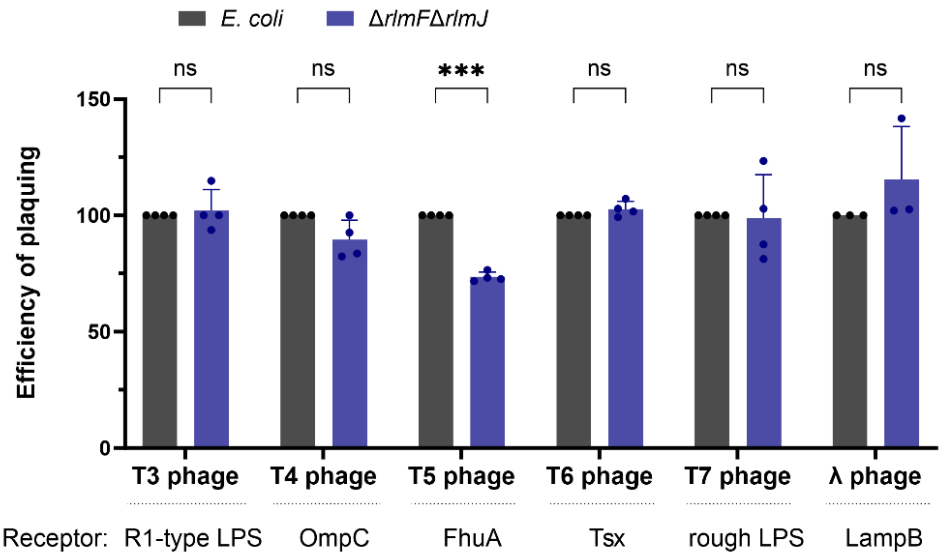

Figure 3.4 Depletion of m^{6}A-RNA in *E. coli* MG1655 and its effect on infection by different lytic phages. *E. coli* wild type and the Δ*rlmF*Δ*rlmJ* mutant were grown to an OD_{600} = 0.5 before infection with the different phages. The EOP was calculated by dividing the number of plaque-forming units (PFU) of the Δ*rlmF*Δ*rlmJ* mutant by the number of PFU of the wild type. The EOP of the wild type was set to 100. Data are presented as the mean ± standard error of at least three independent experiments. *** $p < 0.001$ (Student's t-test). ns, not significant. The primary receptors are indicated below the diagram. Figure was cited from publication: Bibakhya Saikia, Sebastian Riquelme-Barrios, Thomas Carell, Sophie Brameyer and Kirsten Jung. 2024. Depletion of m^{6}A-RNA in *Escherichia coli* reduces the infectious potential of T5 bacteriophage. Microbiology Spectrum, 12 (12), e0112424. Doi: 10.1128/spectrum.01124-24.

Of all lytic phages tested, the T5 phage showed significantly reduced plaque formation in the Δ*rlmF*Δ*rlmJ* mutant compared to the wild type (Fig 3.4). This effect was not observed with the other phages (Fig 3.4). The infection by T5 phage was further analysed at different growth stages of *E. coli*. It was found that the number of plaques was consistently lower in the Δ*rlmF*Δ*rlmJ* mutant compared to the wild-type strain regardless of the growth phase, an effect that was no longer observed in the complemented mutant (ΔΔ-compl.) (Fig 3.5). These observations suggest that m^6A-RNA modification influences T5 phage infection in *E. coli.*

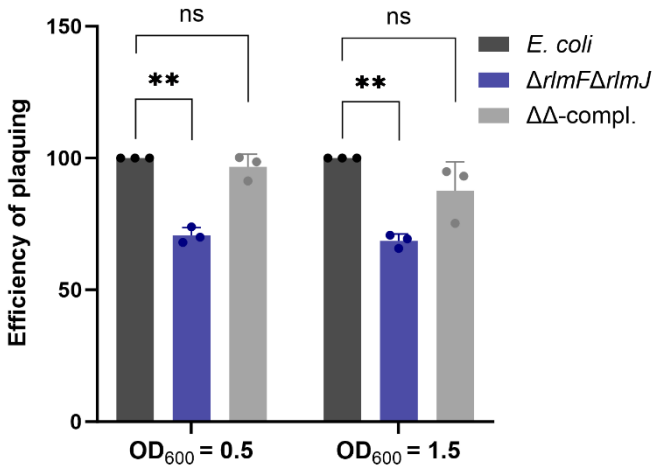

Figure 3.5 Efficiency of plaquing of phage T5 to exponential and stationary phase *E. coli* wild-type strain, its Δ*rlmF*Δ*rlmJ* mutant and the complemented mutant (ΔΔ-compl.). The strains were infected with T5 in the exponential growth phase (OD_{600} = 0.5) or stationary phase (OD_{600} = 1.5). The efficiency of plaquing was calculated as in Fig. 3.4. Data are presented as the mean ± standard deviation of three independent experiments. ** $p < 0.01$ (Student's *t*-test). Figure was cited from publication: Bibakhya Saikia, Sebastian Riquelme-Barrios, Thomas Carell, Sophie Brameyer and Kirsten Jung. 2024. Depletion of m^6A-RNA in *Escherichia coli* reduces the infectious potential of T5 bacteriophage. Microbiology Spectrum, 12 (12), e0112424. Doi: 10.1128/spectrum.01124-24.

3.2.2 m^{6}A-RNA depletion in *E. coli* does not impact most T5-like phages

A more targeted screening was conducted to establish whether the observed reduction in plaque formation by T5 phage is a conserved trait among T5-like phages. With this objective in mind, T5-like phages from the BASEL phage collection (Maffei et al., 2021) were tested for their ability to infect *E. coli* Δ*rlmF*Δ*rlmJ* mutant compared to the wild-type (Fig 3.6). According to ICTV, all nine T5-like phages tested are classified within the *Demerecviridae* family, which falls under the class *Caudoviricetes*. Of the nine T5-like phages, four — DaisyDussoix (Bas31), IrisVonRoten (Bas32), HildyBeyeler (Bas33), and SelmaRatti (Bas43) — are classified in the genus *Tequintavirus*, like phage T5 (Maffei et al., 2021). The remaining five phages — GreteKellenberger (Bas26), TrudiGerster (Bas27), IrmaTschudi (Bas28), SuperGirl (Bas29), and TrudiRoth (Bas30) — are classified under the genus *Eseptimavirus* (Maffei et al., 2021).

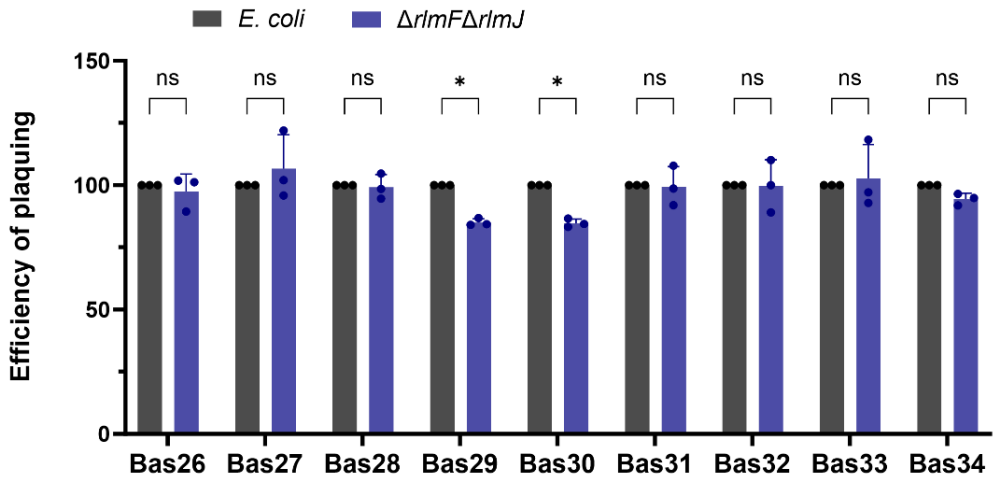

Figure 3.6 Depletion of m^{6}A-RNA in *E. coli* MG1655 and its effect on infection by different T5-like phages. *E. coli* wild type and the Δ*rlmF*Δ*rlmJ* mutant were grown to an OD_{600} = 0.5 and infected with different T5-like phages. The EOP was calculated as in Fig 3.4. The EOP of the wild type was set to 100. Data are presented as the mean ± standard deviation of three independent experiments. * $p < 0.05$ (Student's *t*-test). Figure was cited from publication: Bibakhya Saikia, Sebastian Riquelme-Barrios, Thomas Carell, Sophie Brameyer and Kirsten Jung. 2024. Depletion of m^{6}A-RNA in *Escherichia coli* reduces the infectious potential of T5 bacteriophage. Microbiology Spectrum, 12 (12), e0112424. Doi: 10.1128/spectrum.01124-24.

The results demonstrated a statistically significant reduction in plaque formation efficiency for phages Bas29 and Bas30 in the Δ*rlmF*Δ*rlmJ* mutant (Fig. 3.6), suggesting that m^6A-RNA depletion also reduces the infectivity of other T5-like phages. However, this is not a shared feature among T5-like phages. Particularly, the T5 phage exhibited a more pronounced reduction in plaque formation (Fig 3.5) compared to Bas29 and Bas30 (Fig. 3.6). Given this, further investigations were carried out to characterise the phenotype displayed by the T5 phage.

3.2.3 m^6A modification did not change during the T5 phage infection

This work was done in collaboration with Leonardo Vásquez Camus from the AG Kirsten Jung at LMU. Mr. Camus performed the Rol-LAMP method with the samples.

RlmF specifically methylates the A1618 position, while RlmJ specifically methylates the A2030 position in the 23S rRNA of *E. coli* (Golovina et al., 2012; Sergiev et al., 2007). By using the rolling circle extension-assisted loop-mediated isothermal amplification (Rol-LAMP) method (Li et al., 2023), the abundance of m^6A modification in the A2030 position of the 23S rRNA during different stages of T5 infection was measured (Fig. 3.7). The uninfected Δ*rlmF*Δ*rlmJ* mutant was used as the negative control, while the uninfected wild-type strain served as the positive control. Comparison of threshold cycle (Ct) values between the wild-type and Δ*rlmF*Δ*rlmJ* strains for the A2030 position indicated that the Rol-LAMP method successfully detected this position (Fig. 3.7). The Ct values for the wild-type strain were significantly higher than those of the Δ*rlmF*Δ*rlmJ* mutant, demonstrating the presence of m^6A modification at this site (Fig. 3.7). Higher Ct values are indicative of unsealed padlock probes resulting from the presence of m^6A modification, which prevents the provision of starting material for LAMP. In contrast, the Rol-LAMP method failed to detect the A1618 position in the samples. The Ct values between the wild-type and Δ*rlmF*Δ*rlmJ* strains for the A1618 position did not reveal any significant difference. This may be attributed to the detection limit of the method or the absence of m^6A modification in the A1618 position under experimental conditions used in this study.

To monitor the m^6A modification abundance in the A2030 position during T5 phage infection, an additional internal control was maintained to normalise against the basal transcription of the 23S

rRNA. A surrounding non-modified adenine served as the internal control. The results showed that the non-modified adenine control (23S control) had lower Ct values as compared to the modified A2030 position (Fig. 3.7), demonstrating the lack of m^6A modification in the control site. Lower Ct values correspond to an increase in the production of LAMP products, which is due to the sealing of the padlock probes. Additionally, the Ct values remained fairly constant throughout the course of T5 phage infection in *E. coli* wild type, which implies that the abundance of the m^6A modification remained unaltered and did not vary during infection (Fig. 3.7).

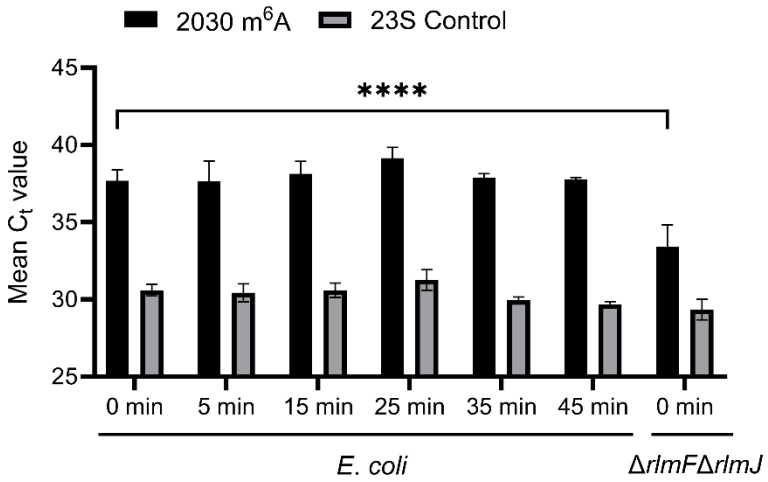

Figure 3.7 Abundance of m^6A modification in the A2030 position of 23S rRNA of *E. coli* during T5 phage infection. Uninfected *E. coli* Δ*rlmF*Δ*rlmJ* mutant served as the negative control. Uninfected *E. coli* wild type served as the positive control. Data are presented as the mean ± standard deviation of three independent experiments. **** $p < 0.0001$ (Two-way ANOVA; Tukey's multiple correction test).

3.2.4 T5 phage lacks its own m^6A methyltransferases

To investigate whether the T5 phage possesses its own methyltransferases that could modulate m^6A-RNA levels during infection, the T5 phage genome was examined for any potential methyltransferase-encoding genes. Since none of the annotated proteins encoded for methyltransferases, the focus was shifted to on non-annotated T5 proteins in the range of 100–350 amino acid. Twenty-five candidate proteins (T5.002, T5.011, T5.018, T5.019, T5.023, T5.026, T5.028, T5.033, T5.038, T5.039, T5.047, T5.048, T5.054, T5.055, T5.067, T5.076, T5.077, T5.078, T5.80, T5.089, T5.100, T5.106, T5.107, T5.123 and T5.134) fitting this criterion were

compiled and their structural predictions were made using AlphaFold 3.0 (Abramson et al., 2024). Comparative structural analysis was conducted in PyMOL (Version 3.0 by Schrödinger) to the known structure of RlmJ and the predicted structure of RlmF. Additionally, these candidate proteins were assessed for structural similarities to SAM lyase, which is found in T3 phage. However, no structural similarities were found, suggesting that the T5 phage does not possess its own methyltransferases or SAM lyase that could modulate m^6A. Thus, the lower infection potential of T5 phage is due to the depleted m^6A-RNA modification in the host (Fig 3.5).

3.2.5 m^6A-RNA depletion delays *E. coli* cell lysis during T5 phage infection

Efficiency of plaquing data suggests that T5 phage may impact survival rates differently between the wild-type *E. coli* and Δ*rlmF*Δ*rlmJ* mutant strains in liquid culture. To test this hypothesis on a population level, bacterial growth experiments were conducted with different multiplicities of infection (MOI), defined as the ratio of bacteriophage particles to bacterial cells. In the control experiment (Fig. 3.8 A), bacterial cells proliferated and no lysis was observed. However, the addition of T5 phage resulted in the lysis of bacterial cells (Fig. 3.8 B-E), confirming that the observed phenomenon was a consequence of phage infection. Infection at an MOI of 10 or 1 led to rapid, complete collapse of both wild-type and mutant populations, with earlier collapse at the higher MOI (Fig. 3.8 B, C and F). Similarly, infection at an MOI of 0.1 resulted in earlier collapse of both populations than at an MOI of 0.01 (Fig. 3.8 D, E and F). Strain-specific differences in lysis timing became evident at an MOI of 0.01 during infection with T5 phage (Fig. 3.8 E).

Additionally, the peak bacterial density time and the extinction time were calculated from growth curve data (Fig 3.8 A-E) to act as a proxy for T5 phage susceptibility to the host strains using the package gcplyr (Blazanin, 2024). The time taken for the first local maxima in bacterial density to be reached before a decline due to T5 phage infection is referred to as the peak bacterial density time. In uninfected samples, both *E. coli* wild-type and Δ*rlmF*Δ*rlmJ* mutant strains reached peak density at approximately 5.6 h, with no substantial difference (Fig. 3.8 F). Under T5 phage infection, an increase in MOI resulted in a decrease in peak bacterial density and time taken to reach it. At MOI of 0.01, the wild-type strain attained peak bacterial density at 4.3 h, whereas the Δ*rlmF*Δ*rlmJ* mutant attained peak density at 5.2 h, indicating that the mutant withstood phage-induced lysis for nearly an hour longer than the wild type (Fig. 3.8 F). Extinction time, calculated

as the time required to drive bacterial density below a detectable optical density (Turner et al., 2012), in this case, a threshold of 0.15 due to T5 phage infection was also examined. A notable overall trend was observed, whereby the Δ*rlmF*Δ*rlmJ* mutant exhibited a delayed extinction time in comparison to the wild-type strain, particularly evident at MOIs of 1 and 0.01 (Fig 3.8 G). At an MOI of 1, the *E. coli* wild-type strain reached the extinction threshold at 1.8 h, while Δ*rlmF*Δ*rlmJ* mutant reached it at 2.1 h, signifying a delay of 0.3 hours (Fig 3.8 G). Furthermore, a more profound delay of five hours was noted in the Δ*rlmF*Δ*rlmJ* mutant at an MOI 0.01, with the extinction threshold being reached at 13.7 h, in contrast to the wild-type strain, which reached it at 8.7 h (Fig 3.8 G). When the threshold is set to an optical density of 0.3, the trend remains unchanged. The mutant reaches extinction time at 8.4 hours, compared to 5.7 hours in the wild type, indicating a delay of three hours (Fig 3.8 E). This delay in both peak bacterial density time and extinction time is suggestive of a prolonged period of bacterial viability in the m^6A-RNA depleted (Δ*rlmF*Δ*rlmJ*) mutant.

To further validate this at the level of individual cells, time-lapse phase contrast microscopy was used for live-cell imaging. Exponential phase *E. coli* wild type and Δ*rlmF*Δ*rlmJ* mutant were infected with T5 phage at an MOI of 10 to ensure synchronous phage infection or with nutrient broth as a control. After adsorption for 10 min, samples were spotted on an agarose pad and imaged up to 3 hours post-infection. Images were captured every 2 min in several positions at a constant temperature of 37 °C. Intact cells could be easily distinguished from burst cells. A significantly higher proportion of cells from the Δ*rlmF*Δ*rlmJ* population survived after 2.5 hours of T5 infection compared to the *E. coli* wild-type population (Fig. 3.8 H). This indicates that cell lysis was delayed in the Δ*rlmF*Δ*rlmJ* mutant, which is consistent with the observation made in the survival experiments.

The next stage of the investigation was to examine T5 phage-host interactions in order to ascertain the cause of the prolonged cell lysis observed in the Δ*rlmF*Δ*rlmJ* mutant. Since adsorption is the initial step in the phage infection process, an adsorption assay was performed to evaluate whether the delayed lysis in the Δ*rlmF*Δ*rlmJ* mutant was due to inefficient binding of the phage to the host cells. The adsorption rates of T5 phage to both host strains were found to be comparable, with a minimum of 60 % adsorption occurring within 15 min of the infection (Fig 3.9 A). By 25 min, almost 85 % of T5 was adsorbed by the strains (Fig 3.9 A). These results suggest that the higher

percentage of surviving cells observed in the Δ*rlmF*Δ*rlmJ* mutant after T5 phage infection is likely not due to differences in binding to host cells but are instead related to processes that occur after phage–receptor interactions.

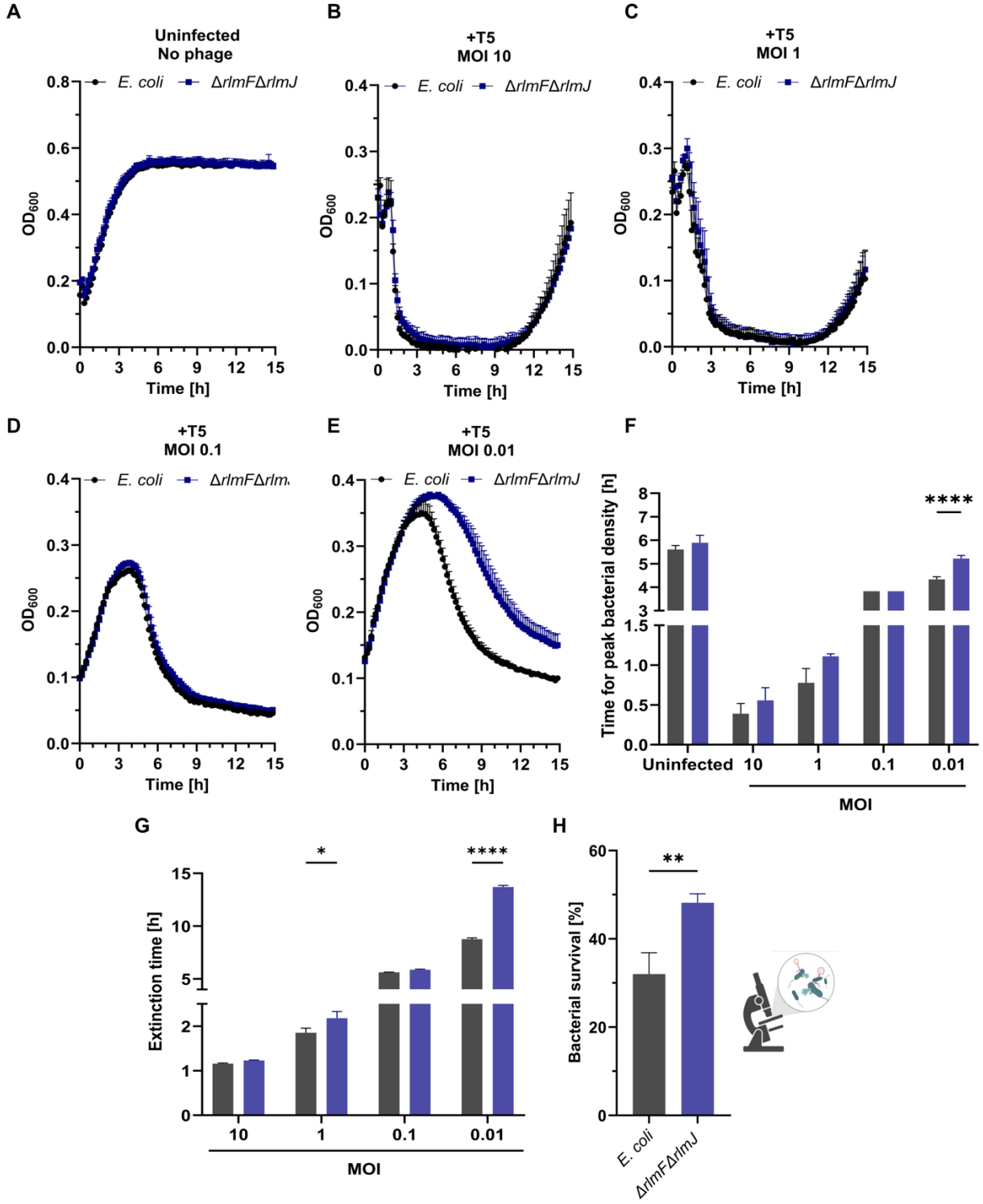

Figure 3.8 Survival of *E. coli* MG1655 wild type and Δ*rlmF*Δ*rlmJ* mutant after phage T5 infection at different MOIs. (A–E) *E. coli* wild type and Δ*rlmF*Δ*rlmJ* mutant were grown to the exponential growth phase in nutrient broth. About 2×10^8 cells were uninfected (A) or infected with T5 phage at MOI of 10 (B), 1 (C), 0.1 (D), and 0.01 (E). The mixtures were transferred to 96-well plates (150 µL per well), and the OD_{600} was measured every 10 min at 37°C with continuous shaking. (F) The time taken to reach the peak bacterial density of the strains was calculated based on growth curves A to E. (G) Extinction time was estimated using growth curves A to E to measure the time required for the T5 phage to cause bacterial cell death and reduce the optical density to a threshold of 0.15. (H) *E. coli* strains were infected with T5 phage at MOI of 10. Single cells were monitored by phase contrast time-lapse microscopy, imaged every 2 min, and the percentage of surviving cells after 2.5 hours was determined. A total of 2,080 wild type and 1,923 Δ*rlmF*Δ*rlmJ E. coli* cells were quantified at time point 2.5 hours post-infection. Data are presented as the mean ± standard error (A–E) or as mean ± standard deviation of the mean (F-H) of three independent biological replicates. *** $p < 0.001$ (Student's *t*-test). Part of the figure (A-E and H) was cited from publication: Bibakhya Saikia, Sebastian Riquelme-Barrios, Thomas Carell, Sophie Brameyer and Kirsten Jung. 2024. Depletion of m^6A-RNA in *Escherichia coli* reduces the infectious potential of T5 bacteriophage. Microbiology Spectrum, 12 (12), e0112424. Doi: 10.1128/spectrum.01124-24.

To test this, one-step growth curves were performed with the *E. coli* wild type and the Δ*rlmF*Δ*rlmJ* mutant, with the aim of characterising the dynamics of T5 phage replication. Through this assay, it was possible to determine (i) the latent period, the time for the production of phage components, and virion assembly until phage-induced lysis of infected cells, (ii) the rise period, which includes the rise in phage concentration and asynchronous bursts, and (iii) the burst size, a measure of phage virions produced per infected cell. For both strains, the latent period was observed to be 45 min, followed by a rise period for another 45 min, followed by a burst period (Fig. 3.9 B). In the Δ*rlmF*Δ*rlmJ* mutant, a significant delay in the increase of the phage titer was observed during the rise period compared to the wild type, which was particularly evident at the 60- and 75-min time points (Fig 3.9 B). This period indicates the rise in phage number due to the release of progeny phage particles by lysis of infected bacterial cells. The slight delay in the rise period during T5 phage infection may indicate a delay in phage assembly and/or host cell lysis. However, it could also be due to host factors such as differences in overall metabolic activity, ribosomal heterogeneity or host immune responses that were altered due to the deletion of *rlmF* and *rlmJ*.

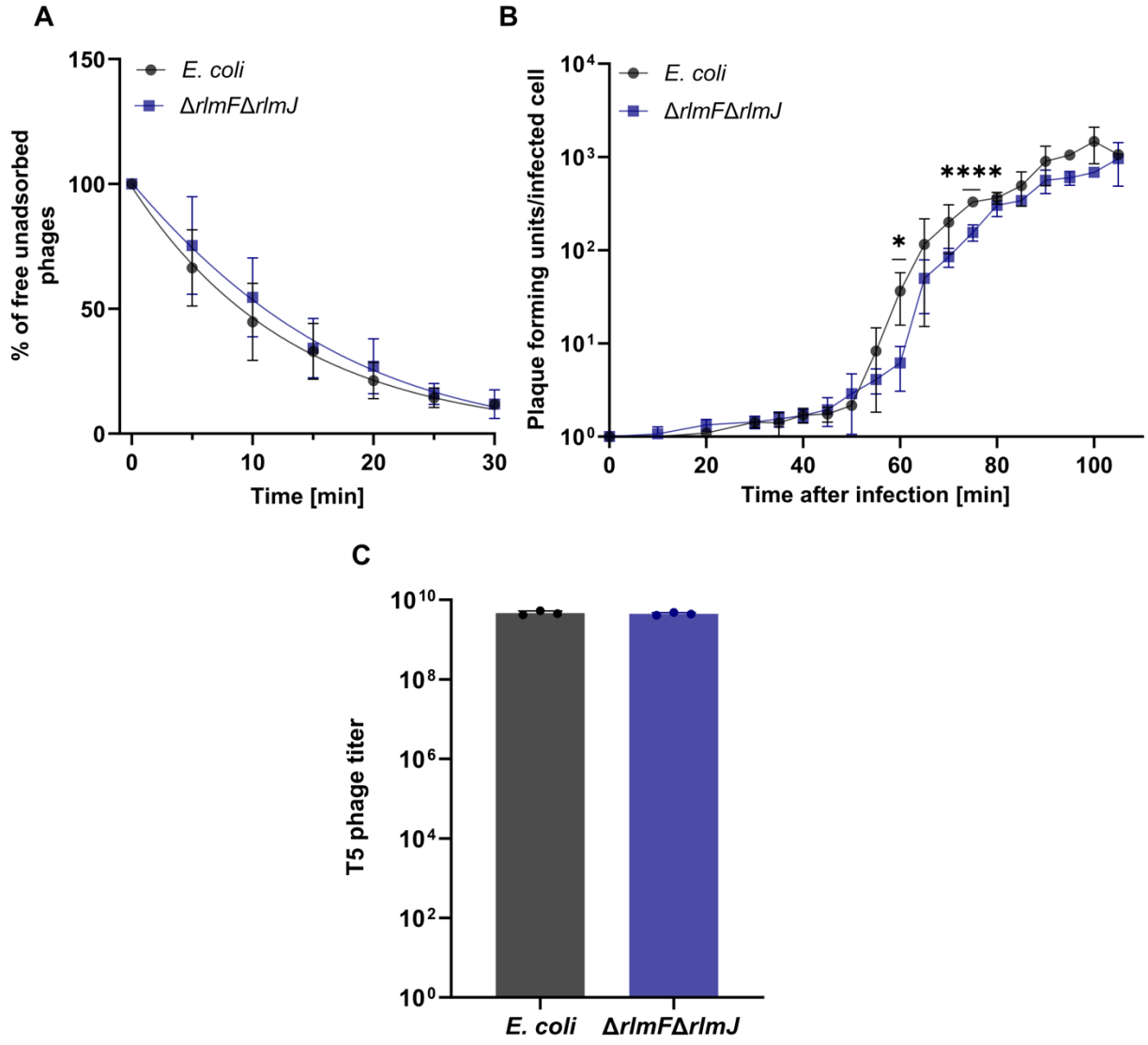

Figure 3.9 Characterisation of T5 phage infection in *E. coli* MG1655 wild type and Δ*rlmF*Δ*rlmJ* mutant. (A) Adsorption kinetics of T5 phage to wild type and Δ*rlmF*Δ*rlmJ* mutant *E. coli* at MOI 0.1. Free phages were collected at the indicated time points after infection (0 min), and the concentration of free phages was determined using plaque assays. (B) One-step growth curve of T5 phage determined for wild type and Δ*rlmF*Δ*rlmJ* mutant at MOI 0.01. (C) Wild type and Δ*rlmF*Δ*rlmJ* mutant *E. coli* were infected with phage T5 at an MOI of 0.1 for 24 hours, followed by centrifugation. The supernatant containing T5 phage particles was titer using *E. coli* DSM613 to check for defective phages produced by the mutant. Data are presented as the mean ± standard deviation of at least three independent experiments. * $p < 0.05$; **** $p < 0.0001$ (paired Student's *t*-test). Part of the figure (A-B) was cited from publication: Bibakhya Saikia, Sebastian

Riquelme-Barrios, Thomas Carell, Sophie Brameyer and Kirsten Jung. 2024. Depletion of m^6A-RNA in *Escherichia coli* reduces the infectious potential of T5 bacteriophage. Microbiology Spectrum, 12 (12), e0112424. Doi: 10.1128/spectrum.01124-24.

The burst size analysis demonstrated that *E. coli* wild-type cells produced an average of 364 phages per infection cycle, with the Δ*rlmF*Δ*rlmJ* mutant producing a slightly lower number with an average of 339 phages. This corresponds to a reduction of approximately 7 % per infection cycle. These results suggest that the Δ*rlmF*Δ*rlmJ* mutant releases progressively fewer phages over multiple rounds of infection, which may contribute to the higher survival rates observed in the mutant (Fig. 3.8E and H) and the lower PFU (Fig. 3.5). To ascertain with greater clarity whether a reduction in the number of phages is occurring in each infection cycle, a comparison was made between the titers of phages from infections of both the wild-type and Δ*rlmF*Δ*rlmJ* mutant strains (Fig 3.9C). The titers were similar, indicating that there is no production of defective phages and that the reduction in total phage output per replication cycle is not a factor.

In brief, the results demonstrate that m^6A-RNA modification in *E. coli* delays host cell lysis following T5 infection. This is supported by findings from bacterial growth experiments, live-cell imaging, and one-step growth curve assay.

3.3 T5 phage-host interactions at the molecular level

This work was done in collaboration with Dr. Ignasi Forné and Dr. Siobhan Cusack. Dr. Forné from the Protein analysis unit at the LMU performed the LC-MS/MS analysis and conducted initial statistical tests. Dr. Cusack from AG Kirsten Jung at the LMU performed the weighted gene co-expression network analysis (WGCNA) and generated the corresponding figures to illustrate the results from the analysis.

3.3.1 Dual-proteome analysis of T5 phage infection in *E. coli*

In the previous section, the interactions between T5 phage and its hosts were explored at both cellular and population levels. To delve deeper into the molecular dynamics of this interaction, a quantitative dual-proteome analysis was performed. The term ‘dual-proteome analysis’ in this context refers to the simultaneous profiling of both the host and T5 phage proteomes during the

course of T5 infection. This approach was used to investigate the changes in protein abundance during T5 infection in wild-type and m^6A-RNA depleted (Δ*rlmF*Δ*rlmJ*) *E. coli* strains. Exponential phase cultures were infected with T5 at an MOI of 10 to ensure synchronous phage infection. Proteomes from uninfected bacterial control (0 min) and infected samples at 15- and 35-min post-infection in biological triplicates were analysed by DIA label-free quantification (LFQ) using LC-MS/MS. The uninfected controls served as a baseline to visualise the basal proteome of the host strains before infection (Fig 3.10 A). Interestingly, LFQ intensities for T5 phage proteins were also detected at 0 min (Fig 3.10 B), likely due to certain sequence similarities between the hosts and phage proteins. Sequences of T5 proteins were first obtained from Uniprot (Bateman et al., 2021) and then aligned to *E. coli* MG1655 using the Protein Basic Local Alignment Search Tool (pBLAST; Camacho et al., 2009), focusing on specific T5 proteins found in at least two out of three biological replicates in either host. For example, T5 exonuclease I and side-tail fiber protein share sequence similarity with the *E. coli* endonuclease and cryptic prophage tail fiber, respectively. Additionally, similarities were also found for the T5 DNA replication primase, replication binding protein and ribonucleoside diphosphate reductase. These results suggest that some *E. coli* proteins share homology with T5 proteins, leading to cross-identification during proteomic analysis. Therefore, T5 LFQ intensities at 0 min should be interpreted cautiously, as they likely reflect the presence of host proteins with similar sequences rather than the actual abundance of the phage proteins.

LFQ intensities from the host proteomes showed a normal distribution across all infection times and biological replicates (Fig 3.10 A). Similarly, T5 proteins also followed a normal distribution at 15- and 35-min time points (Fig 3.10 B), suggesting that imputation based on the normal distribution would be reasonable. Consequently, imputation was performed to account for missing values, which facilitated the analysis and minimised bias due to missing data. T5 LFQ intensities were then visualised according to the phase of infection, revealing a clear shift from 15 min to 35 min in early and late proteins (Fig 3.10 C). Importantly, the overall distribution pattern of the LFQ values remained unaltered by the imputation process (Fig 3.10 C).

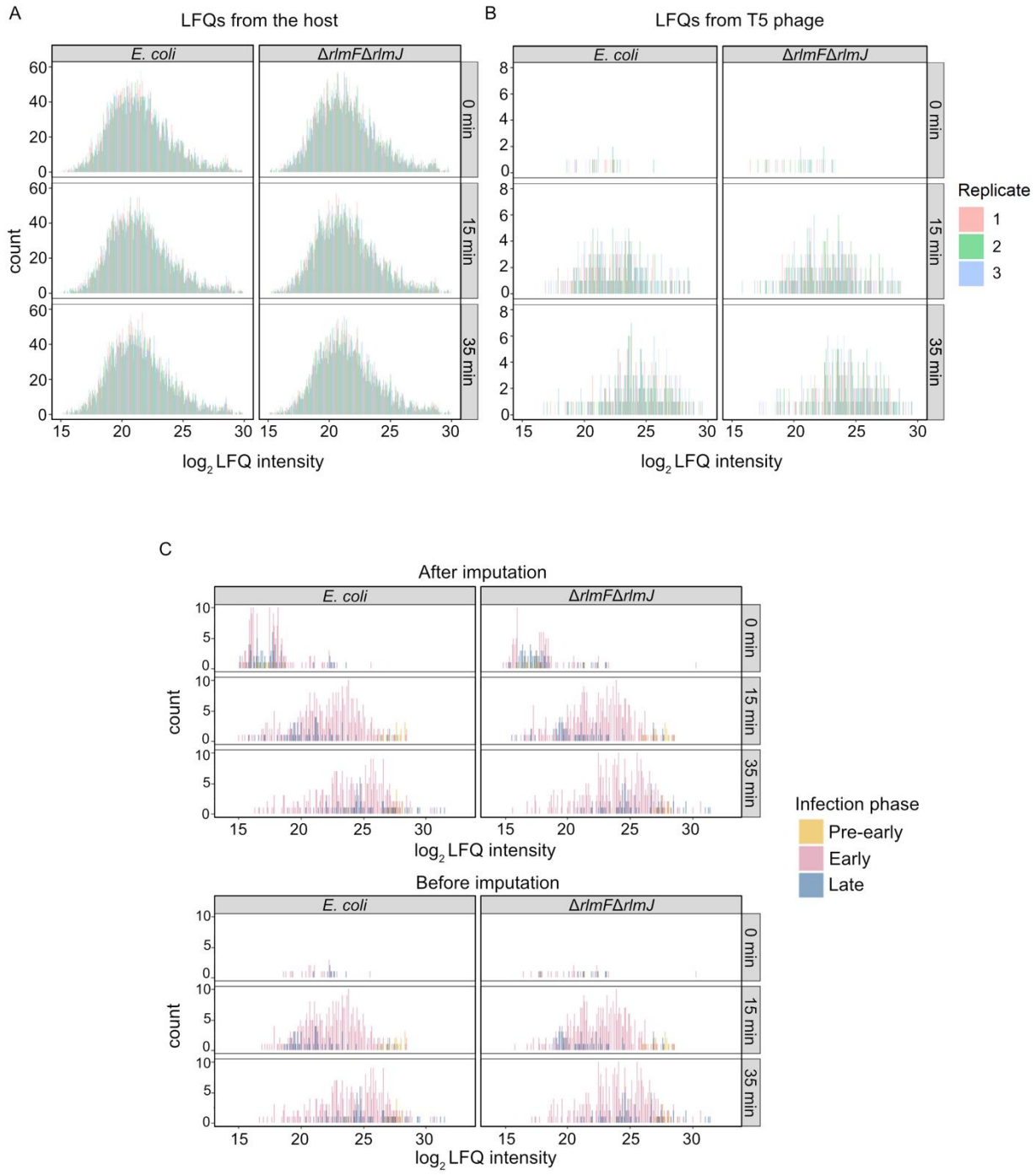

Figure 3.10 Normalised histograms of LFQ intensities contributed by T5 phage as well as *E. coli* wild type and Δ*rlmF*Δ*rlmJ* mutant. A) Histograms of LFQ intensities from the hosts are shown for all time points (0 min, 15 min and 35 min) including all biological replicates (R1-R3) per time point. B) Histograms of LFQ

intensities from the T5 phage are shown for all time points (0 min, 15 min and 35 min) including all biological replicates (R1-R3) per time point. All histograms show normal distribution except for time point 0 min for T5 phage proteins. C) Histograms of imputed and non-imputed LFQ intensities are shown in only T5 phage proteins as per their phase of infection across all time points and including all biological replicates (R1-R3).

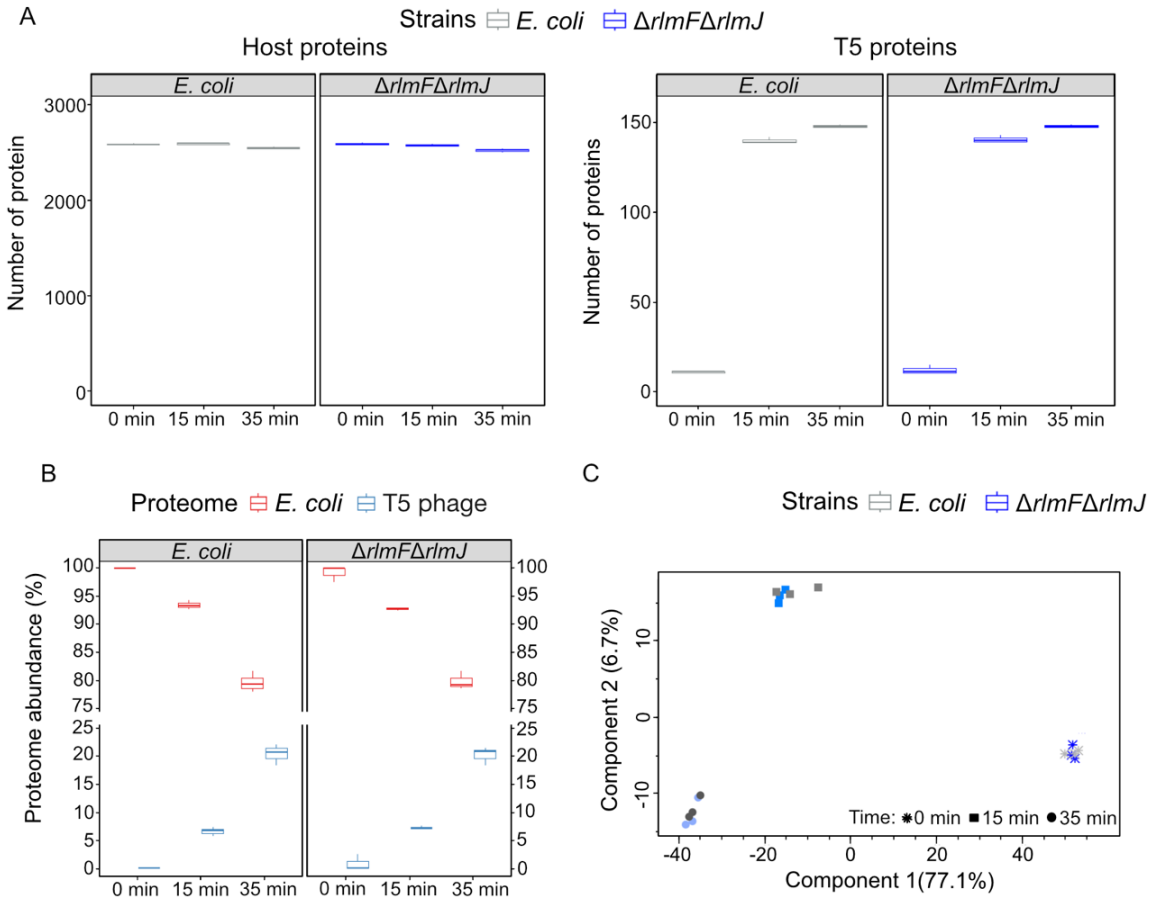

Figure 3.11 Initial analysis of the dual-proteome of T5 phage infected *E. coli* wild type and Δ*rlmF*Δ*rlmJ* mutant. A) Absolute number of proteins detected from the hosts and T5 phage before and after infection. B) Fractions of LFQ intensities from the host or T5 proteomes were calculated relative to the total LFQ intensities per sample across the course of T5 infection. Data are presented as the mean ± standard deviation of three independent experiments. C) PCA analysis of the proteomics samples based on z-score normalised LFQ intensities from three biological replicates.

A total of 2746 proteins were identified from both the hosts and phage proteomes. Of these, 2598 proteins represented 59 % coverage of the host proteome, while 148 T5 phage proteins were detected, accounting for 91 % of the phage proteome (Fig. 3.11 A). Throughout the infection, the LFQ signals were predominantly derived from *E. coli* proteins (Fig. 3.10 A), with a gradual rise in the contribution of T5 proteins, reaching a maximum of 22 % at 35 min post-infection (Fig. 3.11 B). Principal component analysis (PCA) further supported the quality of the dataset, revealing tight clustering of biological triplicates within the same time point, demonstrating consistency and reproducibility (Fig. 3.11 C). Additionally, the PCA clustering pattern distinctly separated the uninfected control (0 min) from the T5 infected time points (Fig. 3.11 C), reinforcing the robustness and reliability of the proteomics dataset.

The increase in the LFQ contribution from T5 phage proteins (Fig. 3.10 A) and the subsequent decrease in host protein contribution to the overall proteome abundance (Fig. 3.11 B) suggests a progressive T5-driven takeover and host translational reprogramming to prioritise phage protein synthesis. Such temporal proteomic shift also impacts host protein abundance. To investigate differences in protein abundance during T5 infection, a volcano plot analysis was performed. Since volcano plot analysis is limited to pairwise comparisons, differences in protein abundance were calculated comparing 15 min to 0 min post-infection and 35 min to 15 min post-infection for each strain. The analysis revealed both host and T5 protein changes during infection (Fig. 3.12). Most T5 phage proteins increased in abundance in 15 min vs 0 min post-infections and 35 min vs 15 min post-infections in both strains (Fig. 3.12). However, some T5 phage proteins, especially those belonging to the pre-early phase of infection (Dmp and A2) decreased in abundance in 35 min vs 15 min post-infections for both strains. In the case of host proteins, a statistically significant increase or decrease in protein levels was observed in response to T5 infection. The T5 proteome is examined in section 3.3.2, while the proteome of the hosts are addressed in sections 3.3.4 and 3.3.5.

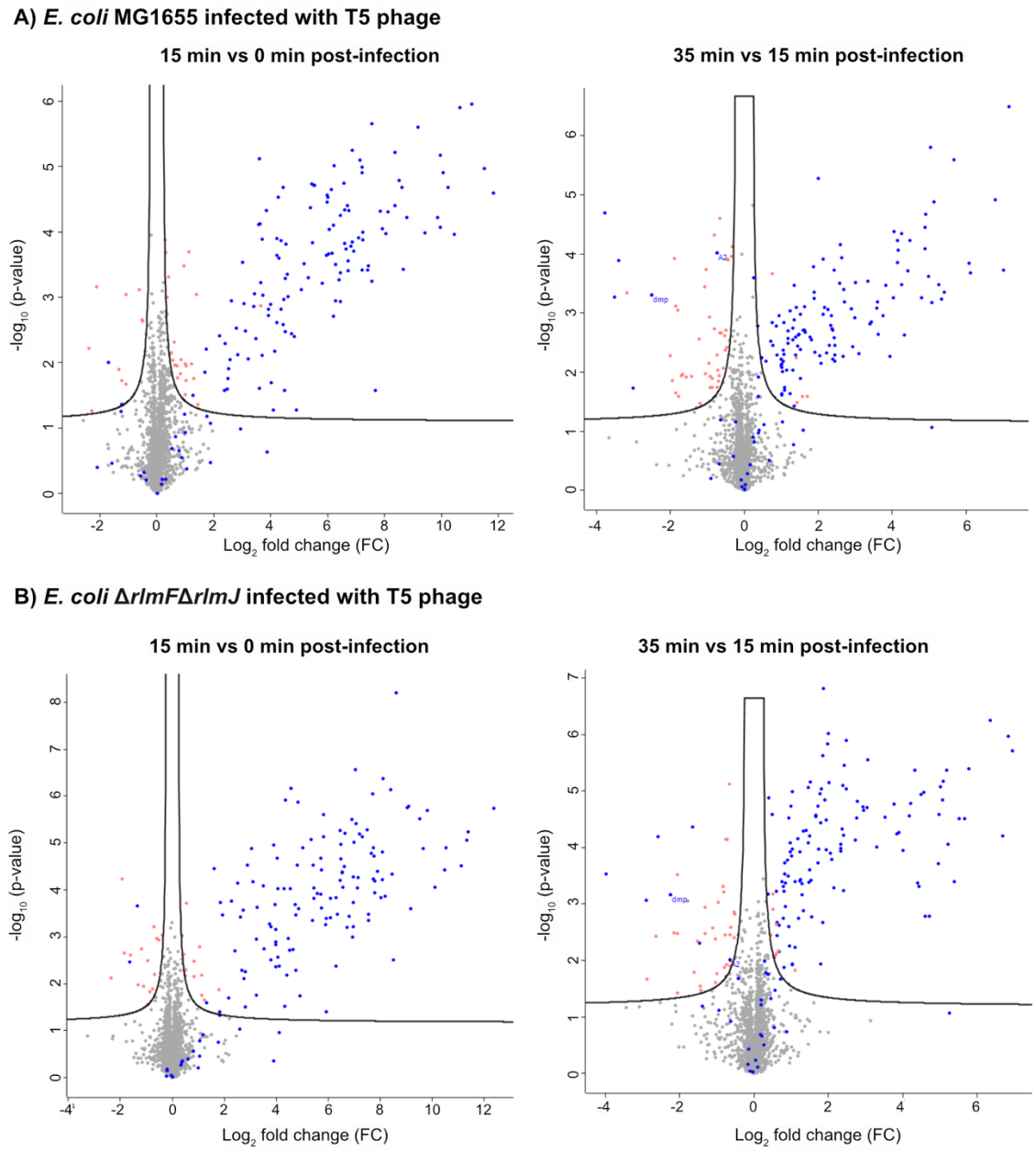

Figure 3.12 Volcano plots of the dual-proteome of T5 phage infected *E. coli* wild type and Δ*rlmF*Δ*rlmJ* mutant. Differential protein abundance was visualised using volcano plots for T5-infected *E. coli* MG1655 (A) and *E. coli* Δ*rlmF*Δ*rlmJ* mutant (B). Volcano plots indicate -$\log_{10}$ (p-value) for proteins against their respective $\log_2$ fold change. They revealed several differentially regulated host and T5 proteins. Blue dots refer to T5 phage proteins, orange dots refer to significantly upregulated and downregulated host proteins and grey indicates no significant difference. The black line represents the significance threshold ($p < 0.05$) in the analysis. Data is derived from three biological replicates.

3.3.2 Temporal progression of T5 phage proteome

T5 phages are known to inject their genomic dsDNA via a two-step transfer process (Davison, 2015). In the first step transfer (FST), approximately 8 % of the genome is injected, and the translated proteins then enable the entry of the remaining dsDNA during the second step transfer (SST) (Lanni, 1968). The FST region contains 17 open reading frames (ORFs) that encode pre-early proteins while the SST region contains 119 ORFs corresponding to early proteins and 25 ORFs for late proteins (Wang et al., 2005). The early proteins of T5 are primarily involved in DNA replication, repair, transcription, and regulation, as well as in phage lytic processes, including proteins such as endolysin and holin (Wang et al., 2005). In contrast, the late proteins are mainly structural and morphogenesis proteins (Wang et al., 2005). By hijacking the host's transcriptional and translational machinery, the early proteins drive the synthesis of phage-specific structural proteins, which are then assembled into mature virions. The complete replication cycle, from injecting the genome to lysing the host cells, takes approximately 50-60 minutes (Sirbasku and Buchanan, 1970a) (Fig 3.13 A).

The T5 phage proteome was found to be similar between the wild type and Δ*rlmF*Δ*rlmJ* mutant (Fig. 3.13 B and C). Moreover, the T5 phage proteome analysis revealed an increase in the abundance of T5-related proteins throughout the infection, indicating the dynamic progression of T5 infection in both strains (Fig. 3.13 B). At 15 min post-infection, 86 % of the annotated T5 proteins were detected (Fig. 3.11 A and B). By 35 minutes, this increased to 91 % of the annotated T5 proteins, accounting for roughly 22 % of the total LFQs (Fig. 3.11 B). This increase in the proportion of T5 proteins corresponds to the expression of late-phase proteins, which showed a consistent increase in abundance from 15 to 35 min (Fig. 3.13 C). Certain late proteins such as D20 (major capsid proteins), N4 (major tail protein pb6) and N5 (decoration protein) exhibited higher abundance at 15 min compared to other late proteins (Fig 3.13 C). The analysis also uncovered distinct patterns among pre-early and early proteins (Fig. 3.13 C). The majority of early proteins such as D5 (putative transcriptional factor), D6 (putative replicative DNA helicase), D11 (probable ssDNA-binding protein), and DUT (deoxyuridine 5'-triphosphate nucleotidohydrolase) demonstrated an increase in abundance throughout the infection process. Conversely, some early proteins such as T5.083 (cell wall hydrolase SleB domain-containing protein) and ORF7

(hypothetical phage protein) exhibited stability, while others, like ORF20 (hypothetical phage protein) and T5.097 (hypothetical phage protein), displayed a discernable decrease in abundance.

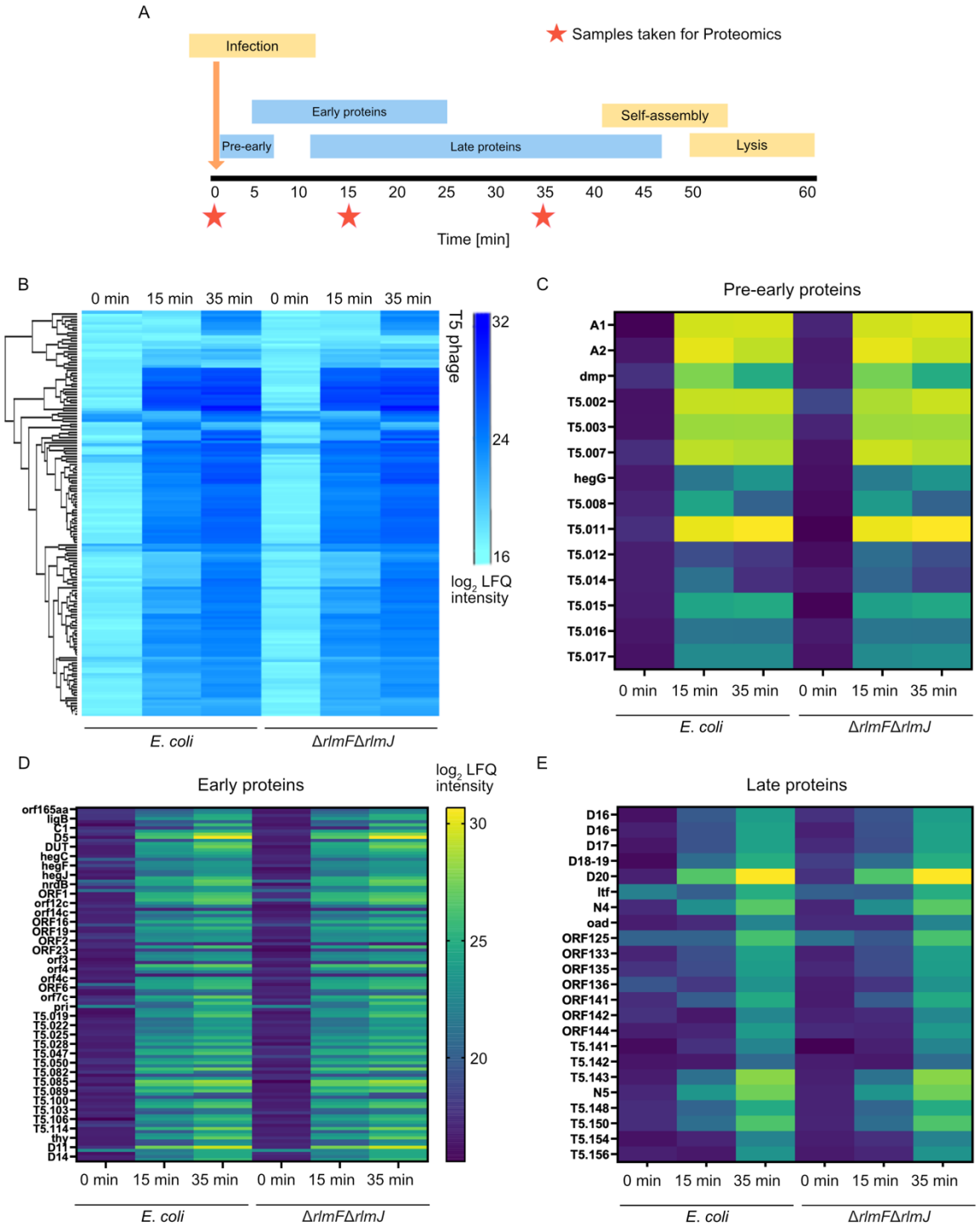

Figure 3.13 Analysis of T5 phage proteome over the course of infection in *E. coli* wild type and Δ*rlmF*Δ*rlmJ* mutant. A) Schematic representation of time-dependent infection-phase-specific protein

expression during T5 phage infection (Sirbasku and Buchanan, 1970b, 1970a). The red star denotes the time at which the samples were collected and subjected to dual-proteome analysis. B) Hierarchical clustering heatmap of all the clustered T5 protein log_2-LFQ intensity over the time course of infection with *E. coli* or Δ*rlmF*Δ*rlmJ* mutant. Y-axis represents functionally clustered T5 proteins. C) Heatmap representation of log_2-LFQ intensities of pre-early, early and late proteins of T5 phage throughout infection with *E. coli* or Δ*rlmF*Δ*rlmJ* mutant. Y axis represents that T5 phage proteins temporally classified into pre-early, early and late proteins (Wang et al., 2005). Data is derived from three biological replicates.

A subset of pre-early proteins such as A2, Dmp (5'-deoxynucleotidase), T5.008, T5.012 and T5.014 decreased in abundance as the infection progressed from 15 min to 35 min (Fig. 3.12 and 3.13 C). In contrast, other pre-early proteins — A1, T5.002, T5.003, T5.007, T5.011, T5.015 (DNA endonuclease), T5.016, and T5.017 — remained stable over the same period (Fig. 3.13 C), despite the shutdown of FST-DNA transcription by A1 protein within 3-4 minutes of infection (Davison, 2015). In addition, HegG, a putative H-N-H endonuclease, increased in abundance from 15 min to 35 min (Fig. 3.13 C), distinguishing it from other pre-early proteins and suggesting a more complex regulatory mechanism controlling the expression of pre-early proteins throughout the infection cycle. These findings highlight the similar dynamic progression and temporal regulation of T5 protein expression in both host strains during infection.

3.3.3 Host proteome stability and changes during T5 infection

The dual-proteome analysis revealed that some host proteins increased or decreased in abundance while others remained stable over the course of T5 infection in both wild-type and Δ*rlmF*Δ*rlmJ E. coli* strains (Fig. 3.12). FhuA, the ferrichrome outer membrane transporter that also functions as the receptor for T5 phage, showed no significant change in abundance during infection across both strains (Fig. 3.14). Similarly, RpoA, the RNA polymerase subunit alpha, remained stable during T5 infection (Fig. 3.14). However, a significant difference between wild type and Δ*rlmF*Δ*rlmJ E. coli* was observed in the CP4-44 cryptic prophage region, specifically in the abundance of Flu (Antigen 43) — a key determinant for auto-aggregation — and inner membrane protein YeeR. These two proteins are predicted to be part of the putative *flu-yeeR* operon, which is reported to be repressed by OxyR, an oxidative stress regulator (Ju et al., 2021). It is noteworthy that the

difference in abundance of Flu and YeeR was already discernible between the uninfected host strains (0 min) and remained unaltered throughout the course of T5 infection (Fig. 3.14). This observation suggests that this discrepancy is an inherent attribute of the host strains as opposed to a response to T5 infection. In the Δ*rlmF*Δ*rlmJ* mutant, both Flu and YeeR were significantly less abundant than in the wild-type strain (Fig. 3.14), implying a potential impact of the deletion of *rlmF* and *rlmJ* on the regulation of this operon.

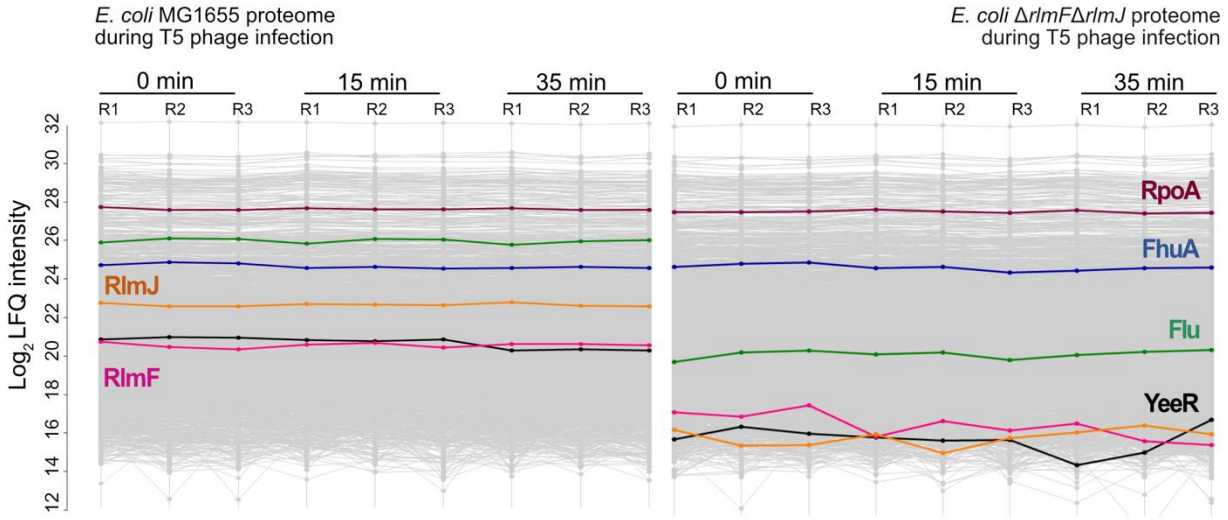

Figure 3.14 Proteomes of *E. coli* wild type and Δ*rlmF*Δ*rlmJ* mutant during T5 phage infection. Log_2 LFQ intensities of the host proteins are shown for the three biological replicates across time points (0 min [before infection] and 15- and 35-min post-infection). Specific proteins are highlighted in different colours.

To confirm this at the transcript levels, infection time-dependent RT-qPCR was performed for *flu* and *yeeR* along with *rpoA* (Fig. 3.15 A). 16S rRNA was used as an internal reference to normalise basal transcriptional levels. Despite stable protein abundances, a decline in *rpoA* transcript levels was observed relative to 16S rRNA during T5 infection in both wild-type and Δ*rlmF*Δ*rlmJ E. coli* strains (Fig. 3.15 A). Similarly, *flu* and *yeeR* transcripts in *E. coli* wild type showed a decline during infection (Fig. 3.15 A) despite stable protein levels (Fig. 3.14). In the Δ*rlmF*Δ*rlmJ* mutant, *flu* and *yeeR* transcripts were significantly downregulated compared to the wild type, both in the uninfected control (0 min) and through the course of T5 infection (Fig. 3.15 A). This finding aligns

with the observed lower protein abundances in the *E. coli* Δ*rlmF*Δ*rlmJ*. To understand if the low transcript abundance of *flu* was due to reduced transcription or post-transcriptional regulation, such as transcript instability or degradation, promoter fusion of *flu* (P_{flu}-*mNeonGreen*) was integrated at the native locus in wild type and Δ*rlmF*Δ*rlmJ E. coli*. Cells expressing mNeonGreen reporter under the control of the *flu* promoter were grown to an OD_{600} of 1.0 and analysed using fluorescence microscopy (Fig. 3.15 B and C). Fluorescence intensities were measured as a readout for *flu* promoter activity.

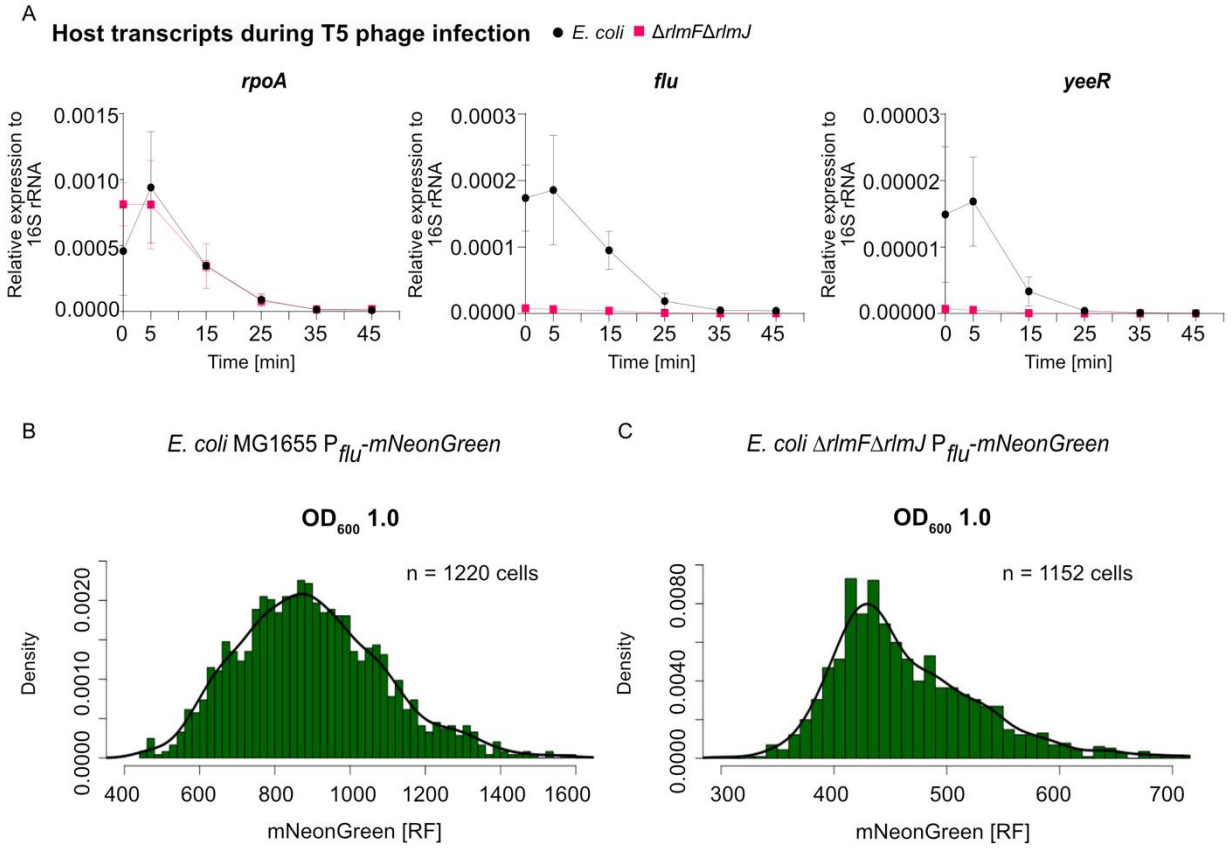

Figure 3.15 Assessment of transcript levels and promoter activities. A) Transcript levels of *rpoA*, *flu* and *yeeR* from *E. coli* wild type and Δ*rlmF*Δ*rlmJ* mutant were quantified using RT-qPCR. Data is acquired from three biological replicates, each with two technical replicates. Wild type and Δ*rlmF*Δ*rlmJ E. coli* transcriptional reporters were constructed by fusing the promoter region of *flu* with *mNeonGreen*. *E. coli* MG1655 P_{flu}-*mNeonGreen* (B) and *E. coli* Δ*rlmF*Δ*rlmJ* P_{flu}-*mNeonGreen* (C) were grown to an OD_{600} of 1.0 and the cells were analysed by fluorescence microscopy. The distribution of the relative fluorescence intensities (RF) from *E. coli* MG1655 P_{flu}-*mNeonGreen* (B) and *E. coli* Δ*rlmF*Δ*rlmJ* P_{flu}-*mNeonGreen* (C)

are depicted in the form of density histograms, wherein the y-axis represents the density, calculated as the frequency of observations in each bin divided by total number of observations and width of the bin. Each bin represents the relative frequency of the corresponding class of fluorescence intensities. Data is derived from one biological replicate.

Density histograms of relative fluorescence intensity (RF) revealed distinct subpopulations in both host strains (Fig. 3.15 B and C). The mean RF of *E. coli* wild type was recorded at 898, while that of *E. coli* Δ*rlmF*Δ*rlmJ* was 466 (Fig. 3.15 B and C). This finding indicates that the average promoter activity of the Δ*rlmF*Δ*rlmJ* mutant was lower than that of the wild type. This was consistent with the observed transcript abundance (Fig. 3.15 A), suggesting that the lower transcript levels in the Δ*rlmF*Δ*rlmJ* mutant were primarily due to reduced promoter activity and, consequently, lower transcription. Thus, the lower abundance of Flu in *E. coli* Δ*rlmF*Δ*rlmJ* is an intrinsic characteristic of the strain as confirmed by dual-proteomic analysis, RT-qPCR and promoter activity studies. Moreover, Flu can be evaluated as a proxy for m^6A-RNA modification by employing a fluorescently tagged *flu*-based translational reporter.

The differential protein abundance analysis revealed a significant increase or decrease in host protein abundance in response to T5 phage infection (Fig. 3.12). Gene Ontology (GO) analysis was performed to elucidate the functional roles of differentially abundant host proteins, including the biological pathways and processes in which they are involved. For *E. coli* wild type (15 min vs 0 min post-infection), proteins with increased abundance were primarily involved in the peptide transport and metabolic processing of glucarate, glyoxylate and aldaric acid (Fig. 3.16). In contrast, proteins with decreased abundance in *E. coli* wild type (15 min vs 0 min post-infection) were significantly enriched in pathways associated with bacterial transcription and motility (Fig. 3.16). Moreover, as the infection progressed in the Δ*rlmF*Δ*rlmJ* mutant, host proteins involved in bacterial transcription, defence systems and motility were significantly downregulated (Fig. 3.16). In both wild-type and Δ*rlmF*Δ*rlmJ* mutant strain, there was a significant downregulation of flagellar component proteins, particularly flagella basal-body and hook-related proteins FlgB and FlgC (Fig. 3.16).

***E. coli* MG1655 infected with T5 phage**

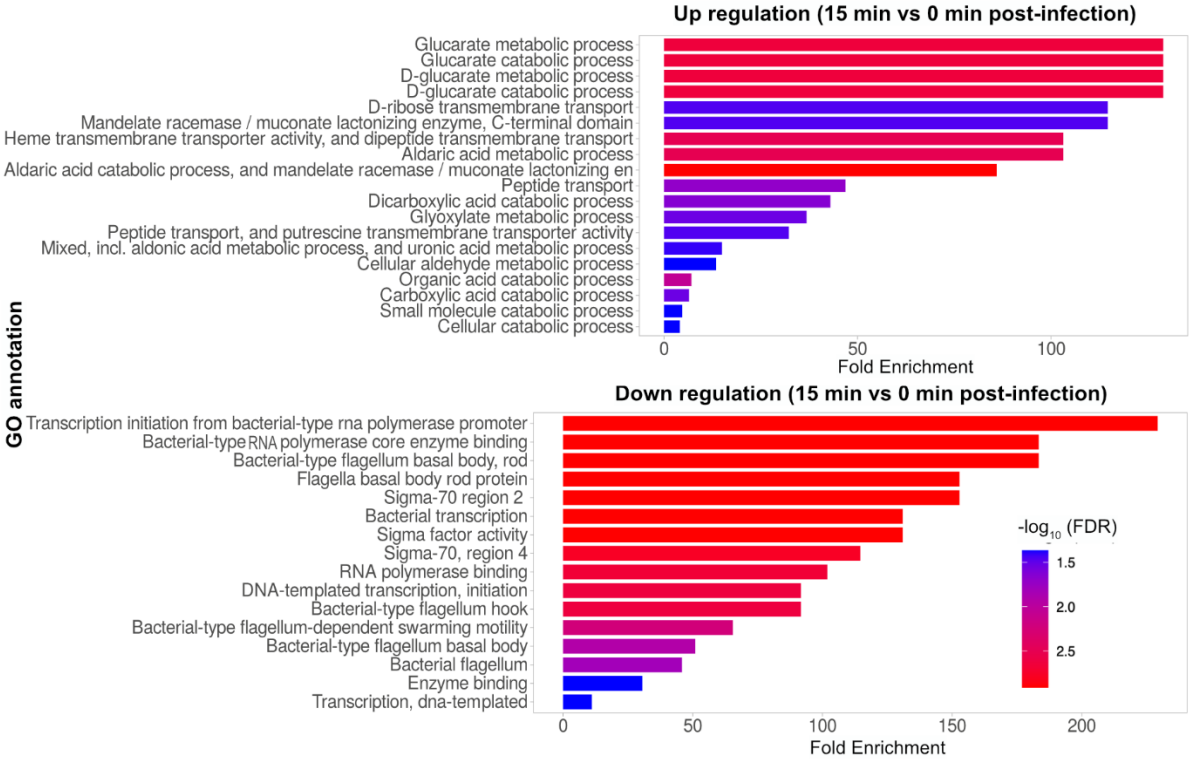

***E. coli* ΔrlmFΔrlmJ infected with T5 phage**

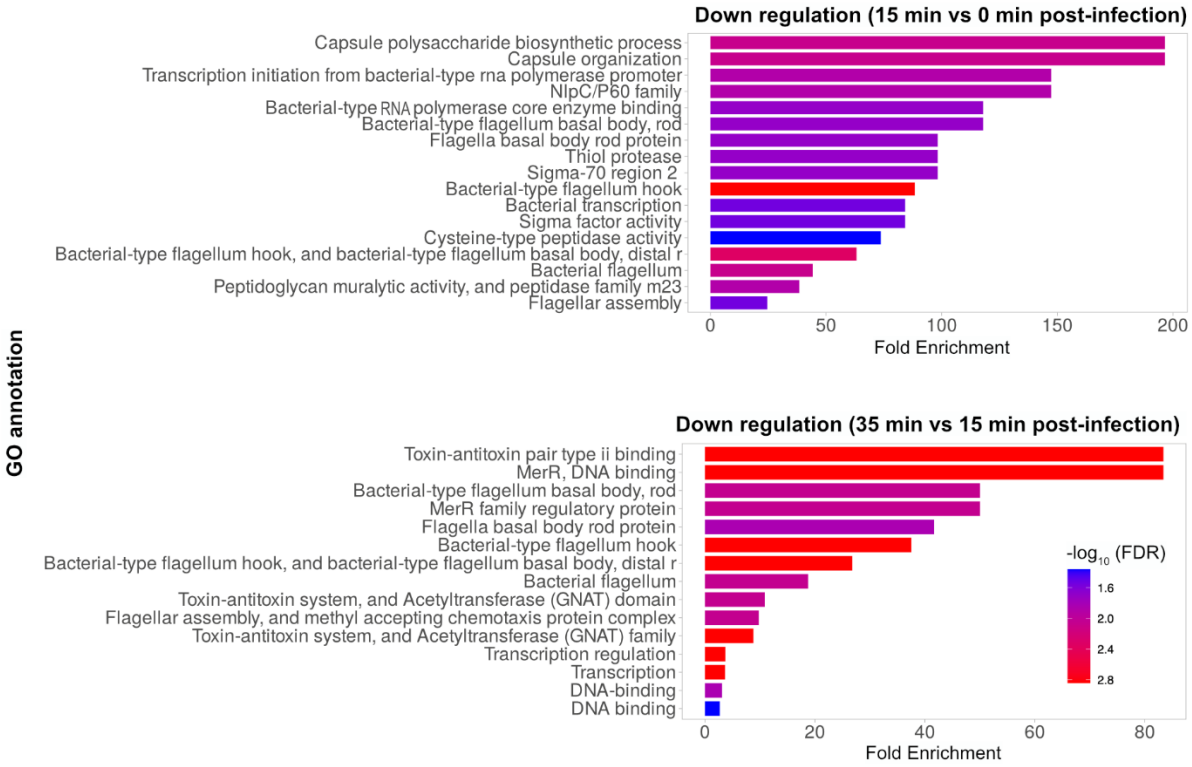

Figure 3.16 Significantly enriched Gene Ontology (GO) terms for host proteins in response to T5 phage infection. T5-infected *E. coli* MG1655 showed significant enrichment of GO terms for differentially upregulated and downregulated proteins comparing 15 min to 0 min post-infection. T5-infected *E. coli* Δ*rlmF*Δ*rlmJ* showed significant enrichment of GO terms for differentially downregulated proteins comparing 15 min to 0 min and 35 min to 15 min post-infections. Functional enrichment analysis was performed for host proteins using data from volcano plots (Fig. 3.12) and visualised using ShinyGo v0.74 (Ge et al., 2020).

Several differentially abundant host proteins (35 min vs 15 min post-infection) during T5 phage infection in the *E. coli* wild type were visualised in the volcano plots (Fig. 3.12) but these proteins did not reveal significant enrichment of any biological pathway. This suggests that the observed changes in the protein abundances were either too small to impact entire pathways or too spread across different biological processes to reach statistical significance. Similarly, many host proteins also increased in abundance in the *E. coli* Δ*rlmF*Δ*rlmJ* mutant strain during T5 infection (Fig. 3.12), functional annotation analysis did not reveal significant enrichment of any biological pathways. Although volcano plot analyses are a routine method in proteomics for rapid identification of differentially abundant proteins, their limitation to pairwise comparisons make them less suitable for the purpose of monitoring temporal dynamics during infection studies. Moreover, volcano plot analyses may sometimes ignore small but biologically relevant changes, making them less effective method for studying subtle changes within the proteome.

3.3.4 Differential regulation of ribosome and translation-related proteins

In pursuit of detailed insight into the expression patterns of host proteins over the infection timeline from 0 min to 35 min, a weighted gene co-expression network analysis (WGCNA) was performed. The analysis is sensitive to low abundance proteins and small fold changes (Rezaie et al., 2023) which makes it ideal to study subtle yet biologically relevant changes in protein abundance throughout the infection course. WGCNA identified clusters of proteins (called modules) based on expression patterns and offered glimpses into the temporal shifts in host protein responses during T5 infection (Fig. 3.17). Functional enrichment analysis of the identified modules revealed

enrichment in KEGG (Kyoto Encyclopedia of Genes and Genomes) pathways (Fig. 3.17) and GO terms.

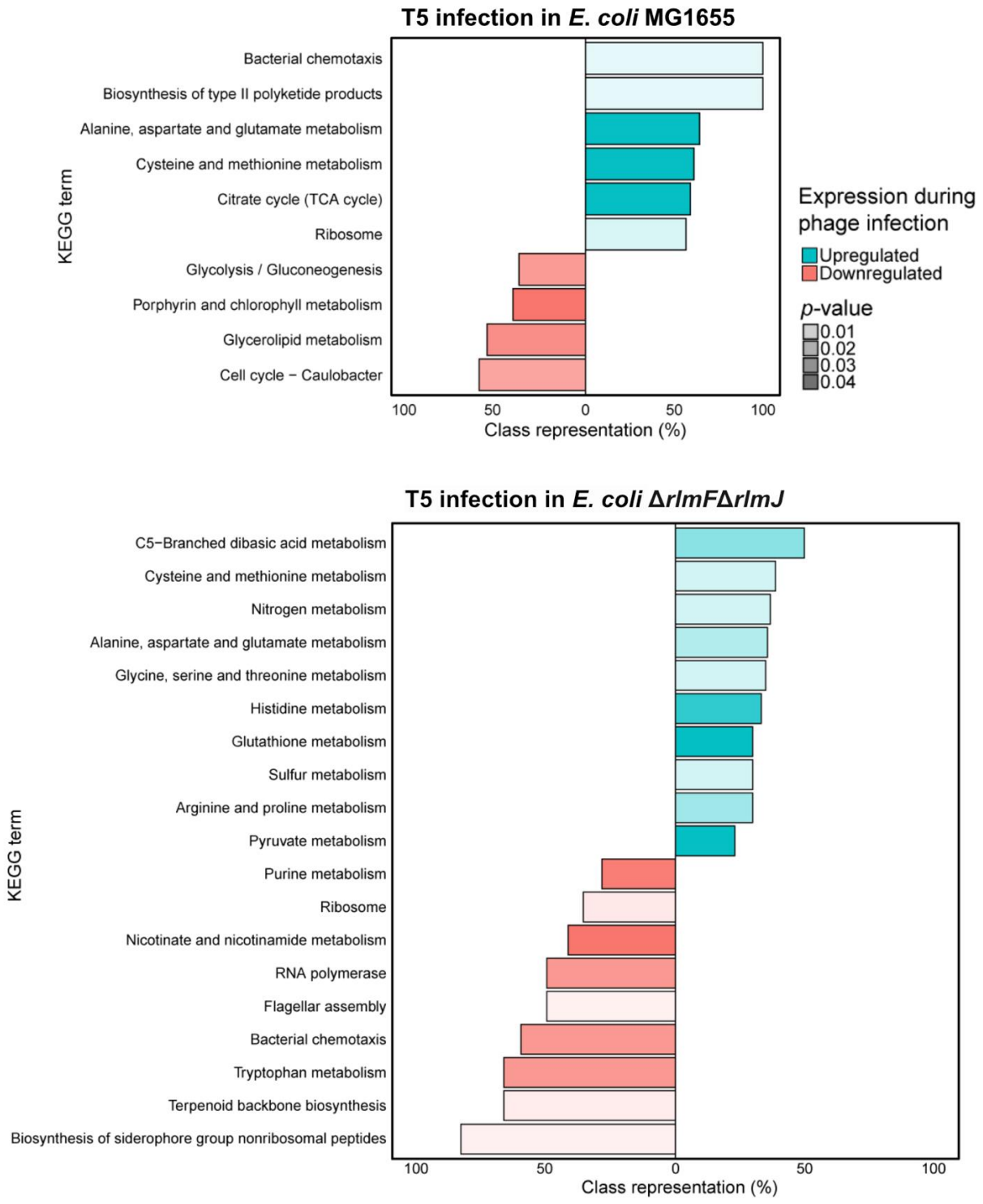

Figure 3.17 Significantly enriched KEGG terms among differentially regulated host proteins during T5 infection revealed by WGCNA analysis. Functional analysis was performed using FUNAGE-Pro v2 (de Jong et al., 2022). Data is derived from three biological replicates.

WGCNA revealed that the chemotaxis related pathway was significantly upregulated in wild-type *E. coli* strain, which contradicts the downregulation of flagella-basal body related GO terms observed for volcano plot analysis comparing 15 min to 0 min post-infection (Fig 3.16). The downregulated proteins in the volcano plot analysis (15 min vs 0 min) did not show significant enrichment in KEGG pathways which suggests that while individual flagellar proteins were affected (Fig. 3.12 and 3.16), they did not collectively form a well-defined KEGG pathway. This likely indicates T5 phage-driven reduction in flagella production to conserve energy during infection. WGCNA confirmed these findings, showing consistent downregulation of flagella basal body components in wild-type *E. coli* strain as demonstrated with GO (but not KEGG enrichment) analysis (Table 1.5). This suggests that structural components were affected, as captured by the relatively broad GO terms, but these components were not part of a single biochemical pathway.

Table 5: List of significantly enriched GO terms associated with chemotaxis and motility in response to T5 infection in *E. coli* wild type. Both upregulated and downregulated biological processes and their associated proteins are shown.

GO Class ID	GO term description	Proteins
Upregulation of biological processes during T5 infection in *E. coli* wild type		
GO:0097588	Archaeal or bacterial-type flagellum-dependent cell motility	CheZ, CheY, MotB, FliO
GO:0009425	Bacterial-type flagellum basal body	YcgR, FliG, FliL, FliM, FliN, FliO, FliP
GO:1902021	Regulation of bacterial-type flagellum-dependent cell motility	CheA, FliZ, PdeH, Tsr
GO:0050920	Regulation of chemotaxis	CheZ, Tar, CheA, Tsr
GO:0098561	Methyl accepting chemotaxis protein complex	Trg, Tar, CheA, Tsr

GO:0006935	Chemotaxis	Trg, CheZ, CheY, Tar, CheW, CheA, MotB, MotA, FliG, FliL, FliN, FliO, Aer, DppA, Tsr
Downregulation of biological processes during T5 infection in *E. coli* wild type		
GO:0030694	Bacterial-type flagellum basal body, rod	FlgB, FlgC

Since WGCNA is more sensitive and can detect subtle expression patterns by considering the collective behaviour of gene networks, it revealed upregulation of bacterial chemotaxis functions in KEGG pathways (Fig. 3.17). A large number of flagellar motor and chemotaxis-related proteins were upregulated upon infection, suggesting that, despite a reduction in flagellar basal body, rod synthesis or assembly, the increased motor activity of existing flagella may facilitate phage particle dispersion (Fig. 3.17 and Table 5). This could be phage-driven upregulation of bacterial motility to promote viral spread. However, this increase in motility may also help bacteria to escape high local phage concentrations, reducing adsorption risk, or enable migration to protective niches where phage access is limited. Thus, the increased abundance of motor proteins could serve also as a potential defence strategy against T5 infection.

In contrast, the Δ*rlmF*Δ*rlmJ E. coli* strain showed a drastic downregulation of flagella and chemotaxis-related proteins throughout T5 infection, as indicated by both the volcano plots WGCNA, with KEGG and GO annotations confirming this trend (Fig. 3.12, Fig. 3.16, Fig. 3.17 and Table 6). This suggests that, unlike the wild-type strain, the Δ*rlmF*Δ*rlmJ E. coli* fails to maintain flagella and chemotaxis function. As motility is an energy-driven process, and reduction in motility-related proteins allows energy and resources to be directed towards supporting the T5 infection.

Table 6: List of significantly enriched GO terms associated with chemotaxis and motility in response to T5 infection in *E. coli* Δ*rlmF*Δ*rlmJ*. Both upregulated and downregulated biological processes and their associated proteins are shown.

GO Class ID	GO term description	Proteins
Upregulation of biological processes during T5 infection in *E. coli* Δ*rlmF*Δ*rlmJ*		
GO:0009425	Bacterial-type flagellum basal body	FliG, FliL, FliO
Downregulation of biological processes during T5 infection in *E. coli* Δ*rlmF*Δ*rlmJ*		
GO:0030694	Bacterial-type flagellum basal body, rod	FlgB, FlgC
GO:0071973	Bacterial-type flagellum-dependent cell motility	FlgA, FlgB, FlgC, FlgF, FlgG, FlgH, FlgI, YcgR, MotA, FliC, FliD, FliS, FliF, FliH, FliI, FliN
GO:1902021	Regulation of bacterial-type flagellum-dependent cell motility	CheA, FliZ, Tsr
GO:0097588	Archaeal or bacterial-type flagellum-dependent cell motility	CheZ, CheY, MotB
GO:0044780	Bacterial-type flagellum assembly	FlgN, FlgA, FlhD, FliS, FliI
GO:0044781	Bacterial-type flagellum organisation	FlgM, FlgD, FliT, FliH
GO:0071978	Bacterial-type flagellum-dependent swarming motility	FlgD, FlgF, MotA
GO:0009424	Bacterial-type flagellum hook	FlgD, FlgF, FliD
GO:0009288	Bacterial-type flagellum	CheZ, FliH
GO:0050920	Regulation of chemotaxis	CheZ, Tar, CheA, Tsr
GO:0006935	Chemotaxis	Trg, CheZ, CheY, Tap, Tar, CheW, CheA, MotB, MotA, FliN, Tsr
GO:0098561	Methyl accepting chemotaxis protein complex	Trg, Tar, CheA, Tsr

In both wild type and Δ*rlmF*Δ*rlmJ E. coli*, proteins related to amino acid metabolism showed increased abundance during T5 infection (Fig. 3.17). Amino acids can mediate metabolic cross-talk in host-pathogen interactions (Ren et al., 2018). Key amino acids, such as arginine, asparagine,

and tryptophan are pivotal to the competition between the host and phage (Ren et al., 2018). The host might initiate amino acid metabolism to mount defensive responses. However, the phages can manipulate these pathways to enhance their replication and survival, exploiting the host's metabolic resources to its advantage. This increase in amino acid transport and metabolism is consistent in both strains, highlighting its strategic role during T5 infection.

Polyketides are specialised metabolites involved in a range of functions, including defence, communication, protection and virulence (Toopaang et al., 2022; Kai, 2019; Han et al., 2018). Despite the absence of polyketide production in *E. coli*, certain proteins implicated in the polyketide pathway, such as Dps and OxyR, are upregulated during T5 infection (Fig. 3.17), where they fulfil functions that are not related to polyketide synthesis. A study has shown that Dps and OxyR contribute to the downregulation of replication initiation in *E. coli* (Zhu et al., 2023). Moreover, an increase in alanine, aspartate and glutamate metabolism in *E. coli* wild type during T5 infection may influence the observed increase in abundance for proteins associated with tricarboxylic acid (TCA) cycle (Fig.3.17). Transamination of alanine and aspartate produces pyruvate and oxaloacetate, TCA cycle intermediates. Moreover, glutamate dehydrogenase and aspartate aminotransferase catalyse the reversible reaction between glutamate and α-ketoglutarate, the initial step for glutamate to enter TCA cycle metabolism. Therefore, alanine, aspartate and glutamate are metabolised to support TCA cycle intermediary metabolism and energy generation, thereby meeting the high anabolic demand for virion production.

Pathways associated with cell cycle in *E. coli* were downregulated in response to T5 infection (Fig. 3.17), suggesting phage-driven strategy to redirect host resources for phage replication, ensuring efficient virion production before host lysis. It is also notable that glycolysis, gluconeogenesis and glycerolipid metabolism pathways have significantly downregulated in *E. coli* wild type during T5 infection (Fig. 3.17). This suggests phage-driven host metabolic shutdown to redirect energy towards virion production. Moreover, some porphyrin-related proteins have decreased in abundance during T5 infection, possibly impacting cytochrome production. However, no significant enrichment of GO terms associated with electron transport chain function was observed during T5 infection which suggests ATP generation through oxidative phosphorylation may be reduced but not eliminated. This is indicative of a significant shift in the biosynthetic and energy requirements of the wild-type *E. coli* strain during T5 infection. Host metabolic and energy

pathways are also being reprogrammed in *E. coli* Δ*rlmF*Δ*rlmJ* mutant, wherein proteins associated with RNA polymerase and nicotinamide metabolism decreased in abundance during T5 infection (Fig. 3.17). A reduction in RNA polymerase activity implies suppression of host gene expression in favour of increased expression of viral genes (Fig. 3.17). Moreover, *E. coli* Δ*rlmF*Δ*rlmJ* mutant does not produce terpenoids but it does generate basic terpenoid precursors which are essential for ubiquinone synthesis and sugar-carrier lipids for cell wall synthesis (Fujisaki et al., 1986). Pathways involved in these precursor generation are downregulated during T5 infection, suggesting phage-driven diversion of resources from host growth. This could also be a host defence mechanism to slow down T5 replication by affecting energy generation to sustain metabolic needs of the phage.

Interestingly, WGCNA analysis also revealed differential regulation of ribosome-related proteins during T5 infection between wild-type and Δ*rlmF*Δ*rlmJ E. coli* strains (Fig. 3.17 and Fig. 3.18). The observed increase in ribosome-related proteins in the wild-type strain suggests an adaptive host response to T5 infection (Fig. 3.17). This response may be aimed at meeting the protein synthesis demands during phage infection. This is in contrast to the *E. coli* Δ*rlmF*Δ*rlmJ* strain, in which ribosome-related proteins decreased in abundance during T5 infection (Fig. 3.17), indicating a diminished translational response, likely linked to the absence of m^6A-rRNA modification. Significantly enriched GO terms among differentially regulated ribosome-related proteins revealed functional pathways impacting ribosome biogenesis and processing, structural constituent of ribosome, rRNA modification and regulation of translation (Fig. 3.18). This contrast highlights the role of m^6A modification in maintaining ribosomal stability and/or efficient protein synthesis under T5 phage-induced stress. Interestingly, there was an increase in abundance of RlmC and RlmD methyltransferases during T5 infection in *E. coli* wild type (Fig. 3.18). RlmC and RlmD are responsible for the methylation of the 23S rRNA at the U747 and U1939 nucleotide, respectively (Madsen, 2003). Moreover, there was a decrease in abundance of RlmKL, RsmG, RsmF and RsmB methyltransferases during T5 infection in *E. coli* Δ*rlmF*Δ*rlmJ* mutant (Fig. 3.18). RlmKL is responsible for the methylation of the 23S rRNA at positions G2445 and G2069 (Kimura et al., 2012) while RsmG is responsible for the methylation of the 16S rRNA at position G527 (Okamoto et al., 2007). RsmB and RsmF methylate the 16S rRNA at positions C967 and C1407, respectively (Andersen and Douthwaite, 2006; Gu et al., 1999). Such increase or decrease in ribosomal methyltransferases suggest T5-driven reliance on host ribosomes.

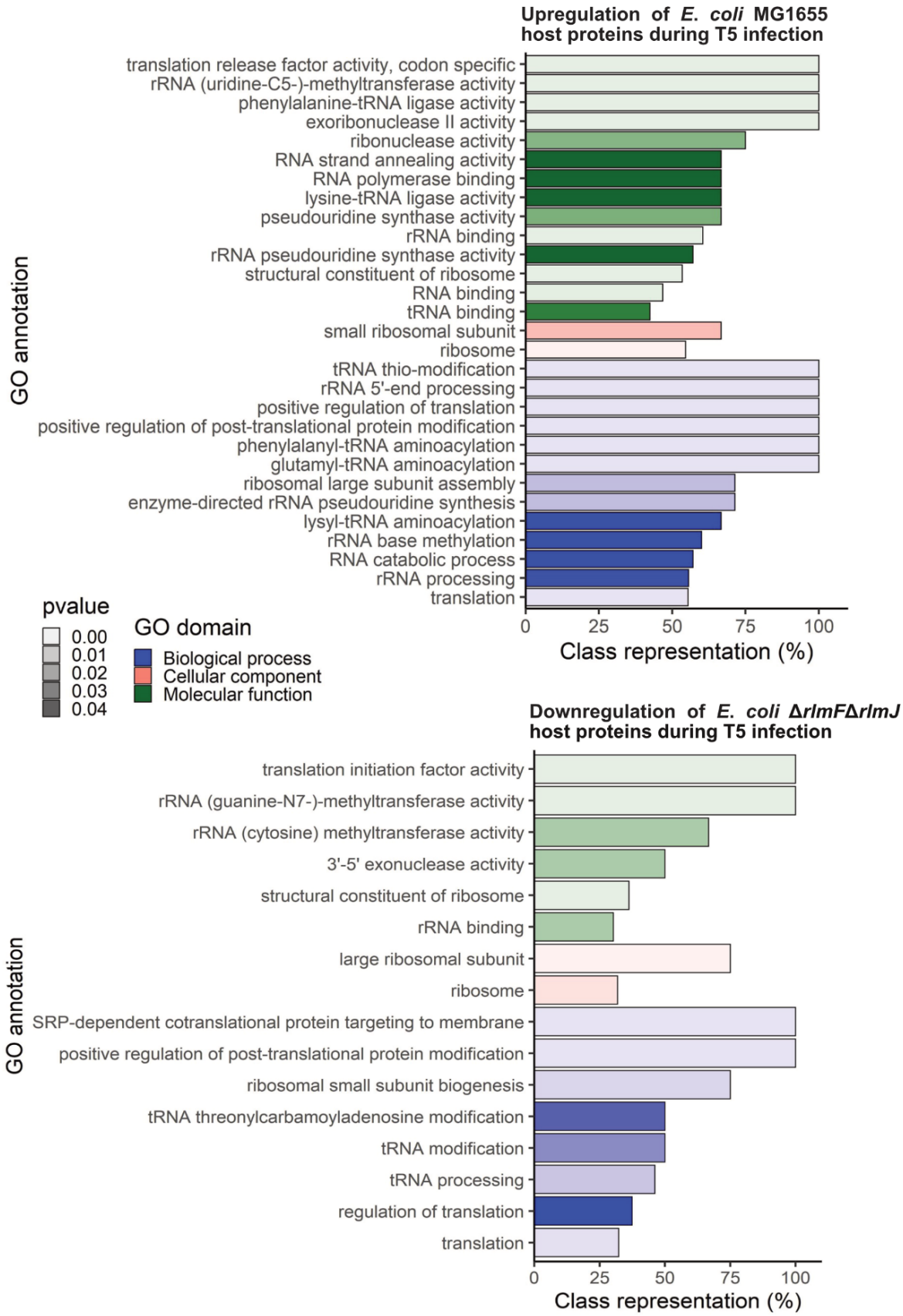
Upregulation of E. coli MG1655 host proteins during T5 infection
translation release factor activity, codon specific
rRNA (uridine-C5-)-methyltransferase activity
phenylalanine-tRNA ligase activity
exoribonuclease II activity
ribonuclease activity
RNA strand annealing activity
RNA polymerase binding
lysine-tRNA ligase activity
pseudouridine synthase activity
rRNA binding
rRNA pseudouridine synthase activity
structural constituent of ribosome
RNA binding
tRNA binding
small ribosomal subunit
ribosome
tRNA thio-modification
rRNA 5'-end processing
positive regulation of translation
positive regulation of post-translational protein modification
phenylalanyl-tRNA aminoacylation
glutamyl-tRNA aminoacylation
ribosomal large subunit assembly
enzyme-directed rRNA pseudouridine synthesis
lysyl-tRNA aminoacylation
rRNA base methylation
RNA catabolic process
rRNA processing
translation
GO annotation
0
25
50
75
100
Class representation (%)
pvalue
0.00
0.01
0.02
0.03
0.04
GO domain
Biological process
Cellular component
Molecular function
Downregulation of E. coli ΔrlmFΔrlmJ host proteins during T5 infection
translation initiation factor activity
rRNA (guanine-N7-)-methyltransferase activity
rRNA (cytosine) methyltransferase activity
3'-5' exonuclease activity
structural constituent of ribosome
rRNA binding
large ribosomal subunit
ribosome
SRP-dependent cotranslational protein targeting to membrane
positive regulation of post-translational protein modification
ribosomal small subunit biogenesis
tRNA threonylcarbamoyladenosine modification
tRNA modification
tRNA processing
regulation of translation
translation
GO annotation
0
25
50
75
100
Class representation (%)

Figure 3.18 Significantly enriched GO terms among differentially regulated ribosome-related proteins during T5 infection revealed by WGCNA analysis. Functional analysis was performed using FUNAGE-Pro v2 (de Jong et al., 2022). Data is derived from three biological replicates.

Following the functional annotation analysis, which revealed significant enrichment in ribosomal structure, biogenesis and translation pathways, the study was expanded to analyse the ribosomal subunits, 70S monosomes and polysomes. This was achieved by separating the ribosomal components using sucrose density centrifugation in uninfected and T5-infected wild-type and Δ*rlmF*Δ*rlmJ E. coli* strains. The polysome profile was then determined for each host strain under T5-infected and uninfected conditions by continuous monitoring of the absorbance at 260 nm. In the uninfected control samples, *E. coli* Δ*rlmF*Δ*rlmJ* mutant consistently demonstrated a lower peak for 70S monosomes in comparison to the wild type across three biological replicates (Fig. 3.19). This implies a reduction in the number of free 70S monosomes in the Δ*rlmF*Δ*rlmJ* mutant, suggesting that RlmF and RlmJ may affect ribosome availability or stability. Remarkably, in T5-infected samples, the trend was reversed - the mutant showed a slightly higher 70S monosome peak and a reproducible reduced number of polysomes as compared to the wild type.

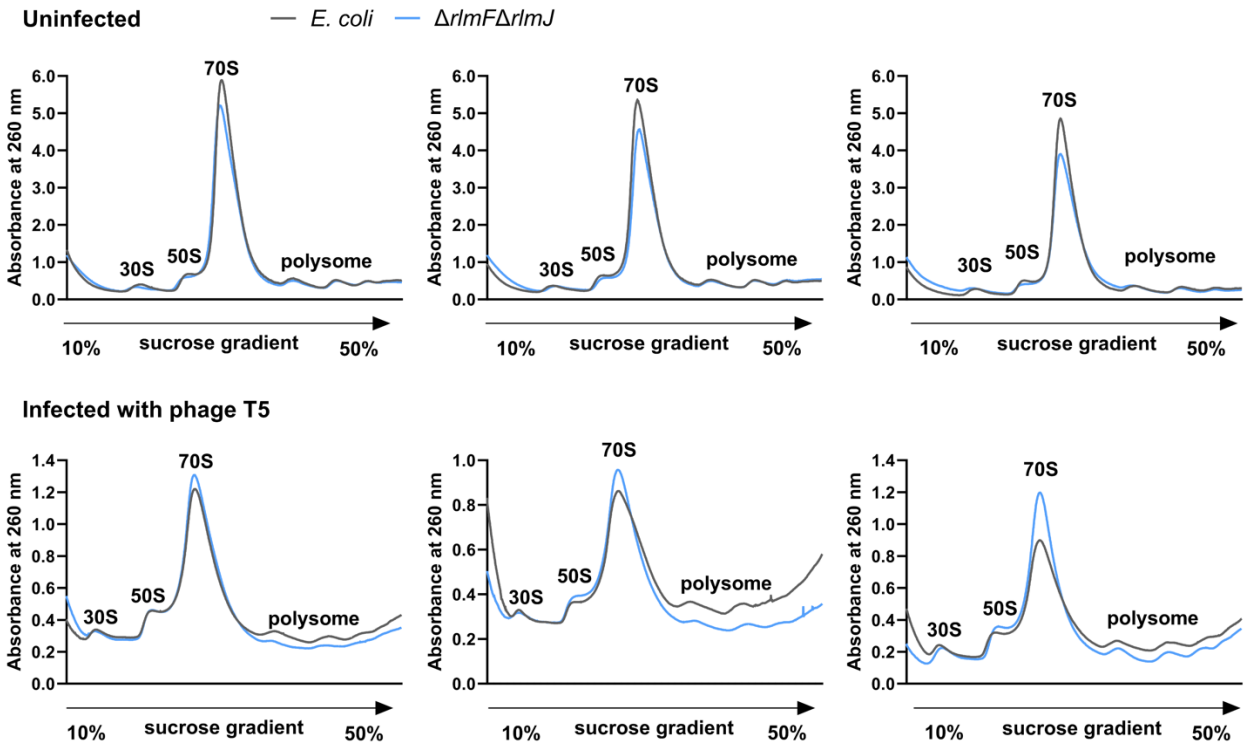

Figure 3.19 Polysome profile of uninfected and T5-infected *E. coli* wild type and Δ*rlmF*Δ*rlmJ* mutant. The host strains were infected with T5 phage at an MOI of 10 and centrifuged after 30 minutes of infection to collect the bacterial crude lysate. The crude lysate was processed and loaded onto a sucrose gradient. Ribosomal components were separated using sucrose density centrifugation, followed by continuous monitoring of the absorbance at 260 nm. Three biological replicates are shown of each condition and strain.

This finding suggests that the mutant, following T5 infection, may not utilise polysomes as effectively for translation or undergo slower translation. It can be hypothesised that the Δ*rlmF*Δ*rlmJ* mutant either has a greater number of free 70S monosomes or relies more on monsome-based translation, in contrast to the wild-type strain, which engages more actively in polysomal translation. The reliance on monosomes could result in a slower translation process.

3.3.5 Increased relative abundance of phage structural transcripts in the m^{6}A-RNA depleted mutant

To investigate the temporal regulation of T5 phage gene transcription, RT-qPCR was conducted on six phage genes, representing both the early and late stages of replication. The late-phase genes include *N4* (encoding major tail fiber protein) and *T5.150* (encoding prohead protease), while the early-phase genes include *C1* (encoding holin), *lys* (encoding endolysin), *orf3* (encoding tail assembly protein) and *T5.025* (capsid and scaffold protein). These genes were selected due to their involvement in one of the three biological roles during T5 infection: structural protein production, protein assembly or cell host lysis (Wang et al., 2005).

Wild-type and Δ*rlmF*Δ*rlmJ E. coli* strains were grown to an OD_{600} of 0.5 and infected with T5 phage at an MOI of 10 to ensure synchronous infection. Cells were collected at 0 (uninfected), 5, 15, 25, 35, and 45 min post-infection, followed by RNA extraction and DNAse I treatment. The RNA samples were then reverse transcribed, and qPCR was performed. Basal transcription was normalised using 16S rRNA from respective host. Late genes like *N4* and *T5.150* exhibit a temporal increase in transcript expression around 25 min post-infection with levels remaining stable through 45 min (Fig 3.20). Early genes demonstrate two distinct patterns of gene expression. In the first case, transcripts of *orf3* and *T5.025* are upregulated at 15 min post-infection, peak at this time and subsequently decline from 25 min to 45 min (Fig. 3.20). In the other case, transcripts

of *C1* and *lys* continue to increase progressively from 15 min to 45 min (Fig.3.20). Holin and Endolysin are essential for phage-induced host lysis and their gradual accumulation is critical to ensure proper timed host lysis. The early accumulation of these proteins could lead to premature host cell lysis, which may result in the dysregulation of the T5 infection.

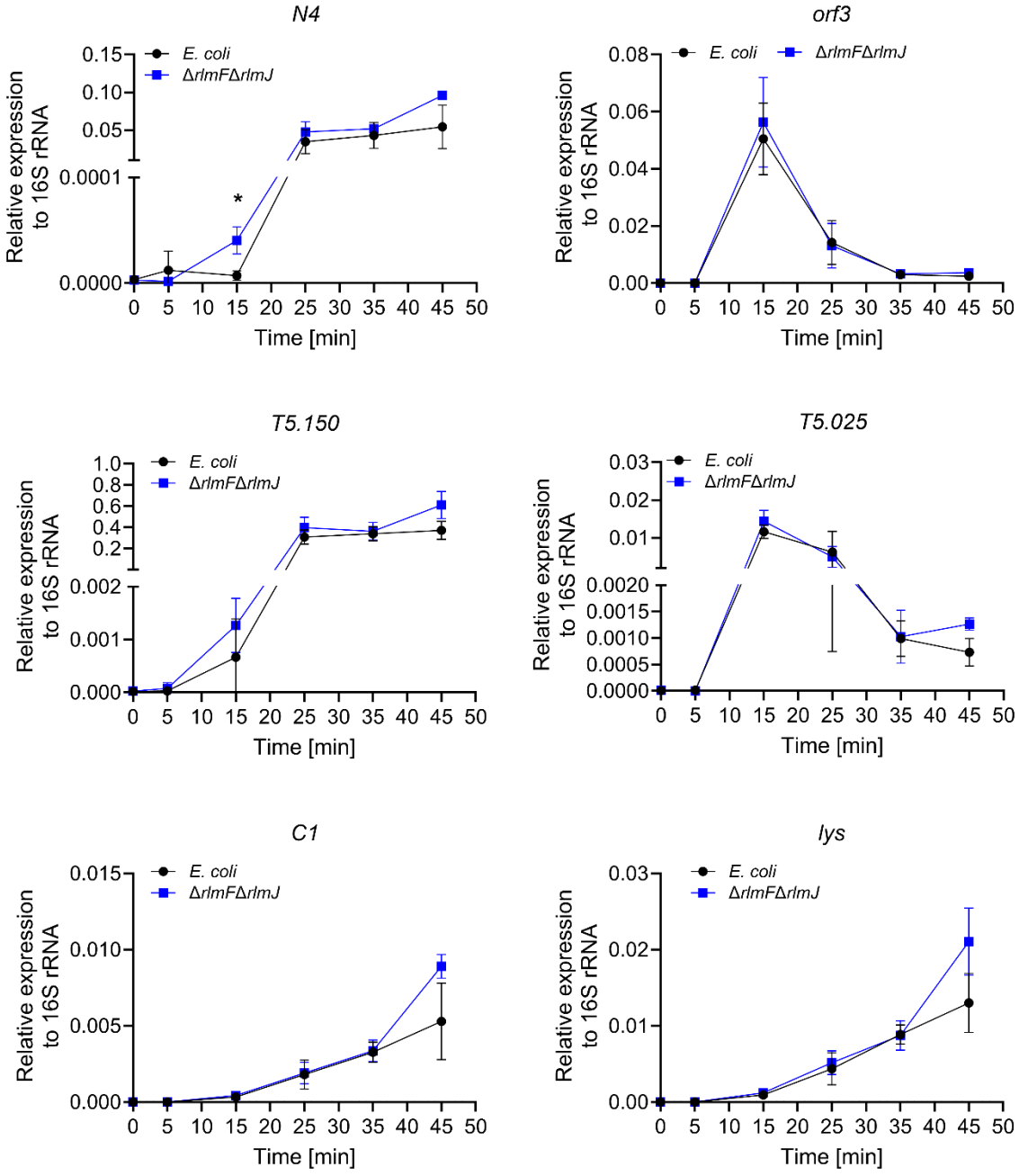

Figure 3.20 Comparison of six selected T5 phage genes during infection in *E. coli* wild type and Δ*rlmF*Δ*rlmJ* mutant. The expression profiles are presented as relative expression to 16S rRNA. Data is derived from three biological replicates and expressed as mean ± standard deviation. * $p < 0.05$ (Two-way ANOVA; Tukey's multiple correction test).

To compare gene expression between the wild-type and Δ*rlmF*Δ*rlmJ E. coli* strains, Pfaffl method (Pfaffl, 2001) was employed as it accounts for differences in primer efficiencies between the target gene and reference gene (i.e., 16S rRNA). The relative expression levels of the target genes in *E. coli* Δ*rlmF*Δ*rlmJ* were quantified by normalising against the wild type across all time points of infection. Time points of 0 min and 5 min were excluded from the analysis due to Ct values of the phage transcripts being similar to the minus RT values, suggesting their absence at these pre-early stages. The analysis revealed three phage transcripts that were more abundant at specific time points during T5 infection in the Δ*rlmF*Δ*rlmJ* mutant (Fig.3.21). Interestingly, all three transcripts encode structural proteins. Transcripts *N4* and *T5.150* were upregulated at 15 min post-infection, while *T5.025* showed increased expression at 45 min post-infection in the Δ*rlmF*Δ*rlmJ* mutant compared to the wild-type strain (Fig. 3.21). Overall, there is a pattern of differential phage transcript abundance. Such altered temporal regulation of certain phage transcripts in Δ*rlmF*Δ*rlmJ* mutant suggests a compensatory mechanism to maintain phage protein production at levels similar to the wild-type strain during T5 infection. The elevated transcript levels are likely indicative of reduced mRNA turnover or enhanced transcription, which is consistent with the requirement to sustain the protein demands associated with phage replication. Moreover, the reduced abundance of polysomes in the Δ*rlmF*Δ*rlmJ* mutant suggests that monosomes also play a compensatory role in maintaining essential T5 phage protein synthesis. Thus, this reliance on monosome-based translation, coupled with higher transcript abundance in the Δ*rlmF*Δ*rlmJ* mutant suggests an effective mechanism to ensure sufficient T5 protein production despite slower translation rates. This adaptive response emphasises the interplay between transcriptional and translational mechanisms in the absence of m^6A modification in the rRNA, highlighting the flexibility of the bacterial machinery.

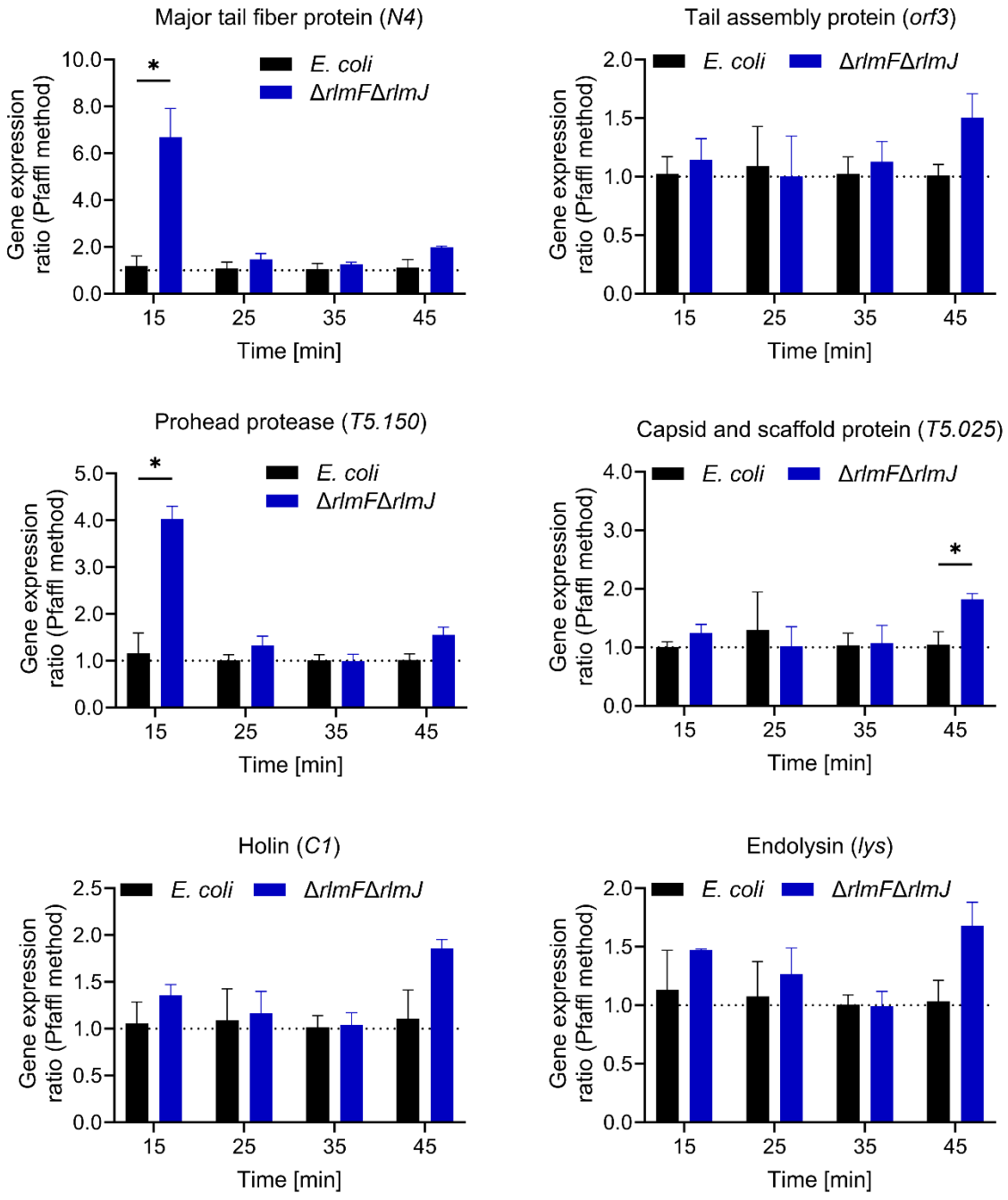

Figure 3.21 Assessment of gene expression levels by RT-qPCR. 16S rRNA was used as the internal reference gene. Pfaffl method was employed to calculate gene expression ratio. Data is derived from three biological replicates and expressed as mean ± standard deviation. * $p < 0.05$ (Two-way ANOVA; Tukey's multiple correction test).

3.4 MS2 and Qβ RNA genomes contain m^6A modifications

Part of this study was conducted in collaboration with Prof. Dr. Stefanie Kaiser Group at Goethe University, Frankfurt. Members of Prof. Kaiser group performed LC-MS/MS analysis with the samples to detect and quantify modifications.

Many eukaryotic RNA viruses, including HIV-1, HCV, ZIKV, DENV and IAV, are reported to carry m^6A modifications on their genomes and viral mRNAs (Imam et al., 2020). These modifications can either promote or suppress their infection. While the modifications present in eukaryotic RNA viruses have been the focus of extensive research, our understanding of modifications in prokaryotic RNA phages remains limited. To close this gap in knowledge, the presence of different modifications was investigated in the RNA genomes of MS2 and Qβ. The genomic RNA (gRNA) was isolated, and the modifications were detected and quantified by LC-MS/MS analysis. Several distinct modifications were identified in both phage genomes (Fig. 3.22). The MS2 phage genome was found to contain m^6A, m^7G, m^2A and $m^{6,6}A$ modifications, while the Qβ phage genome contains m^6A, m^7G and m^2A modifications (Fig. 3.22).

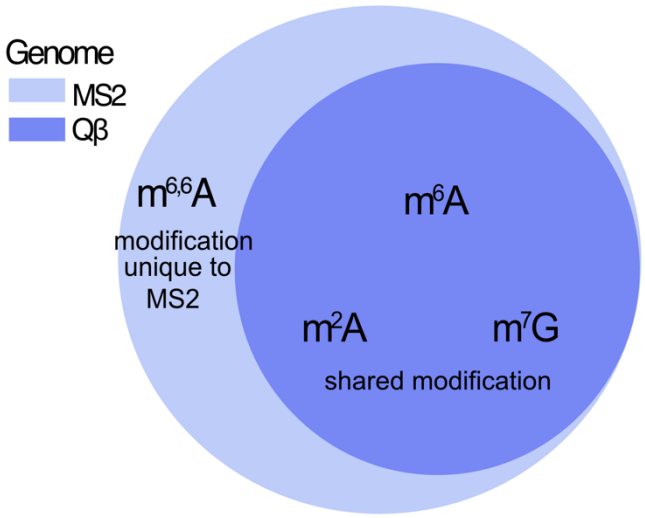

Figure 3.22 Modifications detected on the RNA genomes of MS2 and Qβ using LC-MS/MS analysis.

Quantitative analysis revealed the modification frequencies of various nucleosides in the gRNA of MS2 and Qβ (Fig. 3.23). The m^6A modifications occurred at approximately 0.04 nucleoside per gRNA in MS2 and 0.03 per gRNA in Qβ (Fig. 3.23). The m^7G modifications were observed to occur with greater frequency, with approximately 0.19 nucleoside per gRNA in MS2 and 0.15 per gRNA in Qβ (Fig. 3.23). With regards to m^2A, MS2 exhibited a modification frequency of 0.09 nucleoside per gRNA, compared to 0.05 per gRNA in Qβ (Fig. 3.23). Additionally, the $m^{6,6}A$ modification was detected exclusively in MS2, with a frequency of 0.175 nucleosides per gRNA (Fig. 3.23).

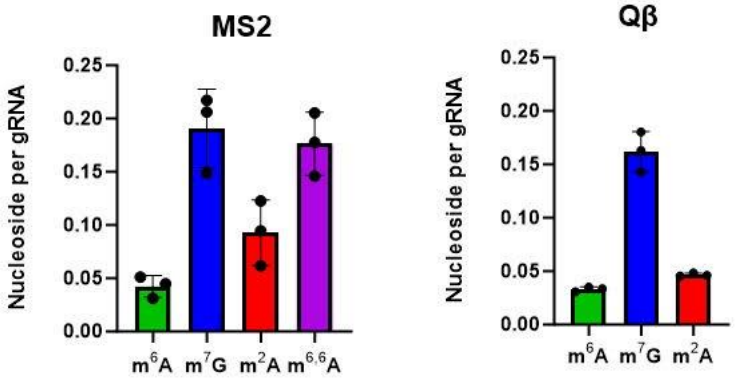

Figure 3.23 Modification frequencies of various nucleosides in the genomic RNA of MS2 and Qβ. Data is derived from three biological replicates.

3.4.1 Impact of RNA modifications on MS2 and Qβ phage infection

MS2 and Qβ are non-enveloped phages containing single-stranded positive sense RNAs (Bastin Guillaume, 2020). They have small genomes and encode four proteins – maturation protein, lysin protein, coat protein and β subunit of the replicase enzyme. Since they lack the necessary enzymes to introduce modifications in their genome, it is more likely that they utilise the host modification machinery to incorporate m^6A, m^7G, m^2A and $m^{6,6}A$ into their genomes. In *E. coli*, m^7G modifications are introduced by RsmG and RlmL, which target the rRNA (Kimura et al., 2012; Okamoto et al., 2007) while TrmB methylates the tRNA (De Bie et al., 2003). RlmN is the sole methyltransferase for m^2A modification in the 23S rRNA and tRNA (Benítez-Páez et al., 2012)

and RsmA is responsible for the addition of $m^{6,6}A$ modification in the 16S rRNA of *E. coli* (Poldermans et al., 1979).

The Keio collection was selected for the investigation of the potential involvement of host methyltransferases in modifying the phage gRNA. This collection offers single knockout mutants for all the mentioned methyltransferases known to add these modifications to the rRNA and tRNA of *E. coli* BW25113 (Baba et al., 2006). Furthermore, an m^6A-RNA depleted (Δ*rlmF*Δ*rlmJ*) *E. coli* MG1655 was already available for further analysis. *E. coli* BW25113 and *E. coli* MG1655 do not contain the F-plasmid which is necessary to form the F-pilus, that serves as the receptor through which ssRNA phages attach to the host cell and inject its genome. Since *E. coli* W1485 is the propagation host for MS2 and contains the F-plasmid, it was chosen as a suitable donor for conjugation. Each recipient strain was mixed with the donor strain to allow the transfer of F-plasmid, followed by selection of F+ recipients by plating on a minimal media without methionine. This ensures only F+ recipient cells to survive as *E. coli* W1485 is a methionine auxotroph. Further confirmation of the successful transfer of F-plasmid was done through PCR amplification of *traI* gene. The resulting strains containing the F-plasmid were used in infection assays with MS2 and Qβ to ascertain the role of modifications in the replication of these phages.

The investigation revealed that deletion of *rlmF* and *rlmJ* did not influence MS2 or Qβ replication in *E. coli* MG1655 (Fig. 3.24). Similarly, among the single knockout mutants tested from the Keio collection, none of them impacted the infection of Qβ (Fig. 3.24). Nevertheless, the knockout of *rsmG* or *rsmA* in *E. coli* BW25113 significantly impacted the infection of MS2 (Fig. 3.24). Infection assays were also conducted during the stationary-phase growth of the knockout strains to test whether the influence was reproducible. The results confirmed that the knockout of *rsmG* did not influence MS2 infection during stationary-phase growth. But, the knockout of *rsmA* in *E. coli* BW25113 significantly increased the plaquing efficiency of MS2 during both exponential and stationary-phase growth. These findings suggest that MS2 phage may impact bacterial survival rates differently between wild-type *E. coli* BW25113 and Δ*rsmA* mutant strains in liquid culture.

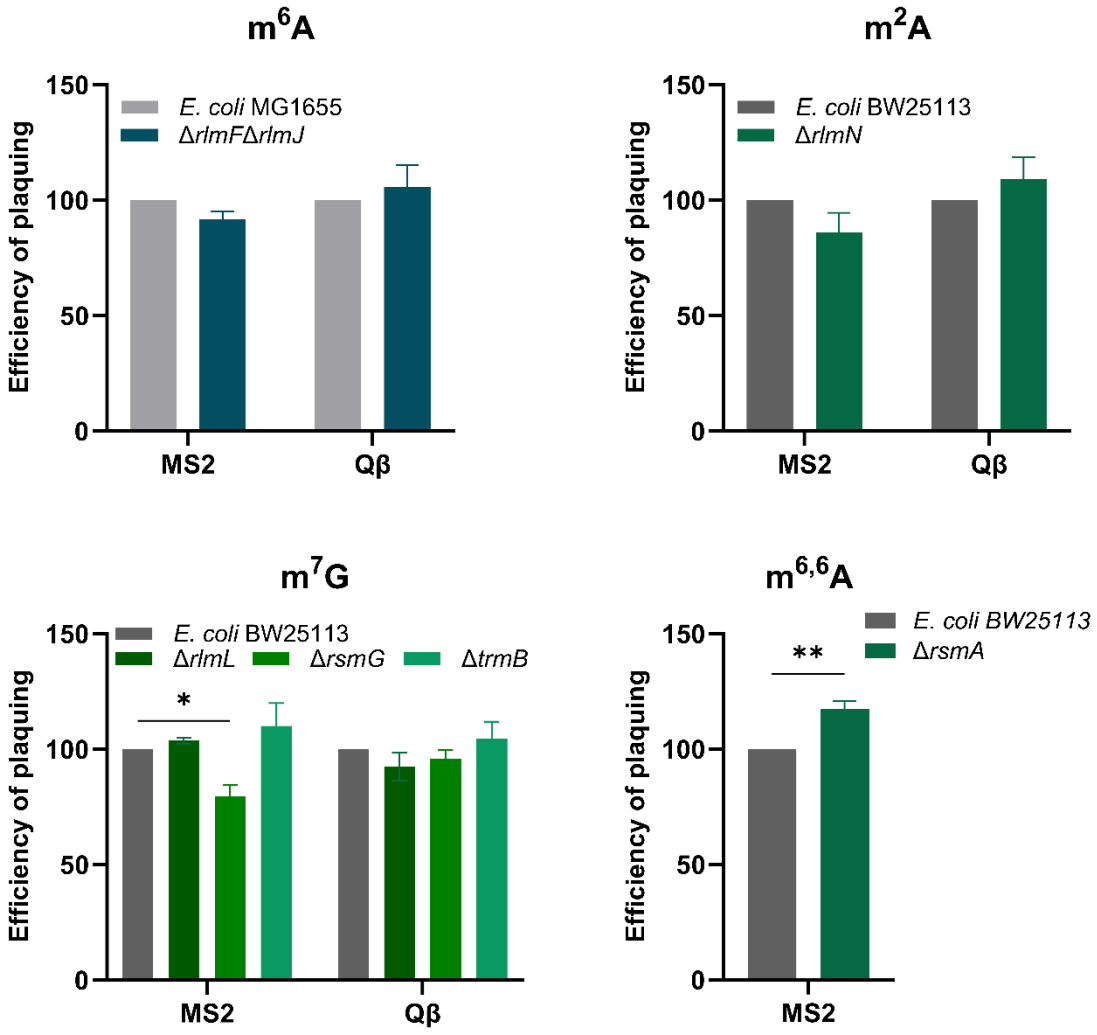

Figure 3.24 Effect of deletion of genes encoding different rRNA methyltransferases on the infection of MS2 and Qβ. All strains containing F-plasmid were grown to an OD_{600} = 0.5 and infected with MS2 or Qβ. The EOP was calculated as in Fig 3.4. The EOP of the wild type was set to 100. Data are presented as the mean ± standard deviation of three independent experiments. * $p < 0.05$, ** $p < 0.01$ (Student's *t*-test).

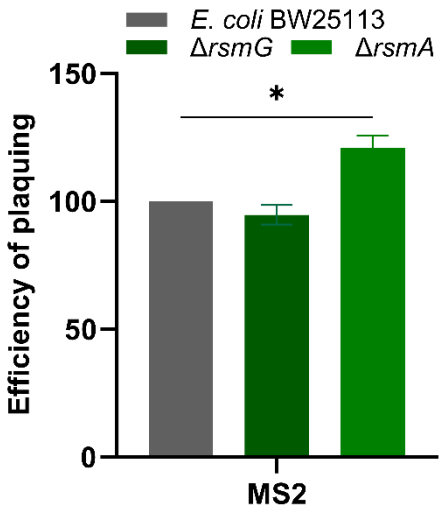

Figure 3.25 Efficiency of plaquing of phage MS2 to stationary phase *E. coli* BW25113 wild type and Δ*rsmG* mutant and Δ*rsmA* mutant. All strains containing F-plasmid were grown to an OD_{600} = 1.5 and infected with MS2. The EOP was calculated as in Fig 3.4. The EOP of the wild type was set to 100. Data are presented as the mean ± standard deviation of three independent experiments. * $p < 0.05$, (Student's *t*-test).

To test this hypothesis, bacterial growth experiments were conducted at MOI of 2.0 and 0.2. In the control experiment (Fig. 3.26), bacterial cells proliferated, and no lysis was observed. However, the addition of MS2 phage resulted in the lysis of bacterial cells, confirming that the observed phenomenon was a consequence of phage infection (Fig. 3.26). Although an earlier population collapse was observed when infected with MS2 at an MOI of 2.0 compared to 0.2, strain-specific differences in lysis timing are evident at both MOIs (Fig. 3.26). The Δ*rsmA* mutant is more susceptible to MS2 infection, as visualised by a faster decline in optical density and higher plaquing efficiency. Moreover, Δ*rsmA* exhibits faster and more robust recovery under both MOI conditions (Fig. 3.26).

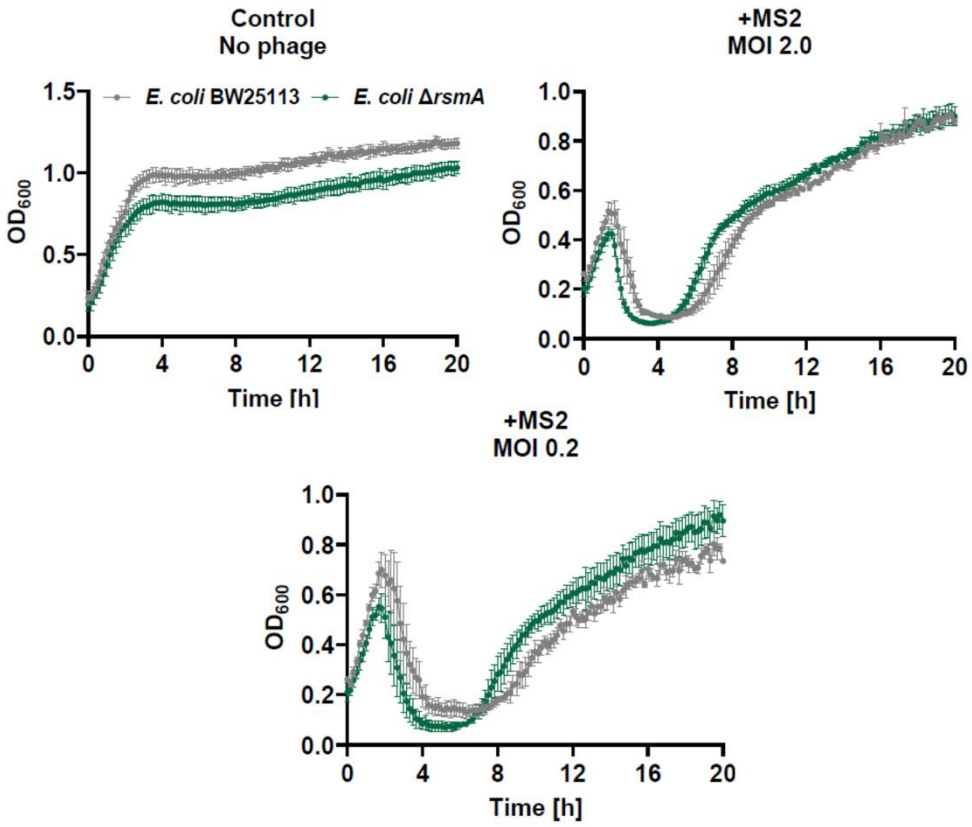

Figure 3.26 Survival curves of *E. coli* BW25113 wild type and Δ*rsmA* mutant in the absence (control) and presence of MS2 phage infection at different MOIs. Optical density was measured over time to assess growth dynamics and recovery. Data is presented as mean ± standard deviation from three biological replicates.

The peak bacterial density time and the extinction time were calculated from growth curve data (Fig 3.26) using the gcplyr package (Blazanin, 2024). In uninfected samples, both *E. coli* wild-type and Δ*rsmA* mutant strains reached peak density at approximately 3.5 h, with no substantial difference observed between the strains (Fig. 3.27). Under MS2 infection, peak bacterial density for both strains was fairly similar due to the high standard deviations that indicate variability in the measurements (Fig. 3.27). Moreover, extinction time was calculated, which measures the time required for the MS2 phage to reduce the bacterial density to an OD_{600} of 0.2. A clear trend emerged, showing that the Δ*rsmA* mutant consistently exhibited an earlier extinction time in comparison to the wild-type strain, particularly evident at MOI of 0.2 (Fig. 3.27).

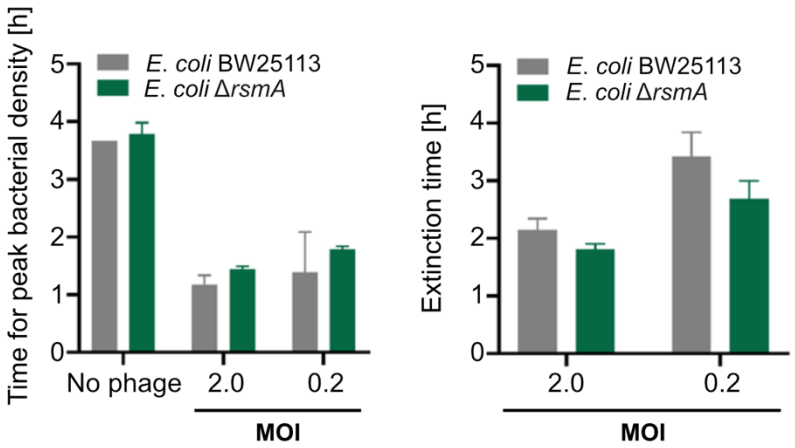

Figure 3.27 Peak bacterial density time and extinction time of *E. coli* BW25113 and Δ*rsmA* mutant during MS2 phage infection at different MOIs. Data is presented as mean ± standard deviation from three biological replicate.

These findings suggest that the deletion of *rsmA* in *E. coli* BW25113 increases susceptibility to MS2 phage infection, which aligns with the higher plaquing efficiency observed in the Δ*rsmA* mutant.

4 Discussion and Outlook

4.1 Discussion

Phage replication is a complex and time-sensitive process that is heavily influenced by various host and viral factors. Recent studies highlight the role of RNA-related modifications in influencing phage replication, particularly mediated by ADP-ribosyltransferases (ARTs) CmdT (Mets et al., 2024; Vassallo et al., 2024). As part of the CmdTAC (toxin-antitoxin-chaperone) defence system, CmdT catalyses the addition of ADP-ribose to phage transcripts, thereby blocking the translation of phage proteins (Vassallo et al., 2024). Another study showed that ARTs found in T4 phages play a role in influencing phage replication by post-translationally modifying several host proteins with ADP-ribose from the substrate NAD^+ (Depping et al., 2005; Tiemann et al., 2004; Koch et al., 1995; Goff, 1974). One of the ARTs found in T4 phage, ModB, can also utilise NAD-capped RNA as a substrate, leading to covalent attachment of RNA chains to host ribosomal proteins in a process termed RNAylation (Wolfram-Schauerte et al., 2023). The absence of functional ModB is linked to delayed cell lysis and reduced burst size, highlighting its significance in the T4 phage replication (Wolfram-Schauerte et al., 2023). Thus, the role of RNA modifications in phage replication is an evolving area of research, opening up possibilities for further exploration into phage-host dynamics.

This thesis provides the first insights into the impact of bacterial rRNA modifications on phage replication, particularly phage-host interactions and the molecular mechanisms influencing their life cycles. Among the various RNA modifications explored in this thesis, the primary focus is on m^6A, given its essential role in viral replication in eukaryotes (Horner and Reaves, 2024; Zhang et al., 2023; Baquero-Perez et al., 2021; Manners et al., 2019). This study employed a strain lacking the *rlmF* and *rlmJ* methyltransferases, responsible for adding m^6A to the 23S rRNA in *V. campbellii* and *E. coli*. Prophage inductions and replication dynamics of lytic phages were analysed in both wild-type and m^6A-RNA depleted (Δ*rlmF*Δ*rlmJ*) strains, thereby highlighting the role of RNA modifications in phage-host interactions.

Most bacteria commonly harbour multiple prophages that may or may not be induced into their lytic cycle. For instance, the *E. coli* genome contains nine prophage elements that are cryptic and

cannot be induced into their lytic cycle (Wang et al., 2010). Nonetheless, these elements are vital for withstanding unfavourable environmental conditions (Wang et al., 2010). In contrast, *V. campbellii* harbours six incomplete or cryptic prophage regions and four intact regions that are capable of induction into their lytic cycles (Lorenz et al., 2016). Among the inducible prophages, *Vibrio* kappa-like and ΦHAP-1-like have been demonstrated through TEM analysis, to enter the lytic phase when exposed to oxidative or heat stress (Lorenz et al., 2016). The major capsid proteins of these prophages were quantified using indirect ELISA, which revealed that induction of ΦHAP-1-like prophage was more pronounced than that of *Vibrio* kappa-like prophage in response to stress (Fig. 3.2). While the depletion of m^6A-RNA modifications was found to not affect prophage induction in *V. campbellii* (Fig. 3.2), other RNA modifications have been shown to regulate prophage induction (Gong et al., 2024). For example, a prophage-encoded RNA methyltransferase that specifically modifies 16S rRNA of Shiga-toxin-producing *E. coli* (STEC) has been identified, which can mediate the induction of Shiga toxin-encoding prophage (Gong et al., 2024). This study highlights a previously unidentified link between RNA modification, prophage activation and bacterial virulence.

The depletion of m^6A-RNA modification in *V. campbellii* did not influence the replication of the lytic phage Virtus (Fig. 3.3), indicating that lack of m^6A modification in the 23S rRNA is not critical for the lifecycle of the phage in this host. In contrast, among the lytic phages tested in *E. coli*, the T5 phage showed significantly reduced plaquing efficiency in the m^6A-RNA depleted mutant compared to the wild-type strain (Fig 3.4). This reduction was consistent across growth phases of *E. coli*, suggesting that m^6A-RNA modification plays a role in facilitating the infection or replication of the T5 phage (Fig. 3.5). Nevertheless, this trait is not conserved among T5-like phages from the BASEL collection, as only two (Bas29 and Bas30) out of nine exhibited a similar phenotype with a markedly less pronounced reduction in plaquing efficiency (Fig. 3.6). The diversity observed in phage-host interaction strategies among T5-like phages is consistent with findings reported in other studies (Maffei et al., 2021; Skutel et al., 2023). For example, T5-like phages used in this study display a considerable range of resistance to bacterial defence systems, such as CRISPR-Cas and restriction-modification (R-M) systems, with some phages showing robust evasion while others are more susceptible (Maffei et al., 2021; Skutel et al., 2023). Furthermore, all the T5-like phages that were tested use BtuB as their primary receptor for infection (Maffei et al., 2021), while phage T5 utilises FhuA to inject its genome. This non-

conservation reflects the evolutionary adaptability of closely related groups of phages to their specific hosts and environments.

The abundance of m^6A modification at position A2030 of the 23S rRNA, methylated by RlmJ, remained stable throughout the course of the T5 infection (Fig. 3.7). This observation leads to the inference that this modification is not dynamic and does not alter during the T5 phage lifecycle. In contrast, the m^6A modification at position A1618, methylated by RlmF, was not detected. This absence may be attributed to the low abundance of the modification, limitations in the detection sensitivity of Rol-LAMP or the environmental conditions used in the study. Interestingly, A1618 is situated within the peptidyl transferase centre (PTC) – a structurally dense and functionally essential region of the ribosome (Sergiev et al., 2007). The proximity of A1618 to the surrounding rRNA, RPs and tRNA interactions further restricts its accessibility, posing significant challenges for detection techniques such as Rol-LAMP. Despite this, the reduced plaquing efficiency observed in the m^6A-RNA depleted mutant suggests that the absence of these modifications collectively impacts the T5 phage lifecycle (Fig. 3.4 and 3.5). Moreover, m^6A-RNA depleted mutant exhibited delayed lysis in comparison to the wild-type strain, as evidenced by bacterial growth experiments and single-cell microscopy (Fig. 3.8). This effect was particularly salient at an MOI of 0.01, where the extinction time of the m^6A-RNA depleted mutant occurred approximately five hours later than that of the wild type, indicating a prolonged period of bacterial viability in the absence of the m^6A-RNA modifications (Fig. 3.8). Supporting this hypothesis, one-step growth curve analysis also revealed a delay in the rise period, which indicates asynchronous bursts (Fig. 3.9). While T5 phage adsorption was unaffected by the depletion of m^6A-RNA modifications (Fig. 3.9), ruling it out as a contributing factor, the observed asynchronous bursts may be attributed to delays in phage component assembly or the host cell lysis. Another key factor contributing to this phenomenon could be ribosomal heterogeneity within the bacterial population.

Ribosomal heterogeneity refers to the presence of distinct ribosomal populations within a cell, which can occur at the level of protein components and their post-translational modifications as well as rRNA sequences and their post-transcriptional modifications (Bickle et al., 1973; Byrgazov et al., 2013; Deusser, 1972; Deusser et al., 1974; Deusser and Wittmann, 1972; Gunderson et al., 1987; Milne et al., 1975; Ramagopal, 1990; Shi et al., 2017). *E. coli* has seven rRNA operons (*rrn*) that vary in their sequences as well as their regulatory features, particularly during different

bacterial growth phases and responses to heat shock or nutrient starvation (Condon et al., 1995, 1992; Hirvonen et al., 2001; Maeda et al., 2015). It has also been reported that *E. coli* grown in different media exhibited differential ribosomal protein (RP) abundance (Deusser, 1972; Deusser and Wittmann, 1972; Milne et al., 1975). Moreover, dynamic and differential rRNA modifications of 23S rRNA in the 50S subunit of *E. coli* ribosomes have been observed under stress conditions (Fasnacht et al., 2022; Byrgazov et al., 2013; Bügl et al., 2000). For instance, heat shock triggers the ribose methylation at nucleotide U2552 while oxidative stress leads to the oxidation of C2501 within the 23S rRNA (Fasnacht et al., 2022; Bügl et al., 2000). Thus, bacteria generate and utilise heterogeneous ribosomes to adapt and respond to environmental challenges.

Given that phage infection represents a critical environmental challenge and a form of biotic stress, the presence of both m^6A-modified and unmodified ribosomes in the wild-type strain may provide functional flexibility during T5 phage infection. This may potentially enhance the translational efficiency and stability for the optimisation of phage protein production and assembly, resulting in more synchronised lysis. A study conducted in *E. coli* reported that the degree of m^6A methylation in the ribosomes is around 70% which leaves a 30% margin for variability in the ribosomal composition (Petrov et al., 2022). This allows for diversification both within individual cells and across cell populations. In contrast, the m^6A-depleted mutant, which lacks m^6A modification and therefore has uniformly unmodified ribosomes, is unable to provide this flexibility. The absence of m^6A-modified ribosomes may result in inefficient translation of essential phage proteins, which could, in turn, delay processes such as phage component assembly and host cell lysis. This delay could contribute to the observed asynchronous bursts, whereby the variability in translation efficiency across the bacterial population amplifies the delays in lysis. It is therefore hypothesised that m^6A-modified ribosomes in the wild-type population serve to buffer such variability and play a critical role in the temporal progression of the T5 phage.

To confirm this hypothesis, a whole-cell proteomics-based approach was employed to analyse changes in the host and phage protein profiles during T5 infection in the wild-type and m^6A-RNA depleted strains (Fig. 3.10, 3.11 and 3.12). The phage protein profiles exhibited comparable dynamic and temporal regulation of T5 infection in both strains (Fig. 3.13). Previous studies have shown that this temporal regulation of T5 phage is driven by pre-early proteins such as A1 and the 11 kDa protein, which suppresses pre-early transcription and enable the expression of early genes

(Davison, 2015). Subsequently, the gpT5.026 protein ensures the initiation of late gene transcription, facilitating the later stages of T5 infection (Klimuk et al., 2020). The host protein profiles showed stability and changes in protein abundance during T5 infection. For instance, the receptor of T5 phage, FhuA, did not increase in protein abundance throughout the infection (Fig. 3.14). This complements the observed similar adsorption rates of T5 phage to *E. coli* wild-type and its m^6A-depleted mutant strain (Fig. 3.9 A). Moreover, the differential abundance of Flu and YeeR proteins, which are part of the CP4-44 cryptic prophage region (Ju et al., 2021), was observed among the host strains (Fig. 3.14). The m^6A-RNA depleted mutant showed significantly less abundance of Flu and Yeer in comparison to the wild-type strain (Fig. 3.14). This finding was further substantiated by promoter activity and transcript expression, which demonstrated that the m^6A-RNA depleted mutant exhibited diminished promoter activity of *flu*, consequently resulting in reduced transcripts in contrast to the wild type (Fig. 3.15). It can thus be concluded that the lower abundance of Flu is an intrinsic characteristic of the m^6A-RNA depleted mutant. This opens the possibility of using Flu as a proxy for m^6A-RNA modification by analysing fluorescently tagged *flu*-based translational reporter. Additionally, the host protein profiles throughout the course of T5 infection, as elucidated by weighted gene co-expression network analysis (WGCNA), revealed several significantly enriched biochemical pathways (Fig 3. 17). For instance, differential regulation of chemotaxis and motility-related pathways between the wild-type and m^6A-RNA depleted strains were observed (Fig. 3.17). Significant downregulation of flagella and chemotaxis-related pathways were observed throughout T5 infection in the m^6A-RNA depleted mutant while these pathways were upregulated in the wild-type strain (Fig. 3.17, Table 5 and Table 6). Of particular relevance was also the differential regulation of host ribosome- and translation-related proteins (Fig. 3.17 and 3.18). In the wild-type strain, an increase in ribosome-related proteins was observed, which may be indicative of altered ribosomal composition to meet the increased protein biosynthesis demands imposed by T5 phage infection (Fig. 3.17 and 3.18). Conversely, a reduction in ribosome-related proteins was observed in the m^6A-RNA depleted strain (Fig. 3.17 and 3.18). Proteins involved in ribosome biogenesis, rRNA processing, structural components of the ribosome, rRNA modifications, and processes related to translation and its regulation exhibited differential abundance between the host strains, suggesting a strong reliance on host ribosomes (Fig. 3.18). Phages exclusively rely on host translational machinery, which includes ribosomes and tRNAs, to translate their proteins. Although T5 phage carries its own set of tRNAs (Wang et al,

2005) that may participate in the translation of phage mRNA in a host with a different GC content or amidst the decaying pool of host resources, it does not encode its own ribosomal genes or proteins. Recent research on jumbo phage ΦKZ highlights phage proteins that target and co-opt host ribosomes, thereby modulating the host translational machinery (Gerovac et al., 2024). The protein ΦKZ014 remains bound to the host ribosomes during the entire translation cycle to effectively allow the translation of specific phage transcripts, fundamentally acting as a specialised ribosome (Gerovac et al., 2024).

The concept of specialised ribosomes was first described by Hui and de Boer in 1987, when they demonstrated that the altered Shine-Dalgarno (SD) sequence, located at the 5' untranslated region (UTR) of mRNA could not be effectively translated by wild-type ribosomes but regained expression when the anti-SD region of 16S rRNA was correspondingly changed. Moreover, the ribosomal protein (RP) S1 of the 30S subunit has the ability to bind to the 5' UTR of SD absent transcripts and initiate translation (Lauber et al., 2012; Tzareva et al., 1994; Boni et al., 1990). This drew attention to the binding specificity of transcripts to different components of the 30S subunit, proving it to be structurally and functionally heterogeneous (Van Duin and Van Knippenbero, 1974; Voynow and Kurlandf, 1971). However, the presence of a subpopulation of ribosomes lacking S1 protein in the 30S subunit immediately challenged the proposed non-discriminatory and homogeneous nature of the ribosomes (Delvillani et al., 2011; Moll et al., 2004, 2002b, 2002a). These S1-depleted ribosomes allowed effective translation of leaderless transcripts in *E. coli,* instigating specialised ribosomes to play a role in the selective functionality of the ribosomal translational machinery (Delvillani et al., 2011; Moll et al., 2004, 2002a, 2002b). Moreover, kasugamycin-induced stress in *E. coli* led to the formation of a specialised ribosome that lacked six RPs which could efficiently translate leaderless transcripts (Kaberdina et al., 2009). Other studies in diverse model organisms also revealed the presence of specialised ribosomes in Eukarya (Ramagopal, 1990). Therefore, specialised ribosomes are common and represent a subset of ribosomal heterogeneity that is specifically adapted to preferentially translate certain mRNAs.

Proteins involved in rRNA modifications and ribosomal components are also differentially abundant in both host strains during T5 infection (Fig. 3.18), highlighting the fair possibility of heterogeneous ribosomes. These differences in ribosomal protein levels may impact the distribution of ribosomal subunits, monosomes, and polysomes. Polysome profiling revealed an

increased 70S monosome peak and reduced polysome abundance in the m^6A-RNA depleted strain compared to the wild-type strain during T5 infection (Fig. 3.19). Increased polysome abundance in the wild-type strain indicates an increased protein biosynthesis burden on the host due to T5 phage infection. However, the reduced polysome abundance in the m^6A-RNA depleted mutant could highlight their inability to effectively utilise polysomes for active translation or preferentially undergo monosome-based translation for certain transcripts. This could explain the asynchronous bursts and the overall delay observed in the m^6A-RNA depleted strain, as confirmed in the growth experiments, single-cell microscopy and one-step growth curves. Similarly, a study on human embryonic kidney cells (HEK293) demonstrated a transition from polysome-based to monosome-based translation during starvation (Schneider et al., 2022). Using polysome profiling, a reduction in polysome abundance coupled with an increase in monosome fractions under starvation conditions was also reported (Schieweck et al., 2023; Schneider et al., 2022). Another study showed that HEK293T cells indeed regulate monosome and polysome levels to balance translation-related stresses by lowering the monosome activity (Schieweck et al., 2023). Interestingly, dendritic and axonal transcripts preferentially associate with monosomes and undergo active monosome-based translation (Biever et al., 2020). Such studies highlight the plasticity and adaptability of the translational system, where monosomes and polysomes are differentially regulated depending on the type of transcript and stress to optimise cellular functioning, survival and resource usage. However, the regulatory mechanisms that govern such plasticity remain to be resolved. The ongoing hypothesis of ribosomal heterogeneity, guided by the modifications of rRNA and RPs as well as the stoichiometry of RPs could explain the plasticity of the translational system. It has already been reported in *E. coli* that the stoichiometry of certain RPs shows variation when compared between polysomes and monosomes (Deusser et al., 1974; Bickle et al., 1973). Additionally, the non-uniform distribution of specific RPs was also reported among free subunits, especially the 30S ribosomal subunit (Van Duin and Van Knippenbero, 1974; Bickle et al., 1973; Voynow and Kurlandf, 1971). Certain RPs have been extensively studied as ribosome interactors that could drive the translation of specific transcripts (Kondrashov et al., 2011). In *Saccharomyces cerevisiae*, sulphur starvation induces the formation of m^6A-bearing ribosomes (Liu et al., 2021) while osmotic and pH stress results in RP S26-depleted ribosomes (Ferretti et al., 2017). These specialised ribosomes preferentially translate target transcripts associated with the respective stress conditions (Liu et al., 2021; Ferretti et al., 2017).

During T5 phage infection, the differential abundance of monosomes and polysomes observed in the host strains suggests that translation in the m^6A-RNA depleted mutant is slower compared to the wild-type strain. Despite this impaired translation, phage protein levels remained similar between the strains as observed by proteomic studies (until 35 mins post-infection), indicating the presence of an undefined compensatory mechanism that maintains protein synthesis in the mutant. To pursue this line of reasoning, RT-qPCR analysis was conducted on multiple phage transcripts, which revealed that transcripts encoding three phage structural proteins (major tail fiber, prohead protease, and capsid and scaffold) exhibited increased transcript levels in the m^6A-RNA depleted mutant relative to the wild type (Fig. 3.21). This finding suggests that the mutant may compensate for diminished translational efficiency by increasing transcript levels or decreasing mRNA turnover to maintain protein levels (Fig. 4.1). Furthermore, the m^6A-RNA depleted mutant may rely more heavily on monosome-based translation during T5 infection, which, although slower, could be sufficient under conditions of increased transcript availability (Fig. 4.1). These findings emphasise the interplay between transcriptional and translational regulation during phage infection, thus giving rise to a hypothesis that m^6A rRNA deletion disrupts ribosome dynamics, thereby driving a shift toward increased transcript production or stability as a compensatory response (Fig. 4.1). It is also possible that this compensation via increase in phage transcripts could be a heterogeneous response in the m^6A-RNA depleted mutant. This could very well explain the observed asynchronous bursts in the m^6A-RNA depleted mutant. Moreover, the average duration of T5 infection is 50-60 minutes, indicating that protein level visualisation (through proteomics) until 35 min post-infection covers only half the infection cycle. Thus, it is possible that differences in the protein levels between the wild-type and m^6A-RNA depleted mutant could be more evident at later time points of infection, not covered in this study. The proposed mechanism of T5 infection in *E. coli* wild type and its m^6A-RNA depleted mutant is shown in Fig. 4.1.

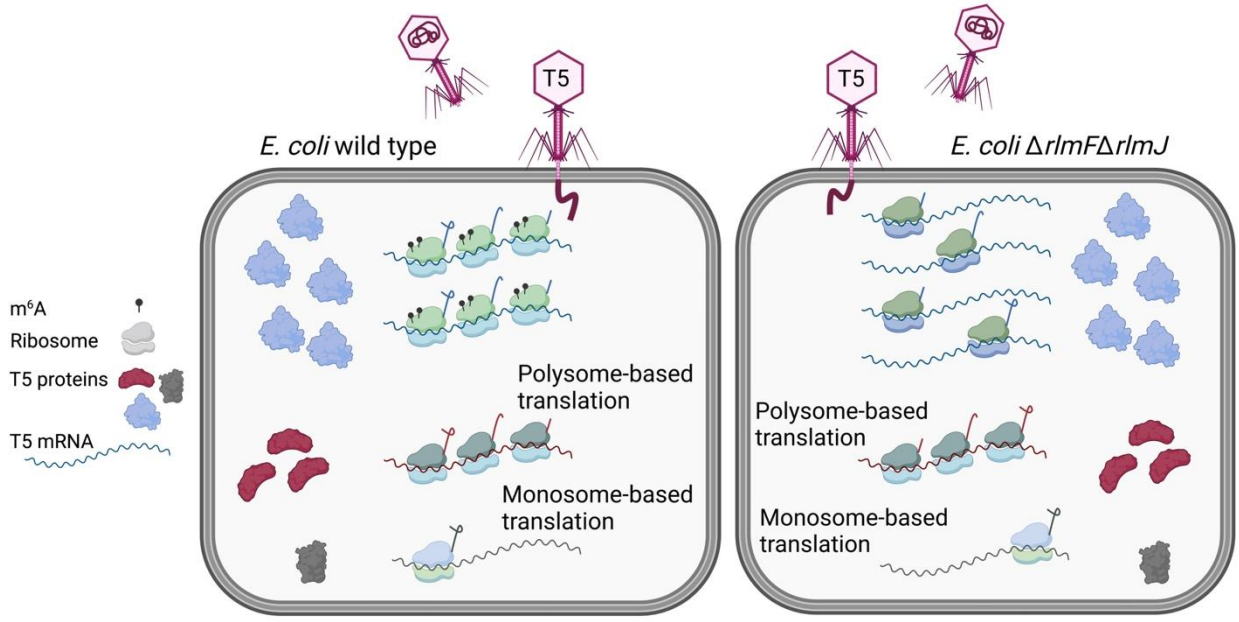

Figure 4.1 Graphical summary of the T5 phage-host interactions at the molecular level. Ribosomal heterogeneity is shown in the T5-infected wild-type (left) or m^{6}A-RNA depleted (right) *E. coli*. In both the hosts, phage proteins are produced using polysome (red) or monosome (grey)-based translation of the transcripts. In the wild-type strain, the presence of m^{6}A-modified ribosomes may be responsible for the effective translation of certain transcripts (blue). However, these transcripts (blue) were upregulated in the m^{6}A-RNA depleted mutant as compared to the wild-type strain as depicted. This increased transcript abundance (blue) is hypothesised to compensate for the lack of m^{6}A-modified ribosomes, the reduced polysome levels and the higher prevalence of 70S monosomes in the m^{6}A-RNA depleted mutant in comparison to the wild-type strain. It is proposed that these transcripts depend on monosome-based translation to satisfy the demand of protein requirements by T5, given that the absence of polysome formation restricts their capacity to undergo the efficient translation observed in the wild-type. This hypothesis may also provide a molecular basis for the observed delay in cell lysis and the asynchronous bursts in the mutant, reflecting the impact of slower and less coordinated protein synthesis. The figure is generated in Biorender.com.

Studies in the eukaryotic RNA viruses that contain cis-regulatory elements such as the internal ribosome entry site (IRES) at the 5' UTR of their transcripts rely on their host ribosomal proteins for efficient non-canonical and cap-independent viral protein translation (Jang et al., 1988;

Pelletier and Sonenberg, 1988). Receptors for activated C kinase 1 (RACK1) and RPS25, components of the 40S subunit of the eukaryotic ribosome, are essential to initiate IRES-dependent translation of viral transcripts (Majzoub et al., 2014; Landry et al., 2009). Specifically, poxvirus phosphorylates RACK1 and RPS2 via virus-encoded B1 kinase to generate specialised ribosomes that preferentially translate polyA leaders in the 5' UTR of viral transcripts and confer a translational advantage (DiGiuseppe et al., 2020; Jha et al., 2017). Moreover, the poxvirus exploits the ubiquitylation of RP S20 by host E3 ligase ZNF598, which enhances viral protein synthesis (DiGiuseppe et al., 2018). Based on this, it is also hypothesised that m^6A-bearing ribosomes may similarly be exploited by T5 phage to selectively translate specific transcripts which enables efficient replication in *E. coli* (Fig. 4.1 and 4.2). This potential mechanism highlights how phages might exploit rRNA modifications to optimise their replication process and lack of these modifications in the host may cause asynchronous bursts due to uncoordinated phage protein production (Fig. 4.2). Thus, the effect of m^6A-RNA depletion on T5 phage replication in *E. coli* is summarised in Fig. 4.2.

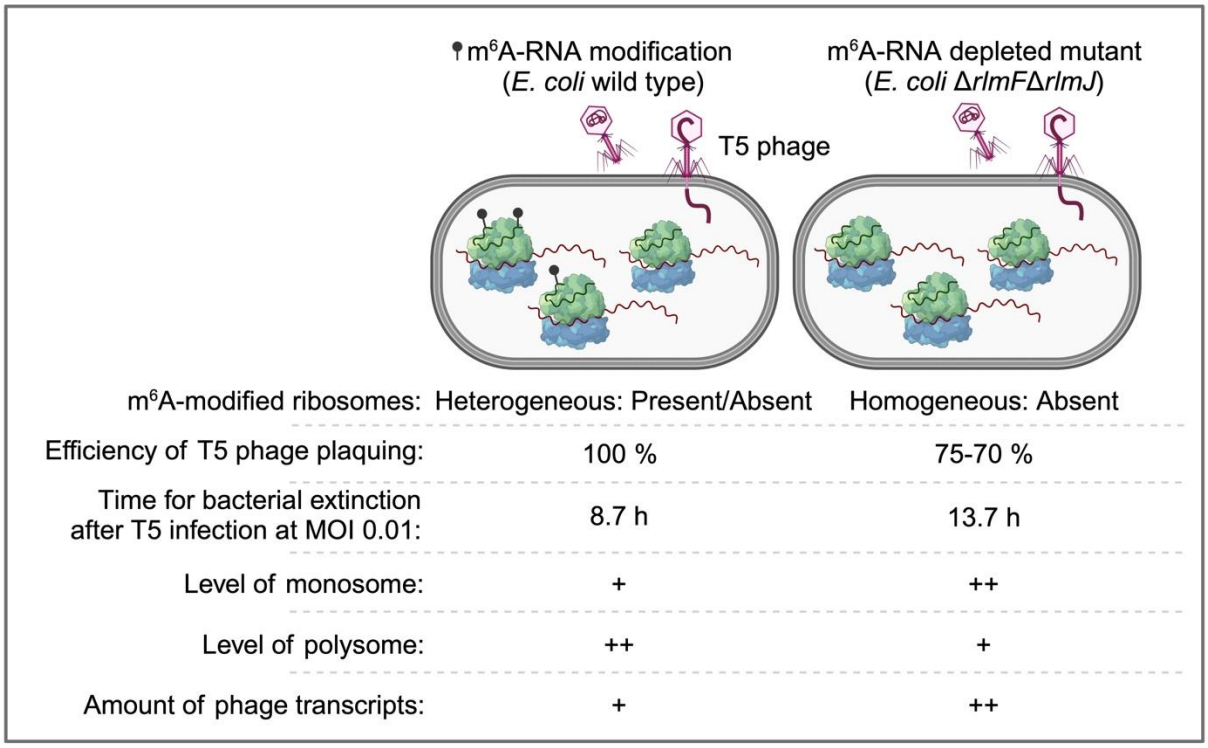

m^6A-modified ribosomes:	Heterogeneous: Present/Absent	Homogeneous: Absent
Efficiency of T5 phage plaquing:	100 %	75-70 %
Time for bacterial extinction after T5 infection at MOI 0.01:	8.7 h	13.7 h
Level of monosome:	+	++
Level of polysome:	++	+
Amount of phage transcripts:	+	++

Figure 4.2 Summary of the effect of m^6A-RNA depletion on T5 phage replication in *E. coli*. The figure is generated in Biorender.com.

The prevalence of RNA modifications, particularly m^6A, in the genomic RNA of numerous eukaryotic viruses, including avian sarcoma virus, Rous sarcoma virus, HIV-1, HCV, ZIKV, DENV and IAV, has been well documented (Beemon and Keith, 1977; Courtney et al., 2017; Gokhale et al., 2016; Kane and Beemon, 1985; Kennedy et al., 2016; Stoltzfus and Dimock, 1976; Tirumuru et al., 2016). These modifications have been demonstrated to influence various stages of viral replication and the interaction of the virus with its host organism. In the present study, multiple RNA modifications were identified for the first time in the genomes of prokaryotic RNA phages MS2 and Qβ (Fig. 3.22). In order to identify the nature of these chemical modifications, the samples were analysed using LC-MS/MS. This analysis revealed the presence of m^6A, m^2A and m^7G in Qβ RNA and m^6A, m^2A, m^7G and $m^{6,6}A$ in MS2 RNA (Fig. 3.22 and 3.23). It is clear that the host's methyltransferases are responsible for introducing these modifications, given that neither phage encodes the necessary enzymatic machinery for the observed modifications. Moreover, positive sense ssRNA phages heavily rely on the host translation machinery to complete their replication cycle (Olsthoorn and van Duin, 2011). Since there are no DNA intermediates involved in the replication cycle of ssRNA phages, it is hypothesised the secondary structure of their RNA genomes plays a predominant role in the temporal progression of their infection (Olsthoorn and van Duin, 2011; de Smit and van Duin, 1993, 1990). For instance, the ssRNA can associate with the host ribosomes to enter translation, with replicase holoenzyme to enter replication or with coat protein to begin packaging (Eigen et al., 1991). But how does ssRNA regulate all these processes efficiently? One study showed that RNA folding kinetics regulates the translation of the MS2 maturation gene by delaying the folding of newly synthesised ssRNA genome which results in a short window wherein the ribosome binding site (RBS) is accessible for the ribosome to initiate translation (Poot et al., 1997). However, the same group later disproved their findings stating that the window during which the folded RBS is open is too short to recruit the 30S ribosomal subunit (de Smit and van Duin, 2003). They argued that a 30S subunit must already be in contact with the ssRNA forming a non-specific and temporally steady state to shift into the RBS as soon as the structure opens (de Smit and van Duin, 2003). But the question remains: How does ssRNA regulate the process of genome replication, translation and packaging? One hypothesis could be that the RNA modifications found on the ssRNA genome of these phages affect and dynamically regulate the secondary structure, making it available for the process of genome replication, translation and

packaging (Fig. 4.3). RNA modifications are known to modulate the stability, fidelity and translational efficiency of tRNAs, the most modified class of RNA (Cappannini et al., 2024; Suzuki, 2021). Since RNA modifications are also essential for the secondary and tertiary structure of tRNA (Biedenbänder et al., 2022; Suzuki, 2021), it is reasonable to speculate that RNA modifications of ssRNA from RNA phages also play a role in maintaining its secondary structure, thereby stabilising RNA folding to regulate the processes for efficient infection (Fig. 4.3). Moreover, RNA modifications may also protect the ssRNA genome from host ribonucleases and aid in immune evasion (Fig. 4.3).

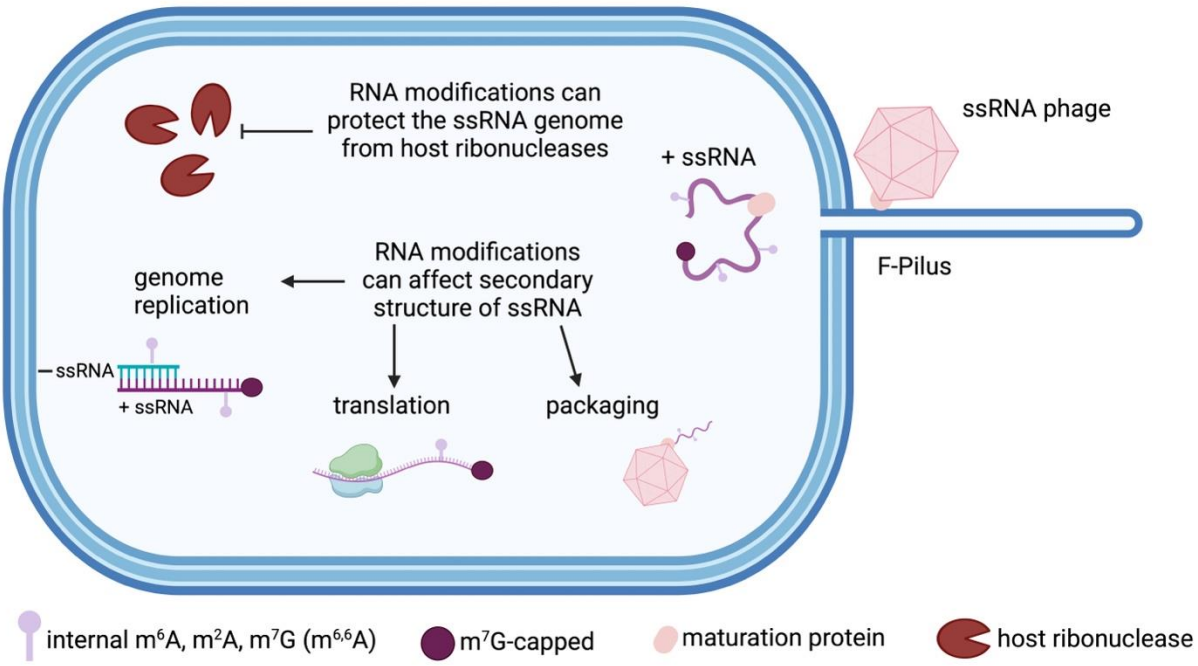

Figure 4.3 Possible roles of RNA modifications in ssRNA genomes of RNA phages. Modifications such as m^6A, $m^{6,6}A$, m^2A, and m^7G may serve as internal modifications in the ssRNA of MS2, while m^6A, m^2A, and m^7G could be internal modifications in the ssRNA of Qβ. In addition, m^7G could also act as a cap for the ssRNA. The figure is generated in Biorender.com.

The functional analysis of these modifications was performed by infecting single methyltransferase knockout mutants with MS2 and Qβ and assessing their plaquing efficiency. Only the deletion of *rsmA*, responsible for the $m^{6,6}A$ modification, led to a significant increase in the plaquing efficiency of MS2, while none of the knockouts affected Qβ (Fig. 3.24 and 3.25).

Growth experiments also demonstrated that the Δ*rsmA* mutant showed an earlier cell death and enhanced recovery following MS2 infection, thus suggesting that it is more susceptible to infection as compared to the wild-type strain (Fig. 3.26). These experimental findings indicate that the $m^{6,6}A$ modification, which is mediated by RsmA, likely plays a physiological role in protecting the host against MS2 infection. It is also possible that *E. coli* has several unidentified methyltransferases in its genome that might be responsible for adding the modification to these RNA phages. For example, prophage-encoded rRNA methyltransferase that modifies the 16S rRNA in *E. coli* STEC was only discovered last year (Gong et al., 2024).

4.2 Outlook

A key avenue for future exploration is the stability and turnover of phage transcripts in the m^6A-RNA depleted mutant. The higher abundance of phage transcripts observed in the mutant suggests that RNA stability may play a critical role in compensating for reduced translational efficiency. Transcript stability can be monitored using rifampicin to inhibit bacterial transcription, followed by transcript quantification using northern blot or RT-qPCR. For a more global understanding of the half-lives of several transcripts, RNA-seq could also be implemented. It is also important to investigate whether m^6A-RNA depletion affects the recruitment or activity of RNA degradation machinery, as this could provide valuable insights into how transcript turnover is regulated during phage infection. This could be explored by generating bacterial mutants lacking essential ribonucleases such as host RNase E or RNase III and monitoring phage transcript stability. A transcriptomic analysis using RNA-seq or Ribo-seq would help clarify whether enhanced stability is a general feature or selectively targeted to certain transcripts. A global RNA-seq analysis would also explain if the increased transcript abundance in the m^6A-RNA depleted mutant is purely a compensatory response or a broader rewiring of transcriptional regulation in the absence of m^6A modification in the 23S rRNA. Moreover, a Ribo-seq would also allow the study of translational efficiency by evaluating the association of phage transcripts with ribosomes. Thus, the distribution of phage transcripts between the monosomes and polysomes in the host strains can be studied to further validate the working hypothesis. Furthermore, a codon usage analysis of the enriched transcripts would provide insights into whether specific codons drive monosome or polysome translation in the hosts.

To answer questions regarding ribosome composition and heterogeneity in the host strains, studies can be conducted to characterise the ribosomal proteome and identify the potential differences in ribosomal protein abundance or post-translational modifications between the wild-type and m^6A-RNA depleted mutant. Cryo-electron microscopy (Cryo-EM) is a method of visualising macromolecular structures at an atomic level. Thus, this technique would provide structural insights into how the absence of m^6A modification in the 23S rRNA affects ribosomal structure and heterogeneity. Moreover, co-immunoprecipitation of ribosomes and associated factors would also provide evidence of potential co-factors that may shape differential ribosomal heterogeneity in the host strains. RNA modification profiling on rRNA would also facilitate the study of ribosomal heterogeneity. This objective could be achieved by extracting T5-infected rRNA from purified ribosomes and conducting LC-MS/MS analysis to quantify different modifications.

The observation that the $m^{6,6}A$ modification mediated by RsmA negatively regulates MS2 infection highlights the importance of further characterising this phage-host interaction. Subsequent studies may include adsorption assays and one-step growth curves to elucidate the dynamics of phage replication, as well as to ascertain critical phage parameters, including the latent period, burst size, and rise period. Moreover, LC-MS/MS analysis of RNA from MS2- or Qβ-infected wild-type and single-knockout strains would provide exciting insights into the role of host methyltransferases in modifying the phage genomic RNA. Comparing RNA modification profiles across these strains would allow for the identification of direct dependencies between specific methyltransferases and modifications. If modifications persist in certain phage-infected knockout strains, it will indicate the potential existence of other methyltransferases capable of introducing these modifications into the phage genomic RNA.

The field of epitranscriptomics during phage infection is at its budding stage. Discovering modified RNA in phages is the first step for exploring their regulation and potential roles during infection. Such studies can also enhance our understanding of phage-host interactions, which could be exploited to use in phage therapy. Moreover, improvement in sequencing accuracy and throughout, as well as advancement in sequencing technologies will drive discoveries in RNA-phage biology, unveiling novel immune strategies and therapeutic targets.

5 References

Abedon, S.T., 2000. The murky origin of snow white and her T-even dwarfs. Genetics 155, 481–486. https://doi.org/10.1093/genetics/155.2.481

Abraham, G., Rhodes, D.P., Banerjee, A.K., 1975. The 5' terminal structure of the methylated mRNA synthesized in vitro by vesicular stomatitis virus. Cell 5, 51–58. https://doi.org/10.1016/0092-8674(75)90091-4.

Abramson, J., Adler, J., Dunger, J., Evans, R., Green, T., Pritzel, A., Ronneberger, O., Willmore, L., Ballard, A.J., Bambrick, J., Bodenstein, S.W., Evans, D.A., Hung, C.C., O'Neill, M., Reiman, D., Tunyasuvunakool, K., Wu, Z., Žemgulytė, A., Arvaniti, E., Beattie, C., Bertolli, O., Bridgland, A., Cherepanov, A., Congreve, M., Cowen-Rivers, A.I., Cowie, A., Figurnov, M., Fuchs, F.B., Gladman, H., Jain, R., Khan, Y.A., Low, C.M.R., Perlin, K., Potapenko, A., Savy, P., Singh, S., Stecula, A., Thillaisundaram, A., Tong, C., Yakneen, S., Zhong, E.D., Zielinski, M., Žídek, A., Bapst, V., Kohli, P., Jaderberg, M., Hassabis, D., Jumper, J.M., 2024. Accurate structure prediction of biomolecular interactions with AlphaFold 3. Nature 630, 493–500. https://doi.org/10.1038/s41586-024-07487-w

Ackermann, H.-W., 2009. Phage classification and characterization, in: Methods Mol Biol. pp. 127–140.

Ackermann, H.-W., 1999. Tailed bacteriophages: The order *Caudovirales*. Adv Virus Res 51, 135–201. https://doi.org/https://doi.org/10.1016/s0065-3527(08)60785-x

Andersen, N.M., Douthwaite, S., 2006. YebU is a m^5C methyltransferase specific for 16S rRNA nucleotide 1407. J Mol Biol 359, 777–786. https://doi.org/10.1016/j.jmb.2006.04.007

Andreolla, A.P., Marina, L., Erpen, S., Frandoloso, R., Kreutz, C., 2018. Development of an indirect ELISA based on recombinant capsid protein to detect antibodies to bovine leukemia virus. Braz J Microbiol. 49 Suppl, 68–75. https://doi.org/10.1016/j.bjm.2018.05.001

Baba, T., Ara, T., Hasegawa, M., Takai, Y., Okumura, Y., Baba, M., Datsenko, K.A., Tomita, M., Wanner, B.L., Mori, H., 2006. Construction of *Escherichia coli* K-12 in-frame, single-gene

knockout mutants: The Keio collection. Mol Syst Biol 2, 2006.0008. https://doi.org/10.1038/msb4100050

Bahena-Ceron, R., Teixeira, C., Jaramillo Ponce, J.R., Wolff, P., Couzon, F., François, P., Klaholz, B.P., Vandenesch, F., Romby, P., Moreau, K., Marzi, S., 2024. RlmQ: a newly discovered rRNA modification enzyme bridging RNA modification and virulence traits in *Staphylococcus aureus*. RNA 30, 200–212. https://doi.org/10.1261/rna.079850.123.

Baltimore, D., 1970. RNA-dependent DNA polymerase in virions of RNA tumour viruses. Nature 226, 1209–1211. https://doi.org/10.1038/2261209a0.

Baquero-Perez, B., Geers, D., Díez, J., 2021. From A to m^6A: The emerging viral epitranscriptome. Viruses 13, 1049. https://doi.org/10.3390/v13061049

Bateman, A., Martin, M.-J., Orchard, S., Magrane, M., Agivetova, R., Ahmad, S., Alpi, E., Bowler-Barnett, E.H., Britto, R., Bursteinas, B., Bye-A-Jee, H., Coetzee, R., Cukura, A., Da Silva, A., Denny, P., Dogan, T., Ebenezer, T., Fan, J., Castro, L.G., Garmiri, P., Georghiou, G., Gonzales, L., Hatton-Ellis, E., Hussein, A., Ignatchenko, A., Insana, G., Ishtiaq, R., Jokinen, P., Joshi, V., Jyothi, D., Lock, A., Lopez, R., Luciani, A., Luo, J., Lussi, Y., MacDougall, A., Madeira, F., Mahmoudy, M., Menchi, M., Mishra, A., Moulang, K., Nightingale, A., Oliveira, C.S., Pundir, S., Qi, G., Raj, S., Rice, D., Lopez, M.R., Saidi, R., Sampson, J., Sawford, T., Speretta, E., Turner, E., Tyagi, N., Vasudev, P., Volynkin, V., Warner, K., Watkins, X., Zaru, R., Zellner, H., Bridge, A., Poux, S., Redaschi, N., Aimo, L., Argoud-Puy, G., Auchincloss, A., Axelsen, K., Bansal, P., Baratin, D., Blatter, M.-C., Bolleman, J., Boutet, E., Breuza, L., Casals-Casas, C., de Castro, E., Echioukh, K.C., Coudert, E., Cuche, B., Doche, M., Dornevil, D., Estreicher, A., Famiglietti, M.L., Feuermann, M., Gasteiger, E., Gehant, S., Gerritsen, V., Gos, A., Gruaz-Gumowski, N., Hinz, U., Hulo, C., Hyka-Nouspikel, N., Jungo, F., Keller, G., Kerhornou, A., Lara, V., Le Mercier, P., Lieberherr, D., Lombardot, T., Martin, X., Masson, P., Morgat, A., Neto, T.B., Paesano, S., Pedruzzi, I., Pilbout, S., Pourcel, L., Pozzato, M., Pruess, M., Rivoire, C., Sigrist, C., Sonesson, K., Stutz, A., Sundaram, S., Tognolli, M., Verbregue, L., Wu, C.H., Arighi, C.N., Arminski, L., Chen, C., Chen, Y., Garavelli, J.S., Huang, H., Laiho, K., McGarvey, P., Natale, D.A., Ross, K., Vinayaka, C.R., Wang, Q., Wang, Y., Yeh, L.-S., Zhang, J., Ruch, P., Teodoro, D., 2021. UniProt: the universal protein

knowledgebase in 2021. Nucleic Acids Res 49, D480–D489. https://doi.org/10.1093/nar/gkaa1100

Batinovic, S., Wassef, F., Knowler, S.A., Rice, D.T.F., Stanton, C.R., Rose, J., Tucci, J., Nittami, T., Vinh, A., Drummond, G.R., Sobey, C.G., Chan, H.T., Seviour, R.J., Petrovski, S., Franks, A.E., 2019. Bacteriophages in natural and artificial environments. Pathogens 8, 100. https://doi.org/10.3390/PATHOGENS8030100

Beemon, K., Keith, J., 1977. Localization of N^6-methyladenosine in the Rous sarcoma virus genome. J Mol Biol 113, 165–179. https://doi.org/10.1016/0022-2836(77)90047-x.

Benítez-Páez, A., Villarroya, M., Armengod, M.E., 2012. The *Escherichia coli* RlmN methyltransferase is a dual-specificity enzyme that modifies both rRNA and tRNA and controls translational accuracy. RNA 18, 1783–1795. https://doi.org/10.1261/rna.033266.112

Bickle, T.A., Howard, G.A., Traut, R.R., 1973. Ribosome heterogeneity: The nonuniform distribution of specific ribosomal proteins among different functional classes of ribosomes. J Biol Chem 248, 4862–4864. https://doi.org/https://doi.org/10.1016/S0021-9258(19)43745-9

Biedenbänder, T., de Jesus, V., Schmidt-Dengler, M., Helm, M., Corzilius, B., Fürtig, B., 2022. RNA modifications stabilize the tertiary structure of $tRNA^{fMet}$ by locally increasing conformational dynamics. Nucleic Acids Res 50, 2334–2349. https://doi.org/10.1093/nar/gkac040

Biever, A., Glock, C., Tushev, G., Ciirdaeva, E., Dalmay, T., Langer, J.D., Schuman, E.M., 2020. Monosomes actively translate synaptic mRNAs in neuronal processes. Science (1979) 367, eaay4991. https://doi.org/10.1126/science.aay4991

Blattner, F.R., Plunkett, G., Bloch, C.A., Perna, N.T., Burland, V., Riley, M., Collado-Vides, J., Glasner, J.D., Rode, C.K., Mayhew, G.F., Gregor, J., Davis, N.W., Kirkpatrick, H.A., Goeden, M.A., Rose, D.J., Mau, B., Shao, Y., 1997. The complete genome sequence of *Escherichia coli* K-12. Science 277, 1453–1462. https://doi.org/https://doi.org/10.1126/science.277.5331.1453

Blazanin, M., 2024. gcplyr: an R package for microbial growth curve data analysis. BMC Bioinformatics 25, 232. https://doi.org/10.1186/s12859-024-05817-3

Blumenthal, T., Landers, T.A., Weber, K., 1972. Bacteriophage Qβ replicase contains the protein biosynthesis elongation factors EF Tu and EF Ts. Proc Natl Acad Sci U S A 69, 1313–1317. https://doi.org/10.1073/pnas.69.5.1313

Bokar, J.A., Shambaugh, M.E., Polayes, D., Matera, A.G., Rottman, F.M., 1997. Purification and cDNA cloning of the AdoMet-binding subunit of the human mRNA (N^6-adenosine)-methyltransferase. RNA 3, 1233–1247.

Boni, I. V, Lsaeva, D.M., Musychenko, M.L., Tzareva, N. V, 1990. Ribosome-messenger recognition: mRNA target sites for ribosomal protein S1. Nucleic Acids Res 19, 155–162. https://doi.org/10.1093/nar/19.1.155

Borland, K., Diesend, J., Ito-Kureha, T., Heissmeyer, V., Hammann, C., Buck, A.H., Michalakis, S., Kellner, S., 2019. Production and application of stable isotope-labeled internal standards for RNA modification analysis. Genes (Basel) 10, 26. https://doi.org/10.3390/genes10010026

Bradford, M.M., 1976. A rapid and sensitive method for the quantitation of microgram quantities of protein utilizing the principle of protein-dye binding. Anal Biochem 72, 248–254. https://doi.org/10.1016/0003-2697(76)90527-3

Brameyer, S., Hoyer, E., Bibinger, S., Burdack, K., Lassak, J., Jung, K., 2020. Molecular design of a signaling system influences noise in protein abundance under acid stress in different *Gammaproteobacteria*. J Bacteriol 202, e00121-20. https://doi.org/10.1128/JB.00121-20

Brandão, A., Pires, D.P., Coppens, L., Voet, M., Lavigne, R., Azeredo, J., 2021. Differential transcription profiling of the phage LUZ19 infection process in different growth media. RNA Biol 18, 1778–1790. https://doi.org/10.1080/15476286.2020.1870844

Breger, K., Kunkler, C.N., O'Leary, N.J., Hulewicz, J.P., Brown, J.A., 2023. Ghost authors revealed: The structure and function of human N^6- methyladenosine RNA methyltransferases. WIREs RNA 15, e1810. https://doi.org/10.1002/wrna.1810

Brüssow, H., Canchaya, C., Hardt, W.-D., 2004. Phages and the evolution of bacterial pathogens: From genomic rearrangements to lysogenic conversion. Microbiol Mol Biol Rev 68, 560–602. https://doi.org/10.1128/MMBR.68.3.560-602.2004

Bügl, H., Fauman, E.B., Staker, B.L., Zheng, F., Kushner, S.R., Saper, M.A., Bardwell, J.C.A., Jakob, U., 2000. RNA methylation under heat shock control. Mol Cell 6, 349–360. https://doi.org/10.1016/s1097-2765(00)00035-6.

Byrgazov, K., Vesper, O., Moll, I., 2013. Ribosome heterogeneity: Another level of complexity in bacterial translation regulation. Curr Opin Microbiol 16, 133–139. https://doi.org/10.1016/j.mib.2013.01.009

Callanan, J., Stockdale, S.R., Shkoporov, A., Draper, L.A., Ross, R.P., Hill, C., 2020. Expansion of known ssRNA phage genomes: From tens to over a thousand. Sci Adv 6, 5981. https://doi.org/10.1126/sciadv.aay5981

Callanan, J., Stockdale, S.R., Shkoporov, A., Draper, L.A., Ross, R.P., Hill, C., 2018. RNA phage biology in a metagenomic era. Viruses 10, 386. https://doi.org/10.3390/v10070386

Camacho, C., Coulouris, G., Avagyan, V., Ma, N., Papadopoulos, J., Bealer, K., Madden, T.L., 2009. BLAST+: Architecture and applications. BMC Bioinformatics 10, 421. https://doi.org/10.1186/1471-2105-10-421

Canaani, D., Kahana, C., Lavi, S., Groner, Y., 1979. Identification and mapping of N^6-methyladenosine containing sequences in Simian Virus 40 RNA. Nucleic Acids Res 6, 2879–2899. https://doi.org/https://doi.org/10.1093/nar/6.8.2879

Cappannini, A., Ray, A., Purta, E., Mukherjee, S., Boccaletto, P., Moafinejad, S.N., Lechner, A., Barchet, C., Klaholz, B.P., Stefaniak, F., Bujnicki, J.M., 2024. MODOMICS: A database of RNA modifications and related information. 2023 update. Nucleic Acids Res 52, D239–D244. https://doi.org/10.1093/nar/gkad1083

Carrolo, M., Frias, M.J., Pinto, F.R., Melo-Cristino, J., Ramirez, M., 2010. Prophage spontaneous activation promotes DNA release enhancing biofilm formation in *Streptococcus pneumoniae*. PLoS One 5, e15678. https://doi.org/10.1371/journal.pone.0015678

Casjens, S., 2003. Prophages and bacterial genomics: What have we learned so far? Mol Microbiol 49, 277–300. https://doi.org/10.1046/j.1365-2958.2003.03580.x

Castillo, D., D'Alvise, P., Middelboe, M., Gram, L., Liu, S., Kalatzis, P.G., Kokkari, C., Katharios, P., 2015. Draft genome sequences of the fish pathogen *Vibrio harveyi* strains VH2 and VH5. Genome Announc 3, e01062-15. https://doi.org/10.1128/genomeA.01062-15

Chen, K., Lu, Z., Wang, X., Fu, Y., Luo, G.Z., Liu, N., Han, D., Dominissini, D., Dai, Q., Pan, T., He, C., 2015. High-resolution N^6-methyladenosine (m^6A) map using photo-crosslinking-assisted m^6A sequencing. Angew Chem Int Ed Engl 54, 1587–1590. https://doi.org/10.1002/anie.201410647

Chen, Y., Liu, M., Lu, M., Luo, L., Han, Z., Liu, X., 2024. Exploring the impact of m^6A modification on immune diseases: Mechanisms and therapeutic implication. Front Immunol 15, 1387582. https://doi.org/10.3389/fimmu.2024.1387582

Cheng, W., Gao, A., Lin, H., Zhang, W., 2022. Novel roles of METTL1/WDR4 in tumor via m^7G methylation. Mol Ther Oncolytics 26, 27–34. https://doi.org/10.1016/j.omto.2022.05.009

Chow, L.T., Gelinas, R.E., Broker, T.R., Roberts, R.J., 1977. An amazing sequence arrangement at the 5' ends of adenovirus 2 messenger RNA. Cell 12, 1–8. https://doi.org/10.1016/0092-8674(77)90180-5.

Clarke, M., Maddera, L., Harris, R.L., Silverman, P.M., 2008. F-pili dynamics by live-cell imaging. Proc Natl Acad Sci U S A 105, 17978–17981. https://doi.org/10.1073/pnas.0806786105

Condon, C., Liveris, D., Squires, C., Schwartz, I., Squires, C.L., 1995. rRNA operon multiplicity in *Escherichia coli* and the physiological implications of *rrn* inactivation. J Bacteriol 177, 4152–4156. https://doi.org/10.1128/jb.177.14.4152-4156.1995

Condon, C., Philips, J., Fu, Z.Y., Squires, C., Squires, C.L., 1992. Comparison of the expression of the seven ribosomal RNA operons in *Escherichia coli*. EMBO J 11, 4175–4185. https://doi.org/10.1002/j.1460-2075.1992.tb05511.x

Connolly, K., Rife, J.P., Culver, G., 2008. Mechanistic insight into the ribosome biogenesis functions of the ancient protein KsgA. Mol Microbiol 70, 1062–1075. https://doi.org/10.1111/j.1365-2958.2008.06485.x

Courtney, D.G., Kennedy, E.M., Dumm, R.E., Bogerd, H.P., Tsai, K., Heaton, N.S., Cullen, B.R., 2017. Epitranscriptomic enhancement of influenza A virus gene expression and replication. Cell Host Microbe 22, 377–386. https://doi.org/10.1016/j.chom.2017.08.004

Crick, F.H., 1970. Central dogma of molecular biology. Nature 227, 561–563. https://doi.org/10.1038/227561a0.

Crick, F.H., 1958. On protein synthesis. Symp Soc Exp Biol 12, 138–63.

Czerwoniec, A., Dunin-Horkawicz, S., Purta, E., Kaminska, K.H., Kasprzak, J.M., Bujnicki, J.M., Grosjean, H., Rother, K., 2009. MODOMICS: A database of RNA modification pathways. 2008 update. Nucleic Acids Res 37, D118–D121. https://doi.org/10.1093/nar/gkn710

Daegelen, P., Studier, F.W., Lenski, R.E., Cure, S., Kim, J.F., 2009. Tracing ancestors and relatives of *Escherichia coli* B, and the derivation of B Strains REL606 and BL21(DE3). J Mol Biol 394, 634–643. https://doi.org/10.1016/j.jmb.2009.09.022

Davis, J.E., Strauss Jr., J.H., Sinsheimer, R.L., 1961. Bacteriophage MS2: Another RNA phage. Science (1979) 134, 1427.

Davison, J., 2015. Pre-early functions of bacteriophage T5 and its relatives. Bacteriophage 5, e1086500. https://doi.org/10.1080/21597081.2015.1086500

Davison, J., Brunel, F., 1979a. Restriction insensitivity in bacteriophage T5. I. Genetic characterization of mutants sensitive to EcoRI restriction. J Virol 29, 11–16. https://doi.org/10.1128/jvi.29.1.11-16.1979

Davison, J., Brunel, F., 1979b. Restriction insensitivity in bacteriophage T5. II. Lack of EcoRI modification in T5+ and T5ris mutants. J Virol 29, 17–20. https://doi.org/10.1128/jvi.29.1.17-20.1979

De Bie, L.G.S., Roovers, M., Oudjama, Y., Wattiez, R., Tricot, C., Stalon, V., Droogmans, L., Bujnicki, J.M., 2003. The *yggH* gene of *Escherichia coli* encodes a tRNA (m^7G46) methyltransferase. J Bacteriol 185, 3238–3243. https://doi.org/10.1128/JB.185.10.3238-3243.2003

de Smit, M.H., van Duin, J., 2003. Translational standby sites: How ribosomes may deal with the rapid folding kinetics of mRNA. J Mol Biol 331, 737–743. https://doi.org/10.1016/S0022-2836(03)00809-X

de Smit, M.H., van Duin, J., 1993. Translational initiation at the coat-protein gene of phage MS2: Native upstream RNA relieves inhibition by local secondary structure. Mol Microbiol 9, 1079–1088. https://doi.org/10.1111/j.1365-2958.1993.tb01237.x

de Smit, M.H., van Duin, J., 1990. Secondary structure of the ribosome binding site determines translational efficiency: A quantitative analysis. Proc Natl Acad Sci U S A 87, 7668–7672. https://doi.org/10.1073/pnas.87.19.7668

de Jong, A., Kuipers, O.P., Kok, J., 2022. FUNAGE-Pro: Comprehensive web server for gene set enrichment analysis of prokaryotes. Nucleic Acids Res 50, W330–W336. https://doi.org/10.1093/nar/gkac441

Delvillani, F., Papiani, G., Dehò, G., Briani, F., 2011. S1 ribosomal protein and the interplay between translation and mRNA decay. Nucleic Acids Res 39, 7702–7715. https://doi.org/10.1093/nar/gkr417

Demerec, M., Fano, U., 1945. Bacteriophage-resistant mutants in *Escherichia coli*. Genetics 30, 119–136. https://doi.org/10.1093/genetics/30.2.119

Deng, X., Chen, K., Luo, G.-Z., Weng, X., Ji, Q., Zhou, T., He, C., 2015. Widespread occurrence of N^6-methyladenosine in bacterial mRNA. Nucleic Acids Res 43, 6557–6567. https://doi.org/10.1093/nar/gkv596

Depping, R., Lohaus, C., Meyer, H.E., Rüger, W., 2005. The mono-ADP-ribosyltransferases Alt and ModB of bacteriophage T4: Target proteins identified. Biochem Biophys Res Commun 335, 1217–1223. https://doi.org/10.1016/j.bbrc.2005.08.023

Desrosiers, R., Friderici, K., Rottman, F., 1974. Identification of methylated nucleosides in messenger RNA from Novikoff hepatoma cells. Proc Natl Acad Sci U S A 71, 3971–3975. https://doi.org/10.1073/pnas.71.10.3971.

Deusser, E., 1972. Heterogeneity of ribosomal populations in *Escherichia coli* cells grown in different media. Mol Gen Genet 119, 249–258. https://doi.org/10.1007/BF00333862

Deusser, E., Weber, H.J., Subramanian, A.R., 1974. Variations in stoichiometry of ribosomal proteins in *Escherichia coli*. J Mol Biol 84, 249–256. https://doi.org/10.1016/0022-2836(74)90583-X

Deusser, E., Wittmann, H.-G., 1972. Ribosomal proteins: Variation of the protein composition in *Escherichia coli* ribosomes as function of growth rate. Nature 238, 269–270. https://doi.org/10.1038/238269a0

d'Hérelle, F., 1917. Sur un microbe invisible antagoniste des bacilles dysentériques. Compte Rendu Académie Sci 165, 373–375.

DiGiuseppe, S., Rollins, M.G., Astar, H., Khalatyan, N., Savas, J.N., Walsh, D., 2020. Proteomic and mechanistic dissection of the poxvirus-customized ribosome. J Cell Sci 134, jcs246603. https://doi.org/10.1242/jcs.246603

DiGiuseppe, S., Rollins, M.G., Bartom, E.T., Walsh, D., 2018. ZNF598 plays distinct roles in interferon-stimulated gene expression and poxvirus protein synthesis. Cell Rep 23, 1249–1258. https://doi.org/10.1016/j.celrep.2018.03.132

Dominissini, D., Moshitch-Moshkovitz, S., Schwartz, S., Salmon-Divon, M., Ungar, L., Osenberg, S., Cesarkas, K., Jacob-Hirsch, J., Amariglio, N., Kupiec, M., Sorek, R., Rechavi, G., 2012. Topology of the human and mouse m^6A RNA methylomes revealed by m^6A-seq. Nature 485, 201–206. https://doi.org/10.1038/nature11112

Droubogiannis, S., Katharios, P., 2022. Genomic and biological profile of a novel bacteriophage, *Vibrio* phage Virtus, which improves survival of *Sparus aurata* larvae challenged with *Vibrio harveyi*. Pathogens 11, 630. https://doi.org/10.3390/pathogens11060630

Duan, H.C., Zhang, C., Song, P., Yang, J., Wang, Y., Jia, G., 2024. C^2-methyladenosine in tRNA promotes protein translation by facilitating the decoding of tandem m^2A-tRNA-dependent codons. Nat Commun 15. https://doi.org/10.1038/s41467-024-45166-6

Duarte, J., Pereira, C., Costa, P., Almeida, A., 2021. Bacteriophages with potential to inactivate *Aeromonas hydrophila* in Cockles: In vitro and in vivo preliminary studies. Antibiotics 10, 710. https://doi.org/10.3390/antibiotics10060710

Ducret, A., Quardokus, E.M., Brun, Y. V., 2016. MicrobeJ, a tool for high throughput bacterial cell detection and quantitative analysis. Nat Microbiol 1, 16077. https://doi.org/10.1038/nmicrobiol.2016.77

Echeverría-Vega, A., Morales-Vicencio, P., Saez-Saavedra, C., Gordillo-Fuenzalida, F., Araya, R., 2019. A rapid and simple protocol for the isolation of bacteriophages from coastal organisms. MethodsX 6, 2614–2619. https://doi.org/10.1016/j.mex.2019.11.003

Edmonds, M., Vaughan, M.H., Nakazato, H., 1971. Polyadenylic acid sequences in the heterogeneous nuclear RNA and rapidly-labeled polyribosomal RNA of HeLa cells: Possible evidence for a precursor relationship. Proc Natl Acad Sci U S A 68, 1336–1340. https://doi.org/10.1073/pnas.68.6.1336.

Eigen, M., Biebricher, C.K., Gebinoga, M., Gardiner, W.C., 1991. The hypercycle: Coupling of RNA and protein biosynthesis in the infection cycle of an RNA bacteriophage. Biochemistry 30, 11005–11018. https://doi.org/10.1021/bi00110a001

Ero, R., Leppik, M., Reier, K., Liiv, A., Remme, J., 2024. Ribosomal RNA modification enzymes stimulate large ribosome subunit assembly in *E. coli*. Nucleic Acids Res 52, 6614–6628. https://doi.org/10.1093/nar/gkae222

Fasnacht, M., Gallo, S., Sharma, P., Himmelstoß, M., Limbach, P.A., Willi, J., Polacek, N., 2022. Dynamic 23S rRNA modification ho^{5}C2501 benefits *Escherichia coli* under oxidative stress. Nucleic Acids Res 50, 473–489. https://doi.org/10.1093/nar/gkab1224

Ferretti, M.B., Ghalei, H., Ward, E.A., Potts, E.L., Karbstein, K., 2017. Rps26 directs mRNA-specific translation by recognition of Kozak sequence elements. Nat Struct Mol Biol 24, 700–707. https://doi.org/10.1038/nsmb.3442

Fiers, W., Contreras, R., Duerinck, F., Haegeman, G., Iserentant, D., Merregaert, J., Min Jou, W., Molemans, F., Raeymaekers, A., Van den Berghe, A., Volckaert, G., Ysebaert, M., 1976. Complete nucleotide sequence of bacteriophage MS2 RNA: Primary and secondary structure of the replicase gene. Nature 260, 500–507. https://doi.org/10.1038/260500a0

Fortier, L.C., Moineau, S., 2009. Phage production and maintenance of stocks, including expected stock lifetimes, in: Methods Mol Biol. pp. 203–219. https://doi.org/10.1007/978-1-60327-164-6_19

Fortier, L.-C., Sekulovic, O., 2013. Importance of prophages to evolution and virulence of bacterial pathogens. Virulence 4, 354–365. https://doi.org/10.4161/viru.24498

Fu, L., Amato, N.J., Wang, P., McGowan, S.J., Niedernhofer, L.J., Wang, Y., 2015. Simultaneous quantification of methylated cytidine and adenosine in cellular and tissue RNA by nano-flow liquid chromatography-tandem mass spectrometry coupled with the stable isotope-dilution method. Anal Chem 87, 7653–7659. https://doi.org/10.1021/acs.analchem.5b00951

Fujisaki, S., Nishino, T., Katsuki, H., 1986. Isoprenoid synthesis in *Escherichia coli*. Separation and partial purification of four enzymes involved in the synthesis. J Biochem 99, 1327–1337. https://doi.org/10.1093/oxfordjournals.jbchem.a135600

Furuichi, Y., 2015. Discovery of m^7G-cap in eukaryotic mRNAs. Proc Jpn Acad Ser B Phys Biol Sci 91, 394–409. https://doi.org/10.2183/pjab.91.394

Furuichi, Y., Miura, K.-I., 1975. A blocked structure at the 5′ terminus of mRNA from cytoplasmic polyhedrosis virus. Nature 253, 374–375. https://doi.org/10.1038/253374a0.

Ge, S.X., Jung, D., Yao, R., 2020. ShinyGO: A graphical gene-set enrichment tool for animals and plants. Bioinformatics 36, 2628–2629. https://doi.org/10.1093/bioinformatics/btz931

Gerovac, M., Chihara, K., Wicke, L., Böttcher, B., Lavigne, R., Vogel, J., 2024. Phage proteins target and co-opt host ribosomes immediately upon infection. Nat Microbiol 9, 787–800. https://doi.org/10.1038/s41564-024-01616-x

Gibson, D.G., Young, L., Chuang, R.Y., Venter, J.C., Hutchison, C.A., Smith, H.O., 2009. Enzymatic assembly of DNA molecules up to several hundred kilobases. Nat Methods 6, 343–345. https://doi.org/10.1038/nmeth.1318

Goff, C.G., 1974. Chemical structure of a modification of the *Escherichia coli* ribonucleic acid polymerase α polypeptides induced by bacteriophage T4 Infection. J Biol Chem 249, 6181–6190. https://doi.org/10.1016/S0021-9258(19)42238-2

Gokhale, N.S., Mcintyre, A.B.R., Mcfadden, M.J., Roder, A.E., Kennedy, E.M., Gandara, J.A., Hopcraft, S.E., Quicke, K.M., Vazquez, C., Willer, J., Ilkayeva, O.R., Law, B.A., Holley, C.L., Garcia-Blanco, M.A., Evans, M.J., Suthar, M.S., Bradrick, S.S., Mason, C.E., Horner, S.M., 2016. N^6-methyladenosine in *Flaviviridae* viral RNA genomes regulates infection. Cell Host Microbe 20, 654–665. https://doi.org/10.1016/j.chom.2016.09.015

Golovina, A.Y., Dzama, M.M., Osterman, I.A., Sergiev, P. V, Serebryakova, M. V, Bogdanov, A.A., Dontsova, O.A., 2012. The last rRNA methyltransferase of *E. coli* revealed: The *yhiR* gene encodes adenine-N^6 methyltransferase specific for modification of A2030 of 23S ribosomal RNA. RNA 18, 1725–1734. https://doi.org/10.1261/rna.034207.112

Golovina, A.Y., Sergiev, P. V, Golovin, A. V, Serebryakova, M. V, Demina, I., Govorun, V.M., Dontsova, O.A., 2009. The *yfiC* gene of *E. coli* encodes an adenine-N^6 methyltransferase that specifically modifies A37 of $tRNA^{Val}_1$ (cmo^5UAC). RNA 15, 1134–1141. https://doi.org/10.1261/rna.1494409

Gong, C., Chakraborty, D., Koudelka, G.B., 2024. A prophage encoded ribosomal RNA methyltransferase regulates the virulence of Shiga-toxin-producing *Escherichia coli* (STEC). Nucleic Acids Res 52, 856–871. https://doi.org/10.1093/nar/gkad1150

Gorzelnik, K.V., Zhang, J., 2021. Cryo-EM reveals infection steps of single-stranded RNA bacteriophages. Prog Biophys Mol Biol 160, 79–86. https://doi.org/10.1016/j.pbiomolbio.2020.07.011

Groslambert, J., Prokhorova, E., Ahel, I., 2021. ADP-ribosylation of DNA and RNA. DNA Repair (Amst) 105, 103144. https://doi.org/10.1016/j.dnarep.2021.103144

Gu, X.R., Gustafsson, C., Ku, J., Yu, M., Santi, D. V., 1999. Identification of the 16S rRNA m^5C967 methyltransferase from *Escherichia coli*. Biochemistry 38, 4053–4057. https://doi.org/10.1021/bi982364y

Gunderson, J.H., Sogin, M.L., Wollett, G., Hollingdale, M., de la Cruz, V.F., Waters, A.P., McCutchan, T.F., 1987. Structurally distinct, stage-specific ribosomes occur in *Plasmodium*. Science 238, 933–937. https://doi.org/10.1126/science.3672135

Han, J.W., Choi, G.J., Kim, B.S., 2018. Antimicrobial aromatic polyketides: a review of their antimicrobial properties and potential use in plant disease control. World J Microbiol Biotechnol 34, 163. https://doi.org/10.1007/s11274-018-2546-0

Harper, J.E., Miceli, S.M., Roberts, R.J.,, Manley, J.L., 1990. Sequence specificity of the human mRNA N^6-adenosine methylase in vitro. Nucleic Acids Res 18, 5735–5741. https://doi.org/10.1093/nar/18.19.5735

Hashimoto, S.-I., Green, M., 1976. Multiple methylated cap sequences in adenovirus type 2 early mRNA. J Virol 20, 425–435. https://doi.org/10.1128/JVI.20.2.425-435.1976.

Hayashi, Y., Osawa, S., Miura, K., 1966. The methyl groups in ribosomal RNA from *Escherichia coli*. Biochim Biophys Acta 129, 519–531. https://doi.org/10.1016/0005-2787(66)90067-0

Heller, K.J., Schwarz, H., 1985. Irreversible binding to the receptor of bacteriophages T5 and BF23 does not occur with the tip of the tail. J Bacteriol 162, 621–625. https://doi.org/10.1128/jb.162.2.621-625.1985

Helser, T.L., Davies, J.E., Dahlberg, J.E., 1972. Mechanism of kasugamycin resistance in *Escherichia coli*. Nat New Biol 235, 6. https://doi.org/10.1038/newbio235006a0.

Helser, T.L., Davies, J.E., Dahlberg, J.E., 1971. Change in methylation of 16S ribosomal RNA associated with mutation to kasugamycin resistance in *Escherichia coli*. Nat New Biol 233, 12–14. https://doi.org/10.1038/newbio233012a0.

Hirvonen, C.A., Ross, W., Wozniak, C.E., Marasco, E., Anthony, J.R., Aiyar, S.E., Newburn, V.H., Gourse, R.L., 2001. Contributions of UP elements and the transcription factor FIS to expression from the seven *rrn* P1 promoters in *Escherichia coli*. J Bacteriol 183, 6305–6314. https://doi.org/10.1128/JB.183.21.6305-6314.2001

Horner, S.M., Reaves, J. V., 2024. Recent insights into N^6-methyladenosine during viral infection. Curr Opin Genet Dev 87, 102213. https://doi.org/10.1016/j.gde.2024.102213

Howard-Varona, C., Hargreaves, K.R., Solonenko, N.E., Meng Markillie, L., Allen White III, R., Brewer, H.M., Ansong, C., Orr, G., Adkins, J.N., Sullivan, M.B., 2018. Multiple mechanisms drive phage infection efficiency in nearly identical hosts. ISME J 12, 1605–1618. https://doi.org/10.1038/s41396-018-0099-8

Hui, A., de Boer, H.A., 1987. Specialized ribosome system: Preferential translation of a single mRNA species by a subpopulation of mutated ribosomes in *Escherichia coli*. Proc Natl Acad Sci U S A 84, 4762–4766. https://doi.org/10.1073/pnas.84.14.4762

Husain, N., Tkaczuk, K.L., Tulsidas, S.R., Kaminska, K.H., Ĉubrilo, S., Maravić-Vlahoviĉek, G., Bujnicki, J.M., Sivaraman, J., 2010. Structural basis for the methylation of G1405 in 16S rRNA by aminoglycoside resistance methyltransferase Sgm from an antibiotic producer: A diversity of active sites in m^7G methyltransferases. Nucleic Acids Res 38, 4120–4132. https://doi.org/10.1093/nar/gkq122

Imam, H., Kim, G.W., Siddiqui, A., 2020. Epitranscriptomic (N^6-methyladenosine) modification of viral RNA and virus-host interactions. Front Cell Infect Microbiol 10. https://doi.org/10.3389/fcimb.2020.584283

Jablonka, E., Lamb, M.J., 2002. The changing concept of epigenetics. Ann N Y Acad Sci 981, 82–96. https://doi.org/10.1111/j.1749-6632.2002.tb04913.x

Jacob, F., Wollman, E.L., 1953. Induction of phage development in lysogenic bacteria. Cold Spring Harb Symp Quant Biol 18, 101–121. https://doi.org/10.1101/SQB.1953.018.01.019

Jang, S.K., Kräusslich, H.G., Nicklin, M.J., Duke, G.M., Palmenberg, A.C., Wimmer, E., 1988. A segment of the 5' nontranslated region of encephalomyocarditis virus RNA directs internal entry of ribosomes during in vitro translation. J Virol 62, 2636–2643. https://doi.org/10.1128/jvi.62.8.2636-2643.1988

Jha, S., Rollins, M.G., Fuchs, G., Procter, D.J., Hall, E.A., Cozzolino, K., Sarnow, P., Savas, J.N., Walsh, D., 2017. Trans-kingdom mimicry underlies ribosome customization by a poxvirus kinase. Nature 546, 651–655. https://doi.org/10.1038/nature22814

Jia, G., Fu, Y., Zhao, X., Dai, Q., Zheng, G., Yang, Y., Yi, C., Lindahl, T., Pan, T., Yang, Y.G., He, C., 2011. N^6-methyladenosine in nuclear RNA is a major substrate of the obesity-associated FTO. Nat Chem Biol 7, 885–887. https://doi.org/10.1038/nchembio.687

Jiang, X., Liu, B., Nie, Z., Duan, L., Xiong, Q., Jin, Z., Yang, C., Chen, Y., 2021. The role of m^6A modification in the biological functions and diseases. Signal Transduct Target Ther 6. https://doi.org/10.1038/s41392-020-00450-x

Ju, X., Fang, X., Xiao, Y., Li, B., Shi, R., Wei, C., You, C., 2021. Small RNA GcvB regulates oxidative stress response of *Escherichia coli*. Antioxidants 10, 1774. https://doi.org/10.3390/antiox10111774

Kaberdina, A.C., Szaflarski, W., Nierhaus, K.H., Moll, I., 2009. An unexpected type of ribosomes induced by kasugamycin: A look into ancestral times of protein synthesis? Mol Cell 33, 227–236. https://doi.org/10.1016/j.molcel.2008.12.014

Kai, K., 2019. Bioorganic chemistry of signaling molecules in microbial communication. J Pestic Sci 44, 200–207. https://doi.org/10.1584/jpestics.J19-02

Kane, S.E., Beemon, K., 1985. Precise localization of m^6A in Rous sarcoma virus RNA reveals clustering of methylation sites: Implications for RNA processing. Mol Cell Biol 5, 2298–2306. https://doi.org/10.1128/mcb.5.9.2298-2306.1985

Kassambara, A., 2023. ggpubr: "ggplot2" based publication ready plots. R package version 0.6.0. https://doi.org/10.32614/CRAN.package.ggpubr

Keen, E.C., 2015. A century of phage research: Bacteriophages and the shaping of modern biology. BioEssays 37, 6–9. https://doi.org/10.1002/bies.201400152

Kennedy, E.M., Bogerd, H.P., Kornepati, A.V.R., Kang, D., Ghoshal, D., Marshall, J.B., Poling, B.C., Tsai, K., Gokhale, N.S., Horner, S.M., Cullen, B.R., 2016. Posttranscriptional m^6A editing of HIV-1 mRNAs enhances viral gene expression. Cell Host Microbe 19, 675–685. https://doi.org/10.1016/j.chom.2016.04.002

Kim, D.-S., Challa, S., Jones, A., Kraus, W.L., 2020. PARPs and ADP-ribosylation in RNA biology: From RNA expression and processing to protein translation and proteostasis. Genes Dev 34, 302–320. https://doi.org/10.1101/gad.334433.119

Kimura, S., Ikeuchi, Y., Kitahara, K., Sakaguchi, Y., Suzuki, Takeo, Suzuki, Tsutomu, 2012. Base methylations in the double-stranded RNA by a fused methyltransferase bearing unwinding activity. Nucleic Acids Res 40, 4071–4085. https://doi.org/10.1093/nar/gkr1287

Koch, T., Raudonikiene, A., Wilkens, K., Rüger, W., 1995. Overexpression, purification, and characterization of the ADP-ribosyltransferase (gpAlt) of bacteriophage T4: ADP-

ribosylation of *E. coli* RNA polymerase modulates T4 “early” transcription. Gene Expr 4, 253–64.

Kojic, M., Topisirovic, L., Vasiljevic, B., 1996. Translational autoregulation of the *sgm* gene from *Micromonospora zionensis*. J Bacteriol 178, 5493–5498. https://doi.org/10.1128/jb.178.18.5493-5498.1996.

Kondrashov, N., Pusic, A., Stumpf, C.R., Shimizu, K., Hsieh, A.C., Xue, S., Ishijima, J., Shiroishi, T., Barna, M., 2011. Ribosome-mediated specificity in hox mRNA translation and vertebrate tissue patterning. Cell 145, 383–397. https://doi.org/10.1016/j.cell.2011.03.028

Kõressaar, T., Lepamets, M., Kaplinski, L., Raime, K., Andreson, R., Remm, M., 2018. Primer3-masker: Integrating masking of template sequence with primer design software. Bioinformatics 34, 1937–1938. https://doi.org/10.1093/bioinformatics/bty036

Koressaar, T., Remm, M., 2007. Enhancements and modifications of primer design program Primer3. Bioinformatics 23, 1289–1291. https://doi.org/10.1093/bioinformatics/btm091

Kowalak, J.A., Bruengei, E., McCloskey, J.A., 1995. Posttranscriptional modification of the central loop of domain V in *Escherichia coli* 23S ribosomal RNA. J Biol Chem 270, 17758–17764. https://doi.org/10.1074/jbc.270.30.17758.

Kropinski, A.M., Mazzocco, A., Waddell, T.E., Lingohr, E., Johnson, R.P., 2009. Enumeration of bacteriophages by double agar overlay plaque assay, in: Methods Mol Biol. pp. 69–76. https://doi.org/10.1007/978-1-60327-164-6_7

Krug, R.M., Morgan, M.A., Shatkin, A.J., 1976. Influenza viral mRNA contains internal N^6-methyladenosine and 5’-terminal 7-methylguanosine in cap structures. J Virol 20, 45–53. https://doi.org/10.1128/JVI.20.1.45-53.1976.

Kutter, E., 2009. Phage host range and efficiency of plating, in: Methods Mol Biol. pp. 141–149. https://doi.org/10.1007/978-1-60327-164-6_14

Kutter, E.M., Wiberu, J.S., 1968. Degradation of cytosine-containing bacterial and bacteriophage DNA after infection of *Escherichia coli* B with bacteriophage T4 wild type and with mutants defective in genes 46,47 and 56. J. Mol. Biol 38, 395411. https://doi.org/10.1016/0022-2836(68)90394-x.

Lafontaine, D., Vandenhaute, J., Tollervey, D., 1995. The 18S rRNA dimethylase Dim1p is required for pre-ribosomal RNA processing in yeast. Genes Dev 9, 2470–2481. https://doi.org/10.1101/gad.9.20.2470.

Landry, D.M., Hertz, M.I., Thompson, S.R., 2009. RPS25 is essential for translation initiation by the *Dicistroviridae* and hepatitis C viral IRESs. Genes Dev 23, 2753–2764. https://doi.org/10.1101/gad.1832209

Lanni, Y.T., 1968. First-step-transfer deoxyribonucleic acid of bacteriophage T5. Bacteriol Rev 32, 227–242. https://doi.org/10.1128/br.32.3.227-242.1968

Lassak, J., Henche, A.L., Binnenkade, L., Thormann, K.M., 2010. ArcS, the cognate sensor kinase in an atypical arc system of *Shewanella oneidensis* MR-1. Appl Environ Microbiol 76, 3263. https://doi.org/10.1128/AEM.00512-10

Lauber, M.A., Rappsilber, J., Reilly, J.P., 2012. Dynamics of ribosomal protein S1 on a bacterial ribosome with cross-linking and mass spectrometry. Mol Cell Proteomics 11, 1965–1976. https://doi.org/10.1074/mcp.M112.019562

Lavi, S., Shatkin, A.J., 1975. Methylated simian virus 40-specific RNA from nuclei and cytoplasm of infected BSC-1 cells. Proc Natl Acad Sci U S A 72, 2012–2016. https://doi.org/10.1073/pnas.72.6.2012.

Lederberg, E.M., 1951. Lysogenicity in *E. coli* K-12. Genetics 36, 560–560.

Lederberg, E.M., Lederberg, J., 1953. Genetic studies of lysogenicity in *Escherichia coli*. Genetics 38, 51–64. https://doi.org/10.1093/genetics/38.1.51

Lederberg, J., Cavalli, L.L., Lederberg, E.M., 1952. Sex compatibility in *Escherichia coli*. Genetics 37, 720–730. https://doi.org/10.1093/genetics/37.6.720

Lee, W.L., Sinha, A., Lam, L.N., Loo, H.L., Liang, J., Ho, P., Cui, L., Chan, C.S.C., Begley, T., Kline, K.A., Dedon, P., 2023. An RNA modification enzyme directly senses reactive oxygen species for translational regulation in *Enterococcus faecalis*. Nat Commun 14, 4093. https://doi.org/10.1038/s41467-023-39790-x

Lesnyak, D. V., Sergiev, P. V., Bogdanov, A.A., Dontsova, O.A., 2006. Identification of *Escherichia coli* m^2G methyltransferases: I. The *ycbY* gene encodes a methyltransferase specific for G2445 of the 23S rRNA. J Mol Biol 364, 20–25. https://doi.org/10.1016/j.jmb.2006.09.009

Li, C., Wang, Z., Zhao, J., Wang, L., Xie, G., Huang, J., Zhang, Y., 2021. A novel vibriophage vB_VcaS_HC containing lysogeny-related gene has strong lytic ability against pathogenic bacteria. Virol Sin 36, 281–290. https://doi.org/10.1007/s12250-020-00271-w

Li, J., Zhou, J., Xia, Y., Rui, Y., Yang, X., Xie, G., Jiang, G., Wang, H., 2023. Rolling circle extension-assisted loop-mediated isothermal amplification (Rol-LAMP) method for locus-specific and visible detection of RNA N^6-methyladenosine. Nucleic Acids Res 51, e51. https://doi.org/10.1093/nar/gkad200

Lichinchi, G., Gao, S., Saletore, Y., Gonzalez, G.M., Bansal, V., Wang, Y., Mason, C.E., Rana, T.M., 2016a. Dynamics of the human and viral m^6A RNA methylomes during HIV-1 infection of T cells. Nat Microbiol 1. https://doi.org/10.1038/NMICROBIOL.2016.11

Lichinchi, G., Zhao, B.S., Wu, Y., Lu, Z., Qin, Y., He, C., Rana, T.M., 2016b. Dynamics of human and viral RNA methylation during Zika virus infection. Cell Host Microbe 20, 666–673. https://doi.org/10.1016/j.chom.2016.10.002

Lin, B., Wang, Z., Malanoski, A.P., O'Grady, E.A., Wimpee, C.F., Vuddhakul, V., Alves, N., Thompson, F.L., Gomez-Gil, B., Vora, G.J., 2010. Comparative genomic analyses identify the *Vibrio harveyi* genome sequenced strains BAA-1116 and HY01 as *Vibrio campbellii*. Environ Microbiol Rep 2, 81–89. https://doi.org/10.1111/J.1758-2229.2009.00100.X

Linder, B., Grozhik, A. V., Olarerin-George, A.O., Meydan, C., Mason, C.E., Jaffrey, S.R., 2015. Single-nucleotide-resolution mapping of m^6A and m^6A_m throughout the transcriptome. Nat Methods 12, 767–772. https://doi.org/10.1038/nmeth.3453

Littlefield, J.W., Dunn, D.B., 1958. Natural occurrence of thymine and three methylated adenine bases in several ribonucleic acids. Nature 181, 254–255. https://doi.org/10.1038/181254a0.

Liu, K., Santos, D.A., Hussmann, J.A., Wang, Y., Sutter, B.M., Weissman, J.S., Tu, B.P., 2021. Regulation of translation by methylation multiplicity of 18S rRNA. Cell Rep 34, 108825. https://doi.org/10.1016/j.celrep.2021.108825

Liu, N., Dai, Q., Zheng, G., He, C., Parisien, M., Pan, T., 2015. N^6-methyladenosine-dependent RNA structural switches regulate RNA-protein interactions. Nature 518, 560–564. https://doi.org/10.1038/nature14234

Liu, W.W., Zheng, S.Q., Li, T., Fei, Y.F., Wang, C., Zhang, S., Wang, F., Jiang, G.M., Wang, H., 2024. RNA modifications in cellular metabolism: Implications for metabolism-targeted therapy and immunotherapy. Signal Transduct Target Ther 9, 70. https://doi.org/10.1038/s41392-024-01777-5

Loeb, T., Zinder, N.D., 1961. A bacteriophage containing RNA. Proc Natl Acad Sci U S A 47, 282–289. https://doi.org/10.1073/pnas.47.3.282

Loomis Jr., W.F., Magasanik, B., 1967. The catabolite repression gene of the *lac* operon in *Escherichia cell*. J Mol Biol 23, 487–494. https://doi.org/10.1016/s0022-2836(67)80120-7.

Lorenz, N., Reiger, M., Toro-Nahuelpan, M., Brachmann, A., Poettinger, L., Plener, L., Lassak, J., Jung, K., 2016. Identification and initial characterization of prophages in *Vibrio campbellii*. PLoS One 11, e0156010. https://doi.org/10.1371/journal.pone.0156010

Lu, Y., Jia, R., Zhang, Z., Wang, M., Xu, Y., Zhu, D., Chen, S., Liu, M., Yin, Z., Chen, X., Cheng, A., 2014. In vitro expression and development of indirect ELISA for Capsid protein of duck circovirus without nuclear localization signal. Int J Clin Exp Pathol 7, 4938–4944.

Lucas, M.C., Novoa, E.M., 2023. Long-read sequencing in the era of epigenomics and epitranscriptomics. Nat Methods 20, 25–29. https://doi.org/10.1038/s41592-022-01724-8

Luo, J., Xu, T., Sun, K., 2021. N^6-methyladenosine RNA modification in inflammation: Roles, mechanisms, and applications. Front Cell Dev Biol 9. https://doi.org/10.3389/fcell.2021.670711

Lwoff, A., 1953. Lysogeny. Bacteriol Rev 17, 269–337. https://doi.org/10.1128/br.17.4.269-337.1953

Ma, H., Wang, X., Cai, J., Dai, Q., Natchiar, S.K., Lv, R., Chen, K., Lu, Z., Chen, H., Shi, Y.G., Lan, F., Fan, J., Klaholz, B.P., Pan, T., Shi, Y., He, C., 2019. N^6-Methyladenosine methyltransferase ZCCHC4 mediates ribosomal RNA methylation. Nat Chem Biol 15, 88–94. https://doi.org/10.1038/s41589-018-0184-3

Macinga, D.R., Parojcic, M.M., Rather, P.N., 1995. Identification and analysis of aarP, a transcriptional activator of the 2'-N-acetyltransferase in *Providencia stuartii*. J Bacteriol 177, 3407. https://doi.org/10.1128/JB.177.12.3407-3413.1995

Madsen, C.T., 2003. Identifying the methyltransferases for m^5U747 and m^5U1939 in 23S rRNA using MALDI mass spectrometry. Nucleic Acids Res 31, 4738–4746. https://doi.org/10.1093/nar/gkg657

Maeda, M., Shimada, T., Ishihama, A., 2015. Strength and regulation of seven rRNA promoters in *Escherichia coli*. PLoS One 10, e0144697. https://doi.org/10.1371/journal.pone.0144697

Maffei, E., Shaidullina, A., Burkolter, M., Heyer, Y., Estermann, F., Druelle, V., Sauer, P., Willi, L., Michaelis, S., Hilbi, H., Thaler, D.S., Harms, A., 2021. Systematic exploration of *Escherichia coli* phage-host interactions with the BASEL phage collection. PLoS Biol 19, e3001424. https://doi.org/10.1371/journal.pbio.3001424

Majzoub, K., Hafirassou, M.L., Meignin, C., Goto, A., Marzi, S., Fedorova, A., Verdier, Y., Vinh, J., Hoffmann, J.A., Martin, F., Baumert, T.F., Schuster, C., Imler, J.-L., 2014. RACK1 controls IRES-mediated translation of viruses. Cell 159, 1086–1095. https://doi.org/10.1016/j.cell.2014.10.041

Mandal, P.K., Ballerin, G., Nolan, L.M., Petty, N.K., Whitchurch, C.B., 2021. Bacteriophage infection of *Escherichia coli* leads to the formation of membrane vesicles via both explosive cell lysis and membrane blebbing. Microbiology (Reading) 167, 001021. https://doi.org/10.1099/mic.0.001021

Manners, O., Baquero-Perez, B., Whitehouse, A., 2019. m^6A: Widespread regulatory control in virus replication. Biochim Biophys Acta Gene Regul Mech 1862, 370–381. https://doi.org/10.1016/j.bbagrm.2018.10.015

Mäntynen, S., Laanto, E., Oksanen, H.M., Poranen, M.M., Díaz-Muñoz, S.L., 2021. Black box of phage-bacterium interactions: Exploring alternative phage infection strategies. Open Biol 11, 210188. https://doi.org/10.1098/rsob.210188

Mattick, J.S., 2003. Challenging the dogma: The hidden layer of non-protein-coding RNAs in complex organisms. BioEssays 25, 930–939. https://doi.org/10.1002/bies.10332

Mekler, P., 1981. Determination of nucleotide sequences of the bacteriophage Qbeta genome: Organization and evolution of an RNA virus (PhD Thesis). University of Zürich, Zürich.

Melo, L.D.R., Monteiro, R., Pires, D.P., Azeredo, J., 2022. Phage-host interaction analysis by flow cytometry allows for rapid and efficient screening of phages. Antibiotics 11, 164. https://doi.org/10.3390/antibiotics11020164

Meng, R., Jiang, M., Cui, Z., Chang, J.-Y., Yang, K., Jakana, J., Yu, X., Wang, Z., Hu, B., Zhang, J., 2019. Structural basis for the adsorption of a single-stranded RNA bacteriophage. Nat Commun 10, 3130. https://doi.org/10.1038/s41467-019-11126-8

Mets, T., Kurata, T., Ernits, K., Johansson, M.J.O., Craig, S.Z., Evora, G.M., Buttress, J.A., Odai, R., Wallant, K.C., Nakamoto, J.A., Shyrokova, L., Egorov, A.A., Doering, C.R., Brodiazhenko, T., Laub, M.T., Tenson, T., Strahl, H., Martens, C., Harms, A., Garcia-Pino, A., Atkinson, G.C., Hauryliuk, V., 2024. Mechanism of phage sensing and restriction by toxin-antitoxin-chaperone systems. Cell Host Microbe 32, 1059–1073. https://doi.org/10.1016/j.chom.2024.05.003

Meyer, F., Weber, H., Weissmann, C., 1981. Interactions of Qβ replicase with Qβ RNA. J Mol Biol 153, 631–660. https://doi.org/10.1016/0022-2836(81)90411-3

Meyer, K.D., Saletore, Y., Zumbo, P., Elemento, O., Mason, C.E., Jaffrey, S.R., 2012. Comprehensive analysis of mRNA methylation reveals enrichment in 3′ UTRs and near stop codons. Cell 149, 1635–1646. https://doi.org/10.1016/j.cell.2012.05.003

Milne, A.N., Mak, W.W., Wong, J.T., 1975. Variation of ribosomal proteins with bacterial growth rate. J Bacteriol 122, 89–92. https://doi.org/10.1128/jb.122.1.89-92.1975

Moll, I., Grill, S., Gründling, A., Bläsi, U., 2002a. Effects of ribosomal proteins S1, S2 and the DeaD/CsdA DEAD-box helicase on translation of leaderless and canonical mRNAs in

Escherichia coli. Mol Microbiol 44, 1387–1396. https://doi.org/10.1046/j.1365-2958.2002.02971.x

Moll, I., Grill, S., Gualerzi, C.O., Bläsi, U., 2002b. Leaderless mRNAs in bacteria: surprises in ribosomal recruitment and translational control. Mol Microbiol 43, 239–246. https://doi.org/10.1046/j.1365-2958.2002.02739.x

Moll, I., Hirokawa, G., Kiel, M.C., Kaji, A., Bläsi, U., 2004. Translation initiation with 70S ribosomes: An alternative pathway for leaderless mRNAs. Nucleic Acids Res 32, 3354–3363. https://doi.org/10.1093/nar/gkh663

Moss, B., Gershowitz, A., Stringer, J.R., Holland, L.E., Wagner, E.K., 1977. 5'-terminal and internal methylated nucleosides in herpes simplex virus type 1 mRNA. J Virol 23, 234–239. https://doi.org/10.1128/JVI.23.2.234-239.1977.

Moss, B., Koczot, F., 1976. Sequence of methylated nucleotides at the 5'-terminus of adenovirus-specific RNA. J Virol 17, 385–392. https://doi.org/10.1128/jvi.17.2.385-392.1976

Murray, N.E., Brammar, W., Murray, K., 1977. Lambdoid phages that simplify the recovery of in vitro recombinants. Mol Gen Genet 150, 53–61. https://doi.org/https://doi.org/10.1007/BF02425325

Narayan, P., Ayers, D.F., Rottman, F.M., Maroney, P.A., Nilsen, T.W., 1987. Unequal distribution of N^6-methyladenosine in influenza virus mRNAs. Mol Cell Biol 7, 1572–1575. https://doi.org/10.1128/mcb.7.4.1572-1575.1987

Narayan, P., Ludwiczak, R.L., Goodwin, E.C., Rottman, F.M., 1994. Context effects on N^6-adenosine methylation sites in prolactin mRNA. Nucleic Acids Res 22, 419–426. https://doi.org/10.1093/nar/22.3.419.

Naureen, Z., Dautaj, A., Anpilogov, K., Camilleri, G., Dhuli, K., Tanzi, B., Maltese, P.E., Cristofoli, F., Antoni, L. De, Beccari, T., Dundar, M., Bertelli, M., 2020. Bacteriophages presence in nature and their role in the natural selection of bacterial populations. Acta Biomedica 91, 1–13. https://doi.org/10.23750/abm.v91i13-S.10819

Nonoyama, M., Atsushi, Y., Ikeda, Y., 1963. On some properties of phage β, a new RNA containing phage. J Gen Appl Microbiol 9, 299–305. https://doi.org/10.2323/jgam.9.299

Nuidate, T., Kuaphiriyakul, A., Surachat, K., Mittraparp-Arthorn, P., 2021. Induction and genome analysis of HY01, a newly reported prophage from an emerging shrimp pathogen *Vibrio campbellii*. Microorganisms 9, 1–18. https://doi.org/10.3390/microorganisms9020400

Ofir, G., Sorek, R., 2018. Contemporary phage biology: From classic models to new insights. Cell 172, 1260–1270. https://doi.org/10.1016/j.cell.2017.10.045

Ohno, S., 1972. So much "junk" DNA in our genome. Brookhaven Symp Biol 23, 366–70.

Okamoto, S., Tamaru, A., Nakajima, C., Nishimura, K., Tanaka, Y., Tokuyama, S., Suzuki, Y., Ochi, K., 2007. Loss of a conserved 7-methylguanosine modification in 16S rRNA confers low-level streptomycin resistance in bacteria. Mol Microbiol 63, 1096–1106. https://doi.org/10.1111/j.1365-2958.2006.05585.x

Olsthoorn, R., van Duin, J., 2011. Bacteriophages with ssRNA, in: Encyclopedia of Life Sciences. Wiley. https://doi.org/10.1002/9780470015902.a0000778.pub3

Orlova, E. V., 2012. Bacteriophages and their structural organisation, in: Ipek Kurtböke (Ed.), Bacteriophages. INTECH Open Access Publisher, Rijeka, Croatia.

Overby, L.R., Barlow, G.H., Doi, R.H., Jacob, M., Spiegelman, S., 1966a. Comparison of two serologically distinct ribonucleic acid bacteriophages I. Properties of the viral particles. J Bacteriol 91, 442–448. https://doi.org/10.1128/jb.91.1.442-448.1966

Overby, L.R., Barlow, G.H., Doi, R.H., Jacob, M., Spiegelman, S., 1966b. Comparison of two serologically distinct ribonucleic acid bacteriophages II. Properties of the nucleic acids and coat proteins. J Bacteriol 92, 739–745. https://doi.org/10.1128/jb.92.3.739-745.1966

Pelletier, J., Sonenberg, N., 1988. Internal initiation of translation of eukaryotic mRNA directed by a sequence derived from poliovirus RNA. Nature 334, 320–325. https://doi.org/10.1038/334320a0

Pendleton, K.E., Chen, B., Liu, K., Hunter, O. V., Xie, Y., Tu, B.P., Conrad, N.K., 2017. The U6 snRNA m^6A methyltransferase METTL16 regulates SAM synthetase intron retention. Cell 169, 824-835.e14. https://doi.org/10.1016/j.cell.2017.05.003

Perry, F.P., Kelley, D.E., 1974. Existence of methylated messenger RNA in mouse L cells. Cell 1, 37–42.

Petrov, D.P., Kaiser, Steffen, Kaiser, Stefanie, Jung, K., 2022. Opportunities and challenges to profile mRNA modifications in *Escherichia coli*. Chembiochem 23, e202200270. https://doi.org/10.1002/CBIC.202200270

Pfaffl, M.W., 2001. A new mathematical model for relative quantification in real-time RT-PCR. Nucleic Acids Res 29, 45e–445. https://doi.org/10.1093/nar/29.9.e45

Ping, X.L., Sun, B.F., Wang, L., Xiao, W., Yang, X., Wang, W.J., Adhikari, S., Shi, Y., Lv, Y., Chen, Y.S., Zhao, X., Li, A., Yang, Y., Dahal, U., Lou, X.M., Liu, X., Huang, J., Yuan, W.P., Zhu, X.F., Cheng, T., Zhao, Y.L., Wang, X., Danielsen, J.M.R., Liu, F., Yang, Y.G., 2014. Mammalian WTAP is a regulatory subunit of the RNA N^6-methyladenosine methyltransferase. Cell Res 24, 177–189. https://doi.org/10.1038/cr.2014.3

Pletnev, P., Guseva, E., Zanina, A., Evfratov, S., Dzama, M., Treshin, V., Pogorel'skaya, A., Osterman, I., Golovina, A., Rubtsova, M., Serebryakova, M., Pobeguts, O. V., Govorun, V.M., Bogdanov, A.A., Dontsova, O.A., Sergiev, P. V., 2020. Comprehensive functional analysis of *Escherichia coli* ribosomal RNA methyltransferases. Front Genet 11, 97. https://doi.org/10.3389/fgene.2020.00097

Poldermans, B., Roza, L., Van Knippenberg, P.H., 1979. Studies on the function of two adjacent N^6,N^6-dimethyladenosines near the 3' end of 16S ribosomal RNA of *Escherichia coli*. III. Purification and properties of the methylating enzyme and methylase-30S interactions. J Biol Chem 254, 9094–9100. https://doi.org/10.1016/s0021-9258(19)86815-1

Poot, R.A., Tsareva, N. V., Boni, I. V., van Duin, J., 1997. RNA folding kinetics regulates translation of phage MS2 maturation gene. Proc Natl Acad Sci U S A 94, 10110–10115. https://doi.org/10.1073/pnas.94.19.10110

Prusiner, S.B., 1998. Prions. Proc Natl Acad Sci U S A 95, 13363–13383. https://doi.org/10.1073/pnas.95.23.13363.

Punekar, A.S., Liljeruhm, J., Shepherd, T.R., Forster, A.C., Selmer, M., 2013. Structural and functional insights into the molecular mechanism of rRNA m^6A methyltransferase RlmJ. Nucleic Acids Res 41, 9537–9548. https://doi.org/10.1093/nar/gkt719

Qin, D., Fredrick, K., 2013. Analysis of polysomes from bacteria, in: Methods Enzymol. pp. 159–172. https://doi.org/10.1016/B978-0-12-420037-1.00008-7.

Ramagopal, S., 1990. Induction of cell-specific ribosomal proteins in aggregation-competent nonmorphogenetic *Dictyostelium discoideum*. Biochem Cell Biol 68, 1281–1287. https://doi.org/10.1139/o90-190

Ren, W., Rajendran, R., Zhao, Y., Tan, B., Wu, G., Bazer, F.W., Zhu, G., Peng, Y., Huang, X., Deng, J., Yin, Y., 2018. Amino acids as mediators of metabolic cross-talk between host and pathogen. Front Immunol 9, 319. https://doi.org/10.3389/fimmu.2018.00319

Rezaie, N., Reese, F., Mortazavi, A., 2023. PyWGCNA: a Python package for weighted gene co-expression network analysis. Bioinformatics 39. https://doi.org/10.1093/bioinformatics/btad415

Rhoades, M., 1982. New physical map of bacteriophage T5 DNA. J Virol 43, 566–573. https://doi.org/10.1128/jvi.43.2.566-573.1982

Riquelme-Barrios, S., Camus, L.V., Cusack, S.A., Burdack, K., Petrov, D.P., Yeşiltaç-Tosun, G.N., Kaiser, S., Giehr, P., Jung, K., 2024. Direct RNA sequencing of the *Escherichia coli* epitranscriptome uncovers alterations under heat stress. bioRxiv. https://doi.org/10.1101/2024.07.08.602490

Rottman, F.M., Bokar, J.A., Narayan, P., Ludwiczak, R., 1994. N^6-Adenosine methylation in mRNA: Substrate specificity and enzyme complexity. Biochimie 76, 1109–1114. https://doi.org/10.1016/0300-9084(94)90038-8.

Saikia, B., Riquelme-Barrios, S., Carell, T., Brameyer, S., Jung, K., 2024. Depletion of m^6A-RNA in *Escherichia coli* reduces the infectious potential of T5 bacteriophage. Microbiol Spectr 12, e0112424. https://doi.org/10.1128/spectrum.01124-24

Saito, K., Kratzat, H., Campbell, A., Buschauer, R., Burroughs, A.M., Berninghausen, O., Aravind, L., Green, R., Beckmann, R., Buskirk, A.R., 2022. Ribosome collisions induce mRNA

cleavage and ribosome rescue in bacteria. Nature 603, 503–508. https://doi.org/10.1038/s41586-022-04416-7

Salmond, G.P.C., Fineran, P.C., 2015. A century of the phage: Past, present and future. Nat Rev Microbiol 13, 777–786. https://doi.org/10.1038/nrmicro3564

Sambrook, J., Russell, D.W., 2006. Purification of nucleic acids by extraction with phenol:chloroform. CSH Protoc 2006, pdb.prot4455. https://doi.org/10.1101/pdb.prot4455

Saneyoshi, M., Harada, F., Nishimura, S., 1969. Isolation and characterization of N^6-methyladenosine from *Escherichia coli* valine transfer RNA. Biochim Biophys Acta 190, 264–273. https://doi.org/10.1016/0005-2787(69)90078-1.

Saneyoshi, M., Ohashi, Z., Harada, F., Nishimrura, S., 1972. Isolation and characterization of 2-methyladenosine from *Escherichia coli* $tRNA^{Glu}_2$, $tRNA^{Asp}_1$, $tRNA^{His}_1$ and $tRNA^{Arg}$. Biochim Biophys Acta 262, 1–10.

Sangseedum, C., Vuddhakul, V., Mittraparp-arthorn, P., 2017. Isolation and host range of *Vibrio campbellii* bacteriophages isolated from Cockles. Proc Natl Internatl Grad Res Conference, 241-247.

Schieweck, R., Ciccopiedi, G., Klau, K., Popper, B., 2023. Monosomes buffer translational stress to allow for active ribosome elongation. Front Mol Biosci 10, 1158043. https://doi.org/10.3389/fmolb.2023.1158043

Schneider, C., Erhard, F., Binotti, B., Buchberger, A., Vogel, J., Fischer, U., 2022. An unusual mode of baseline translation adjusts cellular protein synthesis capacity to metabolic needs. Cell Rep 41, 111467. https://doi.org/10.1016/j.celrep.2022.111467

Schneider, C.A., Rasband, W.S., Eliceiri, K.W., 2012. NIH Image to ImageJ: 25 years of image analysis. Nat Methods 9, 671–675. https://doi.org/10.1038/nmeth.2089

Schwartz, S., Agarwala, S.D., Mumbach, M.R., Jovanovic, M., Mertins, P., Shishkin, A., Tabach, Y., Mikkelsen, T.S., Satija, R., Ruvkun, G., Carr, S.A., Lander, E.S., Fink, G.R., Regev, A., 2013. High-resolution mapping reveals a conserved, widespread, dynamic mRNA methylation program in yeast meiosis. Cell 155, 1409–1421. https://doi.org/10.1016/j.cell.2013.10.047

Schwarz, J., Brameyer, S., Hoyer, E., Jung, K., 2023. The interplay of AphB and CadC to activate acid resistance of *Vibrio campbellii*. J Bacteriol 205, e0045722. https://doi.org/10.1128/JB.00457-22

Sendinc, E., Shi, Y., 2023. RNA m^6A methylation across the transcriptome. Mol Cell 83, 428–441. https://doi.org/10.1016/j.molcel.2023.01.006

Sendinc, E., Valle-Garcia, D., Dhall, A., Chen, H., Henriques, T., Navarrete-Perea, J., Sheng, W., Gygi, S.P., Adelman, K., Shi, Y., 2019. PCIF1 catalyzes m^6A_m mRNA methylation to regulate gene expression. Mol Cell 75, 620-630.e9. https://doi.org/10.1016/j.molcel.2019.05.030

Sergiev, P. V., Golovina, A.Y., Osterman, I.A., Nesterchuk, M. V., Sergeeva, O. V., Chugunova, A.A., Evfratov, S.A., Andreianova, E.S., Pletnev, P.I., Laptev, I.G., Petriukov, K.S., Navalayeu, T.I., Koteliansky, V.E., Bogdanov, A.A., Dontsova, O.A., 2016. N^6-methylated adenosine in RNA: From bacteria to humans. J Mol Biol 428, 2134–2145. https://doi.org/10.1016/J.JMB.2015.12.013

Sergiev, P. V, Serebryakova, M. V, Bogdanov, A.A., Dontsova, O.A., 2007. The *ybiN* gene of *Escherichia coli* encodes adenine-N^6 methyltransferase specific for modification of A1618 of 23S ribosomal RNA, a methylated residue located close to the ribosomal exit tunnel. J Mol Biol 375, 291–300. https://doi.org/10.1016/j.jmb.2007.10.051

Shan, Y., Chen, W., Li, Y., 2024. The role of m^6A RNA methylation in autoimmune diseases: Novel therapeutic opportunities. Genes Dis 11, 252–267. https://doi.org/10.1016/j.gendis.2023.02.013

Shapiro, J.A., 2009. Revisiting the central dogma in the 21st century. Ann N Y Acad Sci 1178, 6–28. https://doi.org/10.1111/j.1749-6632.2009.04990.x

Shatkin, A.J., 1976. Capping of eucaryotic mRNAs review. Cell 9, 5–653. https://doi.org/10.1016/0092-8674(76)90128-8

Shi, H., Chai, P., Jia, R., Fan, X., 2020. Novel insight into the regulatory roles of diverse RNA modifications: Re-defining the bridge between transcription and translation. Mol Cancer 19, 78. https://doi.org/10.1186/s12943-020-01194-6

Shi, H., Wei, J., He, C., 2019. Where, when, and how: Context-dependent functions of RNA methylation writers, readers, and erasers. Mol Cell 74, 640–650. https://doi.org/10.1016/j.molcel.2019.04.025

Shi, Z., Fujii, K., Kovary, K.M., Genuth, N.R., Röst, H.L., Teruel, M.N., Barna, M., 2017. Heterogeneous ribosomes preferentially translate distinct subpools of mRNAs genome-wide. Mol Cell 67, 71–83. https://doi.org/10.1016/j.molcel.2017.05.021

Sirbasku, D.A., Buchanan, J.M., 1970a. Patterns of ribonucleic acid synthesis in T5-infected *Escherichia coli* . II. Separation of high molecular weight ribonucleic acid species by disc electrophoresis on acrylamide gel columns. J Biol Chem 245, 2679–92.

Sirbasku, D.A., Buchanan, J.M., 1970b. Patterns of ribonucleic acid synthesis in T5-infected *Escherichia coli*. III. Separation of low molecular weight ribonucleic acid species by disc electrophoresis on acrylamide gel columns. J Biol Chem 245, 2693–703.

Skutel, M., Andriianov, A., Zavialova, M., Kirsanova, M., Shodunke, O., Zorin, E., Golovshchinskii, A., Severinov, K., Isaev, A., 2023. T5-like phage BF23 evades host-mediated DNA restriction and methylation. Microlife 4, uqad044. https://doi.org/10.1093/femsml/uqad044

Srisangthong, I., Sangseedum, C., Chaichanit, N., Surachat, K., Suanyuk, N., Mittraparp-arthorn, P., 2023. Characterization and genome analysis of *Vibrio campbellii* lytic bacteriophage OPA17. Microbiol Spectr 11, e0162322. https://doi.org/10.1128/spectrum.01623-22

Starr, J.L., Fefferman, R., 1964. The occurrence of methylated bases in ribosomal ribonucleic acid of *Escherichia coli* K12 W-6*. J Biol Chem 239, 3457–3461.

Stoltzfus, C.M., Dimock, K., 1976. Evidence for methylation of B77 avian sarcoma virus genome RNA subunits. J Virol 18, 586–595. https://doi.org/10.1128/JVI.18.2.586-595.1976.

Strauss, J.H., Sinsheimer, R.L., 1963. Purification and properties of bacteriophage MS2 and of its ribonucleic acid. J Mol Biol 7, 43–54. https://doi.org/10.1016/S0022-2836(63)80017-0

Studier, F.W., Moffatt, B.A., 1986. Use of bacteriophage T7 RNA polymerase to direct selective high-level expression of cloned genes. J Mol Biol 189, 113–130. https://doi.org/10.1016/0022-2836(86)90385-2

Subedi, D., Barr, J.J., 2021. Temporal stability and genetic diversity of 48-Year-Old T-series phages. mSystems 6, e00990-20. https://doi.org/10.1128/msystems.00990-20

Suzuki, T., 2021. The expanding world of tRNA modifications and their disease relevance. Nat Rev Mol Cell Biol 22, 375–392. https://doi.org/10.1038/s41580-021-00342-0

Takeshita, D., Tomita, K., 2010. Assembly of Qβ viral RNA polymerase with host translational elongation factors EF-Tu and -Ts. Proc Natl Acad Sci U S A 107, 15733–8. https://doi.org/10.1073/pnas.1006559107

Temin, H.M., Mizutani, S., 1970. RNA-dependent DNA polymerase in virions of Rous sarcoma virus. Nature 1211–1213. https://doi.org/10.1038/2261211a0.

Tiemann, B., Depping, R., Gineikiene, E., Kaliniene, L., Nivinskas, R., Rüger, W., 2004. ModA and ModB, two ADP-ribosyltransferases encoded by bacteriophage T4: Catalytic properties and mutation analysis. J Bacteriol 186, 7262–7272. https://doi.org/10.1128/JB.186.21.7262-7272.2004

Tirumuru, N., Simen Zhao, B., Lu, W., Lu, Z., He, C., Wu, L., 2016. N^6-methyladenosine of HIV-1 RNA regulates viral infection and HIV-1 Gag protein expression. Elife 5, e15528. https://doi.org/10.7554/eLife.15528.001

Toh, S.M., Xiong, L., Bae, T., Mankin, A.S., 2008. The methyltransferase YfgB/RlmN is responsible for modification of adenosine 2503 in 23S rRNA. RNA 14, 98–106. https://doi.org/10.1261/rna.814408

Tokuhisa, J.G., Vijayan, P., Feldmann, K.A., Browse, J.A., 1998. Chloroplast development at low temperatures requires a homolog of DIM1, a yeast gene encoding the 18S rRNA dimethylase. Plant Cell 10, 699–711. https://doi.org/10.1105/tpc.10.5.699

Tomikawa, C., 2018. 7-methylguanosine modifications in transfer RNA (tRNA). Int J Mol Sci 19. https://doi.org/10.3390/ijms19124080

Toopaang, W., Bunnak, W., Srisuksam, C., Wattananukit, W., Tanticharoen, M., Yang, Y.-L., Amnuaykanjanasin, A., 2022. Microbial polyketides and their roles in insect virulence: From genomics to biological functions. Nat Prod Rep 39, 2008–2029. https://doi.org/10.1039/D1NP00058F

Tran, N. van, Ernst, F.G.M., Hawley, B.R., Zorbas, C., Ulryck, N., Hackert, P., Bohnsack, K.E., Bohnsack, M.T., Jaffrey, S.R., Graille, M., Lafontaine, D.L.J., 2019. The human 18S rRNA m^6A methyltransferase METTL5 is stabilized by TRMT112. Nucleic Acids Res 47, 7719–7733. https://doi.org/10.1093/nar/gkz619.

Tsai, K., Courtney, D.G., Cullen, B.R., 2018. Addition of m^6A to SV40 late mRNAs enhances viral structural gene expression and replication. PLoS Pathog 14, e1006919. https://doi.org/10.1371/journal.ppat.1006919

Turner, P.E., Draghi, J.A., Wilpiszeski, R., 2012. High-throughput analysis of growth differences among phage strains. J Microbiol Methods 88, 117–121. https://doi.org/10.1016/j.mimet.2011.10.020

Twest, R. Van, Kropinski, A.M., 2009. Bacteriophage enrichment from water and soil, in: Methods Mol Biol. pp. 15–21.

Twort, F.W., 1915. An Investigation on the nature of ultra-microscopic viruses. The Lancet 186, 1241–1243. https://doi.org/10.1016/S0140-6736(01)20383-3

Tzareva, N. V., Makhno, V.I., Boni, I. V., 1994. Ribosome-messenger recognition in the absence of the Shine-Dalgarno interactions. FEBS Lett 337, 189–194. https://doi.org/10.1016/0014-5793(94)80271-8

Untergasser, A., Cutcutache, I., Koressaar, T., Ye, J., Faircloth, B.C., Remm, M., Rozen, S.G., 2012. Primer3-new capabilities and interfaces. Nucleic Acids Res 40, e115. https://doi.org/10.1093/nar/gks596

Van Duin, J., Van Knippenbero, P.H., 1974. Functional heterogeneity of the 30S ribosomal subunit of *Escherichia coli*. III. Requirement of protein S1 for translation. J Mol Biol 84, 185–195. https://doi.org/10.1016/0022-2836(74)90221-6.

Vassallo, C.N., Doering, C.R., Laub, M.T., 2024. Anti-viral defence by an mRNA ADP-ribosyltransferase that blocks translation. Nature 636, 190–197. https://doi.org/10.1038/s41586-024-08102-8

Vila-Sanjurjo, A., Squires, C.L., Dahlberg, A.E., Laboratory, J.W.W., 1999. Isolation of kasugamycin resistant mutants in the 16S ribosomal RNA of *Escherichia coli*. J Mol Biol 293, 1–8. https://doi.org/10.1006/jmbi.1999.3160.

Voynow, P., Kurlandf, C.G., 1971. Stoichiometry of the 30S ribosomal proteins of *Escherichia coli*. Biochemistry 10, 517–524. https://doi.org/https://doi.org/10.1021/bi00779a026

Wahba, A.J., Miller, M.J., Niveleau, A., Landers, T.A., Carmichael, G.G., Weber, K., Hawley, D.A., Slobin, L.I., 1974. Subunit I of Qβ replicase and 30S ribosomal protein S1 of *Escherichia coli*. Evidence for the identity of the two proteins. J Biol Chem 249, 3314–6.

Wang, Jianbin, Jiang, Y., Vincent, M., Sun, Y., Yu, H., Wang, Jing, Bao, Q., Kong, H., Hu, S., 2005. Complete genome sequence of bacteriophage T5. Virology 332, 45–65. https://doi.org/10.1016/j.virol.2004.10.049

Wang, X., Kim, Y., Ma, Q., Hong, S.H., Pokusaeva, K., Sturino, J.M., Wood, T.K., 2010. Cryptic prophages help bacteria cope with adverse environments. Nat Commun 1. https://doi.org/10.1038/ncomms1146

Warda, A.S., Kretschmer, J., Hackert, P., Lenz, C., Urlaub, H., Höbartner, C., Sloan, K.E., Bohnsack, M.T., 2017. Human METTL16 is a N^6-methyladenosine (m^6A) methyltransferase that targets pre-mRNAs and various non-coding RNAs. EMBO Rep 18, 2004–2014. https://doi.org/10.15252/embr.201744940

Warner, H.R., Drong, R.F., Berget, S.M., 1975. Early events after infection of *Escherichia coli* by bacteriophage T5. Induction of a 5'-nucleotidase activity and excretion of free bases. J Virol 15, 273–280. https://doi.org/10.1128/jvi.15.2.273-280.1975

Weigle, J.J., 1953. Induction of mutations in a bacterial virus. Proc Natl Acad Sci U S A 39, 628–636. https://doi.org/10.1073/pnas.39.7.628

Wendling, C.C., Refardt, D., Hall, A.R., 2021. Fitness benefits to bacteria of carrying prophages and prophage-encoded antibiotic-resistance genes peak in different environments. Evolution 75, 515–528. https://doi.org/10.1111/evo.14153

Wickham, H., 2016. ggplot2: Elegant graphics for data analysis. Springer-Verlag, New York.

Wieckowski, Y., Schiefelbein, J., 2012. Nuclear ribosome biogenesis mediated by the DIM1A rRNA dimethylase is required for organized root growth and epidermal patterning in *Arabidopsis*. Plant Cell 24, 2839–2856. https://doi.org/10.1105/tpc.112.101022

Wilkinson, E., Cui, Y.H., He, Y.Y., 2022. Roles of RNA modifications in diverse cellular functions. Front Cell Dev Biol 10, 828683. https://doi.org/10.3389/fcell.2022.828683

Wolfram-Schauerte, M., Pozhydaieva, N., Grawenhoff, J., Welp, L.M., Silbern, I., Wulf, A., Billau, F.A., Glatter, T., Urlaub, H., Jäschke, A., Höfer, K., 2023. A viral ADP-ribosyltransferase attaches RNA chains to host proteins. Nature 620, 1054–1062. https://doi.org/10.1038/s41586-023-06429-2

Xu, Y., Zhang, W., Shen, F., Yang, X., Liu, H., Dai, S., Sun, X., Huang, J., Guo, Q., 2021. YTH domain proteins: A family of m^6A readers in cancer progression. Front Oncol 11, 629560. https://doi.org/10.3389/fonc.2021.629560

Xu, Z., O'Farrell, H.C., Rife, J.P., Culver, G.M., 2008. A conserved rRNA methyltransferase regulates ribosome biogenesis. Nat Struct Mol Biol 15, 534–536. https://doi.org/10.1038/nsmb.1408

Yang, C., Hu, Y., Zhou, B., Bao, Y., Li, Z., Gong, C., Yang, H., Wang, S., Xiao, Y., 2020. The role of m^6A modification in physiology and disease. Cell Death Dis 11, 960. https://doi.org/10.1038/s41419-020-03143-z

Yaniv, M., Folk, W.R., 1975. The nucleotide sequences of the two glutamine transfer ribonucleic acids from *Escherichia coli*. J Biol Chem 250, 3243–3253.

Zhang, L.S., Liu, C., Ma, H., Dai, Q., Sun, H.L., Luo, G., Zhang, Z., Zhang, L., Hu, L., Dong, X., He, C., 2019. Transcriptome-wide mapping of internal N^7-methylguanosine methylome in mammalian mRNA. Mol Cell 74, 1304–1316. https://doi.org/10.1016/j.molcel.2019.03.036

Zhang, X., Peng, Q., Wang, L., 2023. N^6-methyladenosine modification—a key player in viral infection. Cell Mol Biol Lett 28, 78. https://doi.org/10.1186/s11658-023-00490-5

Zhang, Y., Geng, X., Li, Q., Xu, J., Tan, Y., Xiao, M., Song, J., Liu, F., Fang, C., Wang, H., 2020. M^6A modification in RNA: Biogenesis, functions and roles in gliomas. J Exp Clin Cancer Res 39, 192. https://doi.org/10.1186/s13046-020-01706-8

Zheng, G., Dahl, J.A., Niu, Y., Fedorcsak, P., Huang, C.M., Li, C.J., Vågbø, C.B., Shi, Y., Wang, W.L., Song, S.H., Lu, Z., Bosmans, R.P.G., Dai, Q., Hao, Y.J., Yang, X., Zhao, W.M., Tong, W.M., Wang, X.J., Bogdan, F., Furu, K., Fu, Y., Jia, G., Zhao, X., Liu, J., Krokan, H.E., Klungland, A., Yang, Y.G., He, C., 2013. ALKBH5 is a mammalian RNA demethylase that impacts RNA metabolism and mouse fertility. Mol Cell 49, 18–29. https://doi.org/10.1016/j.molcel.2012.10.015

Zhou, H., Liu, Q., Yang, W., Gao, Y., Teng, M., Niu, L., 2009. Monomeric tRNA (m^7G46) methyltransferase from *Escherichia coli* presents a novel structure at the function-essential insertion. Proteins 76, 512–515. https://doi.org/10.1002/prot.22413

Zhou, Z., Lv, J., Yu, H., Han, J., Yang, X., Feng, D., Wu, Q., Yuan, B., Lu, Q., Yang, H., 2020. Mechanism of RNA modification N^6-methyladenosine in human cancer. Mol Cancer 19, 104. https://doi.org/10.1186/s12943-020-01216-3

Zhu, W., Xi, L., Qiao, J., Du, D., Wang, Y., Morigen, 2023. Involvement of OxyR and Dps in the repression of replication initiation by DsrA small RNA in *Escherichia coli*. Gene 882, 147659. https://doi.org/10.1016/j.gene.2023.147659

Zorbas, C., Nicolas, E., Wacheul, L., Huvelle, E., Heurgué-Hamard, V., Lafontaine, D.L.J., 2015. The human 18S rRNA base methyltransferases DIMT1L and WBSCR22-TRMT112 but not rRNA modification are required for ribosome biogenesis. Mol Biol Cell 26, 2080–2095. https://doi.org/10.1091/mbc.E15-02-0073

Acknowledgements

First and foremost, I extend my heartfelt gratitude to Prof. Dr. Kirsten Jung for welcoming me into her research group and granting me the opportunity to pursue my doctoral thesis under her scientific guidance. I am deeply grateful for her mentorship, which not only honed my scientific skills but also shaped my ability to think critically and solve complex problems. Her unwavering support, insightful feedback, and open-door policy created an encouraging environment that was instrumental in shaping the direction of my research. Despite her demanding schedule, she consistently made herself available to address any questions or doubts I had. Her patience, encouragement, and belief in my abilities have been invaluable throughout this journey.

I would like to express my sincere gratitude to Prof. Dr. Simon Heilbronner for his helpful experimental suggestions during the TAC meetings and for serving as the second examiner of this thesis. I would like to extend my thanks to Prof. Dr. Thomas Nägele for his valuable feedback and his role as a member of the TAC committee. I would also like to express my deepest gratitude to Prof. Dr. Wolfgang Enard, PD Dr. Jörg Meurer and Prof. Dr. Laura Busse for their time and effort in reading this thesis and serving as members of the examination committee.

I am deeply thankful to Dr. Sophie Brameyer for her insightful supervision and engaging discussions. Furthermore, I greatly appreciate the support and expertise provided in teaching me microscopy, which greatly enhanced my research skills and understanding. I would also like to thank Dr. Sebastian Riquelme-Barrios for his helpful scientific and non-scientific discussions and for his support as a colleague and friend. I would also like to thank all collaborators who contributed to this thesis. My sincere gratitude goes to Dr. Ignasi Forné for performing the LC-MS/MS analysis, conducting the initial statistical tests on the proteomics dataset, and engaging in many enriching discussions. I am also thankful to Dr. Siobhan Cusack for conducting the WGCNA analysis on the proteomics dataset and her thoughtful advice in data visualization, which made the process both productive and enjoyable. My appreciation extends to Leonardo Vásquez Camus for performing the Rol-LAMP experiment on my samples. Additionally, I am grateful for the opportunity to supervise my research course student, Inès Wullkopf, who has also become a dear friend. I would like to thank my colleague and friend, Agata Golaszewska, for her support, assistance with experiments, and friendship throughout this journey. I would also like to thank the

Epitranscriptomics team – Agata, Dania, Korinna, Leonardo, Luis, Sebastian, Siobhan, and Sophie – for their constructive feedback, encouragement and shared enthusiasm during our regular meetings, which greatly enriched and inspired my work.

The LSM Graduate School played a significant role throughout my doctoral thesis, providing an excellent framework for building connections and offering outstanding method and soft skill courses as well as scientific retreats. I extend my heartfelt thanks to Korbinian and Nadine for their continuous support and for their commitment to addressing all my queries with patience.

Throughout my PhD journey, I had the pleasure of sharing my office with many wonderful people, and I want to sincerely thank each of them for creating a comfortable and supportive workspace. I am especially grateful to my office mates Julia, Sophia Beck, Kilian, Tatiana, and Luis, as well as Leo, our honorary "pseudo-member". I am also grateful to the former and current lab technicians – Korinna, Sabine, Agata, Tatjana, Slavica, Ingrid and Tina - for their invaluable assistance and expertise, which ensured smooth day-to-day operations in the lab. I would also like to express my sincere appreciation to all the former and current members of the AG K. Jung, H. Jung, S. Heilbronner and Lassak research groups who supported me throughout this journey. My heartfelt thanks go to Jin, Giovanni, Urte, Alina Sieber, Elena, Ana, Nathalie, Steffi, Tess, Nan, Lingyun, Kevser, Alina Bitzer, David, Beatrice, Nicola, Michelle, Tania, Fabienne, Dimitar, Frank, Luciana and Jurgen. I want to express my heartfelt gratitude to Grazyna for her incredible support, whether it was navigating LMU administration, resolving visa issues, tackling life challenges, or simply being there for me through it all. Thank you for everything.

I am profoundly grateful to my friends, whose warmth, kindness, and companionship turned Munich into a home-like feeling – Akash, Andreas, Daniela, Jin, Sophia Beck, Giovanni, Leonardo, Agata, Erica, Björn, Urte, Dania, Livia, Siobhan, Korbinian, Annabel, Kenneth, Matias, Alina, Inès, Tatiana, Luis, Alice, Stefan and David. A heartfelt special mention to the Beck family for warmly welcoming me into their home and lives with so much love. A big thank you to all my long-distance friends from around the world who cheered me on and kept me going with their love and support! Thanks to Angika, Manas, Hemant, Yash, Ankit, Dhairya, Shalmalee, Nikita, Abel, Prashant, Pooja, Vedavathi, Swathi, Sophia Lamkhovah, Saumya, Shreeya, Meghomita, Avirup, Chadni, Lavanya, Ritvik, Snehit, Chaitanya, Lakshmi, Amit and Anirudh.

Finally, I would like to thank my family for their love, patience, support and understanding, for being my greatest source of strength and for always being the light guiding my path. None of this could have been possible without all of you. I want to thank the extended Saikia and Phukan family for cheering me on from the sidelines. I also want to thank the Yanamandra family for their love and support. Moreover, I would like to mention my favourite pups of all time – Ninni, Shiloh, Shiro, Bella and Bhoori – who have showered me with endless unconditional love and brought so much happiness and chaos into my life. Last but definitely not the least, I want to express my heartfelt thanks to Kaushik, my partner in life and crime, who, even from afar, always felt so near. Thank you for being my rock, my cheerleader, and my greatest source of joy. It is a great pleasure for me to close this chapter and start a new one with you.

Curriculum Vitae

Bibakhya Saikia

Education

2021- ongoing
Doctor of Philosophy (Ph.D.)
AG. Kirsten Jung, Faculty of Biology
Ludwig-Maximilians-Universität München

2018-2020
Master of Science (MSc.)
Major in Applied Microbiology
Vellore Institute of Technology (VIT), Vellore

2015-2018
Bachelor of Science (BSc.)
Major in Microbiology and Biochemistry
St. Xavier's College (Autonomous), Mumbai

Awards

Poster Prize – LSM Retreat 2023

Poster Prize – 5th International hands-on phage biotechnology course 2023

Talk Prize – LSM Retreat 2022

2nd Rank in Master's Program 2020

1st Rank in Microbiology during the Bachelor's Program 2018

Talk Prize – Undergraduate Research Scholars' Meet (Jigyaasa) 2018

Qualified the 17th State Level Microbiological Contest organized in collaboration with Association of Microbiologists of India (AMI) 2017

Summar Research Fellowship by Indian Academy of Science, Indian National Science Academy and The National Academy of Sciences, India 2017

Work Experience

October 2021 – March 2025
Research Assistant (Wissenshaftliche Mitarbeiterin)
AG K. Jung, Ludwig-Maximilians-Universität München

March 2021 – August 2021
R&D Consultant
Unilever R&D, Bangalore

December 2019 – June 2020
Research Intern (Master's thesis)
Unilever R&D, Bangalore

May 2019 – June 2019
Research Trainee
Organica Biotech Pvt. Ltd., Mumbai

June 2018 – November 2019
Research Project Intern (SET Project)
Dr. John Thomas, Vellore Institute of Technology, Vellore

November 2017 – March 2018

Research Intern (Bachelor's thesis)
Department of Life Sciences and Biochemistry,
St. Xavier's College (Autonomous), Mumbai

June 2017 – November 2017
Research Intern (Bachelor's thesis)
Department of Microbiology,
St. Xavier's College (Autonomous), Mumbai

April 2017 – June 2017
Summer Research Scholar
Dr. N. Ramesh Kumar, National Institute of Interdisciplinary Science and Technology, Trivandrum

Publication

Saikia, B., Riquelme-Barrios, S., Carell, T., Brameyer, S., & Jung, K. (2024). Depletion of m^6A-RNA in *Escherichia coli* reduces the infectious potential of T5 bacteriophage. Microbiology spectrum, 12(12). Advance online publication. https://doi.org/10.1128/spectrum.01124-24

Conferences and Retreats

Talks:

Saikia B, Riquelme-Barrios, S, Brameyer S, Jung K. m^6A-RNA modification may limit phage replication in *V. campbellii*. In: SPP2330 New Concepts in Prokaryotic Virus-host Interactions Meeting. Rösrath. 2022

Saikia B, Brameyer S, Jung K. Does m^6A-RNA modification limit phage replication in *V. campbellii*? In: Graduate school Life Science Munich retreat. Schliersee-Josefstal. 2022

Saikia B, Kandothankandy L, Chandavarkar R, Fereira L, Pinto S, Chakraborty, P. Effect of plant growth promoting rhizobacteria (PGPR) in consortia on the growth of Moong (*Vigna radiata*). In: Jigyaasa - Undergraduate Research Scholars' Meet. Mumbai. 2018

Posters:

Saikia B, Riquelme-Barrios S, Brameyer S, Jung K. m^6A-RNA modification affects phage replication. In: SPP2330 International Symposium on New Concepts in Prokaryotic Virus-host Interactions Meeting. Berlin. 2023

Saikia B, Brameyer S, Jung K. Does m^6A-RNA modification affect phage replication in *E. coli*? In: Graduate school Life Science Munich retreat. Schliersee-Josefstal. 2023

Saikia B, Riquelme-Barrios S, Brameyer S, Jung K. Does m^6A-RNA modification affect phage replication? In: 5^{th} International hands-on phage biotechnology course. Braga. 2023